Results from deuterium-tritium tokamak confinement experiments

R. J. Hawryluk

Princeton Plasma Physics Laboratory, Princeton, New Jersey 08543

Recent scientific and technical progress in magnetic fusion experiments has resulted in the achievement of plasma parameters (density and temperature) which made possible the production of significant bursts of fusion power from deuterium-tritium fuels and the first studies of the physics of burning plasmas. The key scientific issues in studying the reacting plasma core are plasma confinement, magnetohydrodynamic (MHD) stability, and the confinement and loss of energetic fusion products from the reacting fuel ions. Progress in the development of regimes of operation that both have good confinement and are MHD stable has made possible a broad study of problems in burning-plasma physics. The technical and scientific results from deuterium-tritium experiments on the Joint European Torus (JET) and the Tokamak Fusion Test Reactor (TFTR) are reviewed, with particular emphasis on alpha-particle physics issues. [S0034-6861(98)00602-3]

CONTENTS

I. INTRODUCTION

Over the past three decades, substantial progress has been realized in magnetic fusion science. Recent developments in the understanding of plasma transport, plasma stability, and impurity control have made possible the achievement of record plasma parameters including temperature, pressure, and confinement time and have created conditions under which significant fusion reaction rates, and consequently fusion power, have been demonstrated. The magnetic configuration most successful in achieving the parameters necessary for significant fusion reactions has been the tokamak. A tokamak (Artsimovich, 1972; Furth, 1975) is a toroidal magnetic confinement device that confines the plasma by a helical magnetic field through a combination of an external toroidal magnetic field and the self-field produced by a toroidal plasma current. In tokamak experiments on the Joint European Torus, JET (JET Team, 1992), JT-60U (Kikuchi *et al.*, 1995; Ushigusa *et al.*, 1997), DIII-D (DIII-D Team, 1995; Lazarus *et al.*, 1996), and the Tokamak Fusion Test Reactor, TFTR (Hawryluk *et al.*, 1995; McGuire *et al.*, 1997) many of the plasma parameters expected in an operating fusion reactor have been generated. The extension in operating parameters has been accompanied by a deeper understanding of the underlying physics responsible for the confinement and stability of the discharge. Experiments to date have been conducted primarily using either hydrogen or deuterium plasmas, though tokamak reactors are planned primarily to utilize mixed deuterium (D) and tritium (T) plasmas due to the higher cross sections and higher yield per D-T reaction.

Until the operation of the present generation of large tokamaks, the plasma parameters, which determine the reaction rate and the concentration of fusion products,

were not adequate to warrant the use of tritium fuel, a radioactive isotope of hydrogen, and the consequent increase in machine activation from increased plasma reactivity. However, present experiments on TFTR have produced conditions in which the fusion power density and the resulting population of energetic alpha particles are comparable to those within a reactor. Thus the study of D-T plasmas makes possible the study of critical physics issues associated not only with D-T fuel, but also with alpha-particle physics. The production and confinement of energetic alpha particles and their subsequent thermalization will be the central scientific issues for the study of burning plasmas.

The fusion reactions of most practical interest for fusion power production are

$$\mathrm{D}+\mathrm{T}\Rightarrow n(14.1\ \mathrm{MeV})+\alpha(3.5\ \mathrm{MeV}),$$

$$\mathrm{D}+\mathrm{D}\Rightarrow n(2.5\ \mathrm{MeV})+{}^3\mathrm{He}(0.8\ \mathrm{MeV}),$$

and

$$\mathrm{T}(1\ \mathrm{MeV})+p(3\ \mathrm{MeV}),$$

$$\mathrm{D}+{}^3\mathrm{He}\Rightarrow p(14.7\ \mathrm{MeV})+\alpha(3.7\ \mathrm{MeV}).$$

The transfer of energy from the energetic charged particles produced by fusion to the background plasma can, in principle, be used to heat the plasma and eventually, in a reactor, sustain the temperature. Energetic neutrons leave the plasma and are absorbed or scattered by structures outside. In a reactor, the neutrons would be absorbed in a lithium blanket surrounding the plasma, and the tritium would be regenerated by the reactions

$$n+{}^6\mathrm{Li}\rightarrow{}^4\mathrm{He}(2.1\ \mathrm{MeV})+\mathrm{T}(2.7\ \mathrm{MeV}),\quad Q=4.8\ \mathrm{MeV},$$

$$n+{}^7\mathrm{Li}\rightarrow{}^4\mathrm{He}+\mathrm{T}+n,\quad Q=-2.5\ \mathrm{MeV}.$$

The fusion power density due to D-T reactions in the plasma is given by

$$P_{\mathrm{fus}}=n_{\mathrm{T}}n_{\mathrm{D}}\langle\sigma v\rangle 17.6\ \mathrm{MeV}\ V_p,$$

where n_{T} and n_{D} are the tritium and deuterium densities, $\langle\sigma v\rangle$ for a pure plasma is the rate coefficient, and V_p is the plasma volume. There is a corresponding expression for the other reactions of interest.

The rate coefficients for D-T reactions are substantially larger than for the other possible reactions of interest (Bosch and Hale, 1992), as shown in Fig. 1. Thus a D-T reactor with a lithium blanket is the most easily achievable because a self-sustaining plasma can be achieved with the lowest ion temperature ($T>5$ keV) and lowest requirement for the product $n_i\tau_E^*T_i$, where n_i is the ion density, and the energy replacement time τ_E^* is defined by the power balance equation

$$P_{\mathrm{heat}}-P_{\mathrm{breh}}=\frac{dW_{\mathrm{tot}}}{dt}+P_{\mathrm{loss}}\equiv\frac{W_{\mathrm{tot}}}{\tau_E^*}.$$

W_{tot} is the plasma stored energy, P_{loss} is the loss of power due to plasma transport and synchrotron radiation as well as impurity radiation (excluding bremsstrahlung), P_{heat} is the heating power, and P_{breh} is the radiation loss due to bremsstrahlung. In the current experiments, radiation loss from bremsstrahlung is typically very small in the power balance and can be ignored, but it will be significant when alpha heating becomes the dominant heating mechanism, which is why it is explicitly shown. The brehmsstrahlung power for a pure plasma is approximately given by

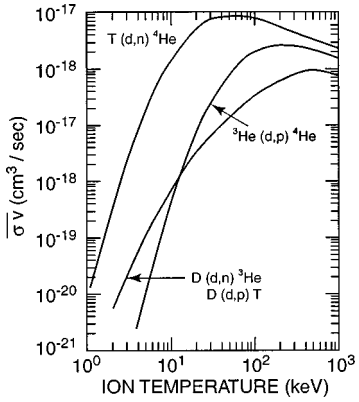

FIG. 1. Rate coefficients for fusion reactions of importance in magnetic fusion, plotted vs ion temperature.

$$P_{\mathrm{breh}}=1.7\times10^{-38}\varepsilon n_e^2\mathrm{T}_e^{0.5}V_p,$$

where ε is the Gaunt factor, and n_e and T_e are the electron density and temperature (Rose and Clark, 1961). $P_{\mathrm{heat}}=P_{\mathrm{aux}}+P_{\mathrm{alpha}}$, where P_{aux} is the auxiliary heating power and P_{alpha} is the alpha heating power,

$$P_{\mathrm{alpha}}=V_p n_{\mathrm{T}}n_{\mathrm{D}}\langle\sigma v\rangle 3.5\ \mathrm{MeV}.$$

The ratio of P_{fus} to P_{aux} equals that of P_{fus} to $(W_{\mathrm{tot}}/\tau_E^*-P_{\mathrm{alpha}}+P_{\mathrm{breh}})$. For a uniform, isothermal plasma ($\mathrm{T}_i=\mathrm{T}_e$) without impurities ($n_i=n_e=2n_{\mathrm{T}}=2n_{\mathrm{D}}$), the ratio of P_{fus} to P_{aux} can be expressed as a function of the triple product $n_i\mathrm{T}_i\tau_E^*$ and T_i. For thermal D-T reactions, $\langle\sigma v\rangle\propto\mathrm{T}_i^2$ for $9<\mathrm{T}_i<19$ keV, and a value of $n_i\mathrm{T}_i\tau_E^*>6\times10^{21}$ m^{-3} keV (Furth *et al.*, 1990) is required for ignition when the power balance is sustained by fusion reactions ($P_{\mathrm{aux}}=0$). Thus it has become customary to illustrate technical progress in magnetic fusion in terms of the triple product, $n_i(0)\mathrm{T}_i(0)\tau_E^*$, as shown in Fig. 2. In large present-day experiments, the value of the triple product achieved corresponds to conditions in which the fusion power produced for D-T plasmas would be somewhat less than the auxiliary power used to heat the plasma. Though the relationship of the triple product to fusion power production applies only to D-T experiments conducted on JET and TFTR, the highest values of triple product achieved in D experiments on several other devices are shown for comparison. The general considerations given here are for a homogeneous, pure, thermal plasma. This analysis has been extended to include important effects associated with profile shapes, impurities, nonthermal ion distributions, synchrotron radiation, and $\mathrm{T}_i\neq\mathrm{T}_e$. Though the precise relationship between the triple product and the ratio of P_{fus} to P_{aux} depends upon these effects, as well as upon

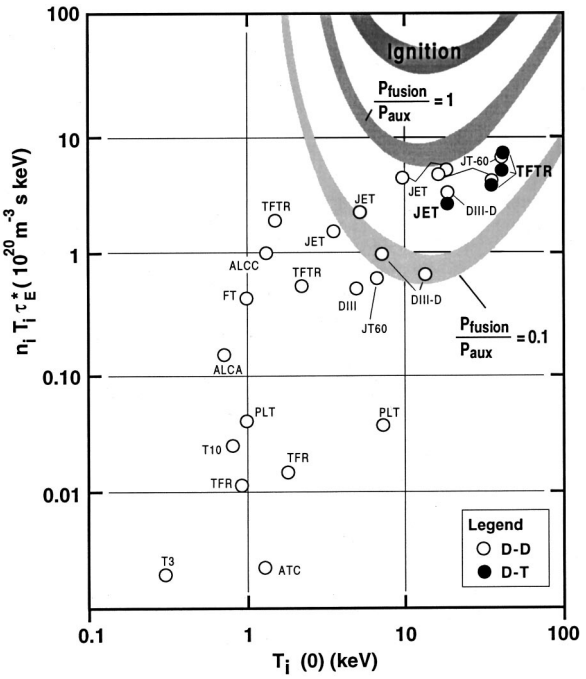

FIG. 2. The achieved product $n_{HYD}(0)\mathrm{T}_i(0)\,\tau_E^*$ where n_{HYD} is the sum of all hydrogenic densities vs $\mathrm{T}_i(0)$ for various tokamak devices. In the present devices, P_{breh} is small compared with P_{aux} and is ignored. For comparison, an estimate of the criteria for $P_{\mathrm{fus}}/P_{\mathrm{aux}}=1$ and ignition in which the alpha heating sustains the plasma is given (Gibson *et al.*, 1987).

the confinement and thermalization of the alpha particles, these very simple considerations highlight the important plasma parameters required for substantial fusion power production.

Present-day deuterium-tritium experiments can address many but not all of the physics issues associated with the use of D-T fuel. Generic issues associated with the use of tritium fuels, such as isotope effects on confinement and heating, have been studied. These do not depend on the plasma reactivity. The production of substantial rates of fusion reactions makes possible the detailed study of the confinement and loss of alpha particles (Strachan *et al.*, 1989). More importantly, the effect of alpha particles on plasma stability can be studied. Because these instabilities depend on alpha-particle pressure (as well as on other parameters), regimes of operation with high rates of alpha-particle production are needed. By operating in regimes in which the ion temperature (or energy) is greater than the electron temperature, it has been possible to achieve fusion power densities comparable to those in a reactor to study this important physics topic, even though the ratio of P_{fus} to P_{aux} is much less than that in a reactor. In the present experiments, alpha heating which depends directly on the ratio of P_{fus} to P_{aux} can be detected; however, a comprehensive study requires operation in regimes in which $P_\alpha > P_{\mathrm{aux}}$, a condition that has not yet been obtained. In this review, approaches used to increase the plasma reactivity are described because they helped to broaden the range of physics topics that could be studied experimentally.

In the world tokamak fusion program, two major facilities, JET and TFTR, have been designed to study the physics associated with the use of D-T fuel. A limited-scope, "Preliminary Tritium Experiment" was performed on JET in 1991. This experiment utilized a ratio of tritium to deuterium fuel of 13% (JET Team, 1992). A more extensive program is planned to begin on JET in 1997. TFTR conducted an extensive campaign of high-power D-T experiments from 1993 to 1996 with a wider range of tritium-to-deuterium fueling (up to 100%; Hawryluk, 1994a; Strachan *et al.*, 1994a). Additional D-T experiments were completed on TFTR in 1997 but are not discussed in this review. The D-T experiments on JET and TFTR during the past several years have provided important new data on the confinement of D-T plasmas, their heating by radio-frequency waves and energetic neutral beams, and confinement and loss of alpha particles.

This paper will review the results from the recent D-T experiments from JET and TFTR and highlight remaining issues and scientific opportunities. In preparing this paper, I have benefited from review papers on alpha-particle and burning-plasma physics issues which were written prior to the use of tritium on JET and TFTR by Kolesnichenko (1980), Goloborod'ko *et al.* (1987), Sigmar (1987), and Furth *et al.* (1990), as well as from several overview papers on experimental results from both machines [JET Team, 1992; JET Team (presented by Gibson), 1993; Hosea *et al.*, 1994; Strachan *et al.*, 1994b; Bell *et al.*, 1995; Johnson, D. *et al.*, 1995; McGuire *et al.*, 1995, 1997; Meade, 1995; Bell *et al.*, 1997]. The experiments on both machines are part of a worldwide effort to study the physics of high-temperature plasmas, and they rely upon theoretical and experimental results from this entire effort. In this paper, it is not possible to give a comprehensive review of tokamak physics research. The presentation of results from D-T experiments on JET and TFTR should be understood within this broader context.

In addition to the present experiments, there is a major international design study underway to develop a device called the International Thermonuclear Experimental Reactor (ITER), which will be able to sustain a burning plasma for a long duration. This device, which will use D-T fuel, is planned to be about three times larger in linear dimension than TFTR or JET and is projected to produce 1500 MW of fusion power. The status of the ITER Project was discussed recently by Aymar *et al.* (1997). The design of the ITER device is based on established physics and technology. However, the design process has identified important issues for burning-plasma research. Many of the results in this paper will be presented in terms of the issues and requirements for ITER.

This review includes a brief description of the JET and TFTR devices, with particular emphasis on the characteristics of importance to D-T experiments. The tritium handling system and the radiological consequences of high-energy neutrons on machine activation and site-boundary dose is in the Appendix. A key element in the

experiments conducted on JET and TFTR has been the development of high-performance regimes characterized by high fusion reactivity. In the present experiments, these regimes have several distinguishing and common characteristics: reduced levels of plasma transport resulting in enhanced confinement; maximum plasma pressure typically limited by the onset of pressure-driven magnetohydrodynamic (MHD) activity; and ion temperatures in excess of the electron temperature caused by the vigorous application of auxiliary heating. Due to differences between these devices, however, different techniques have been employed to achieve these enhanced regimes of operation. These techniques are described, and the present understanding of plasma transport and MHD stability limits in these devices is briefly summarized. An overview of the fusion power production that has been achieved in these regimes of operation follows. Having reviewed the experimental conditions for D-T operation, we turn to the effect of D-T fueling on plasma confinement and heating. In particular, isotope effects on plasma confinement are described, and the effect of a second-harmonic ion-resonance heating by waves in the ion-cyclotron range of frequencies is discussed.

The confinement and thermalization of alpha particles is the key scientific issue for the study of burning plasmas. The confinement of alpha particles in both quiescent and MHD-active discharges is described. An overview of our present understanding of how alpha particles can in turn destabilize plasma is offered. Although in the present experiments alpha heating has been small compared with auxiliary plasma heating, initial evidence for alpha heating is presented. Future research opportunities in the study of D-T plasmas and alpha-particle interactions conclude this review paper.

II. JET AND TFTR DEVICES

Both JET and TFTR are tokamak devices in which a strong toroidal magnetic field, together with the self-field produced by a large toroidal plasma current, is used to confine and heat the plasma. As shown in Figs. 3 and 4, the nearly circular TFTR plasma is limited by a limiter on the inner wall composed of graphite and carbon-fiber-composite (CFC) tiles mounted on a water-cooled Inconel backing plate. A set of poloidal limiters composed of carbon-fiber-composite tiles is used to protect rf launchers on the outboard side, which are used to heat the plasma. The limiters can withstand heat outflow from the plasma of $\sim$30 MW for $\sim$1 s. As shown in Figs. 5 and 6, the JET vacuum vessel is shaped to permit plasma formation with an elongation of $<$1.6 where the plasma elongation is $\kappa = b/a$ with the plasma height $=2b$ and the plasma width$=2a$. The last closed magnetic surface has an X point. The field lines beyond the X point "divert" the heat flux to a toroidally continuous top target composed of CFC tiles used in the Preliminary Tritium Experiments. A continuous inner wall of graphite and CFC tiles, a continuous bottom target clad with beryllium tiles, and a pair of toroidal belt limiters

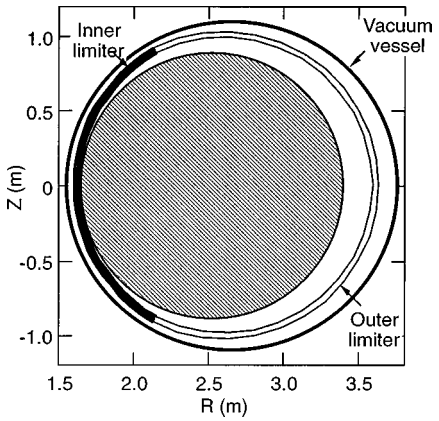

FIG. 3. Plasma boundary for TFTR pulse No. 80539. (The plasma parameters for the pulse are given in Table IV.) Shown are the inboard limiter and the poloidal (outer) limiters.

on the outboard side above and below the midplane, the upper one of beryllium and the lower one of carbon, complete the protection of the JET vessel (JET Team, 1992). A comparison of the principal engineering parameters of JET and TFTR is given in Table I. Since the initial D-T experiments on JET, the machine has been extensively modified with the installation of additional poloidal field coils and particle pumping in the bottom of the vessel. Further D-T experiments are planned to be performed in this modified device [JET Team (presented by Stork) 1995; JET Team (presented by Jacquinot) 1997].

A. Auxiliary heating

During the D-T experiments, neutral-beam heating was used on both devices, and rf heating in the ion-cyclotron range of frequencies (ICRF) was used on TFTR. In addition, an extensive ICRF program was conducted in D discharges on both JET and TFTR.

The TFTR neutral-beam system is composed of four beamlines, each with three positive-ion sources. The sources extract and accelerate a positive-ion beam, which is then neutralized in a gas cell before entering the plasma. The ion sources can operate either in deuterium or in tritium. The maximum operating voltage is 120 kV, and the maximum injected power into a D-T discharge has been 40 MW (Grisham *et al.*, 1995; Stevenson *et al.*, 1995). In addition to heating the discharge, the neutral beams are an effective means of fueling the discharge. On TFTR, the fueling has been varied from all deuterium to all tritium. The JET neutral-beam heating system is composed of two neutral beamlines with eight positive-ion sources each. For the Preliminary Tritium Experiment, two of the ion sources operated in tritium at a voltage of 78 kV to ensure reliable operation. The remaining fourteen sources operated in deuterium, twelve at an operating voltage of 135 kV and two at 75 kV. The injected power into the D-T discharges was 14.3 MW. The tritium fueling rate relative to the total was $\approx$13%.

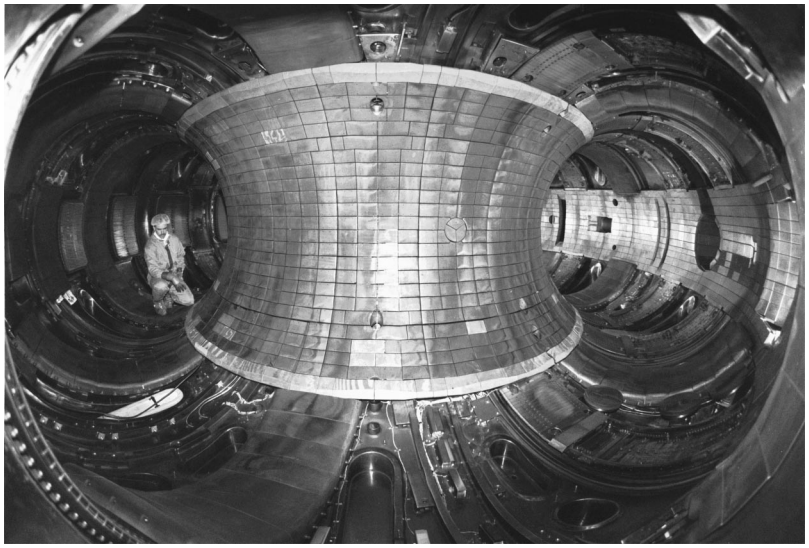

FIG. 4. Interior of the TFTR vacuum vessel. The carbon-fiber-composite and graphite tiles on the inner wall limit the plasma and protect the vacuum vessel wall.

The TFTR ICRF system uses four antennas structured to launch electromagnetic waves, which are dominantly polarized so that the wave electric field parallel to the equilibrium toroidal magnetic field is negligible. For these experiments, the dominant propagating modes are fast magnetosonic waves. Depending on the choice of frequency, magnetic-field strength, and plasma composition, the fast waves can damp in the plasma core on a second-harmonic cyclotron resonance of a majority ion species, such as tritium, or on the fundamental cyclotron resonance of a dilute light-impurity species (minority species) such as hydrogen or ^{3}He. Experiments using coincident fundamental minority ^{3}He and second-harmonic tritium majority absorption have been conducted at 43 MHz, while fundamental hydrogen minority with coincident second-harmonic deuterium majority heating experiments have been conducted at 64 MHz. For multiple-ion-species plasmas, an additional resonance called the ion-ion hybrid resonance is located between the fundamental cyclotron resonance layers of each pair of ions. In the vicinity of this resonance, the launched fast waves can couple to an electrostatic hot-plasma wave called an ion Bernstein wave, which has similar dispersion characteristics in the hybrid layer. This ''mode-conversion'' process can be used to provide localized heating near the D-T ion-ion hybrid layer in TFTR with 30-MHz waves in a plasma with $B_t \sim 5.3$ T or near the D-^{3}He ion-ion hybrid layer with 43-MHz waves in plasma with a small amount of tritium present. A more detailed comparison of the different ICRF heating regimes is given in Sec. VI.B.

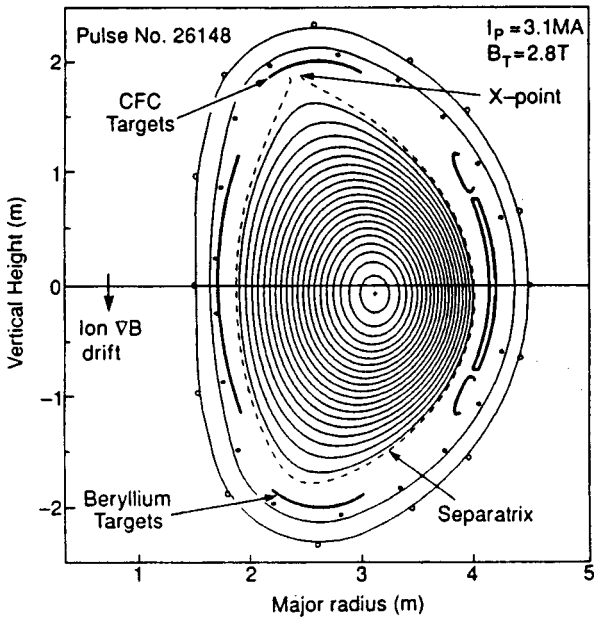

FIG. 5. Magnetic flux surface configuration for JET pulse No. 26148. (The plasma parameters for this pulse are given in Table III.) Shown are the separatrix, the X point, and the carbon-fiber-composite and beryllium targets (JET Team, 1992).

B. Plasma diagnostics

New and novel diagnostics have been an important ingredient in developing an understanding of high-temperature plasmas. A review of recent diagnostic developments is given by Gentle (1995). Information about TFTR and JET diagnostics can be found in Hill *et al.* (1990), Young and Johnson (1992), Young (1997), Johnson *et al.* (1996), and Thomas (1996). In modern tokamak experiments, detailed profile measurements of the plasma electron and ion temperature, electron density, current density, and toroidal rotation are routinely available. Measurements of the fluctuations in the plasma are made by a variety of techniques, including fast-electron cyclotron emission measurements of the electron temperature, x-ray measurements of the chord-averaged x-ray emissivity due to variations in electron

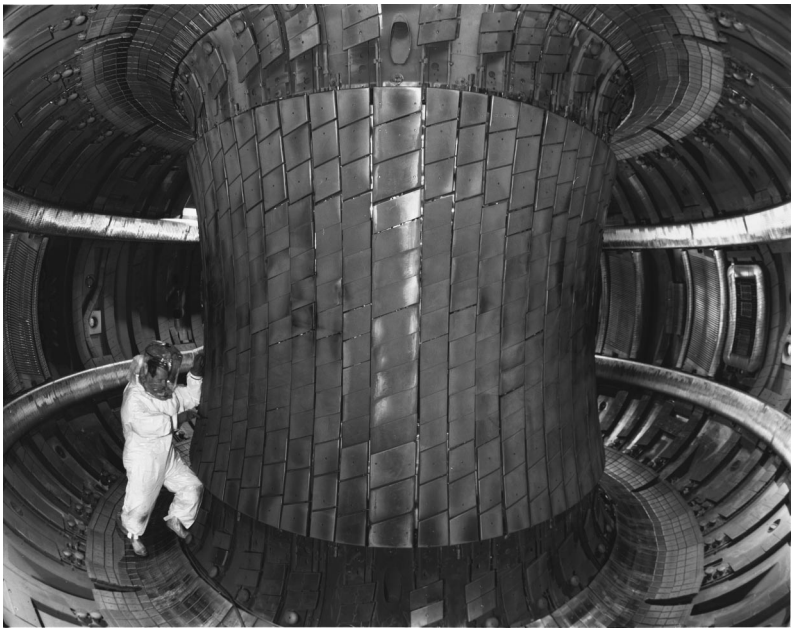

FIG. 6. Interior of the JET vacuum vessel (JET Team, 1992).

temperature, electron density, and impurity concentration, and microwave reflectometer and beam-emission-spectroscopy measurements of the density fluctuations. Table II provides a list of current diagnostics on the TFTR device and the parameters measured. In preparation for the D-T experiments, many TFTR diagnostics were modified to cope with the higher radiation fluxes from both neutrons and gammas during the pulse (Ku *et al.*, 1994; Hill *et al.*, 1995). In addition, the vacuum systems of the diagnostics were modified to be tritium compatible. The D-T experiments also provided an opportunity to assess the effect of neutron damage on fiber optics (Morgan, 1992; Adler *et al.*, 1995; Paul *et al.*, 1995; Ramsey *et al.*, 1995).

For the D-T experiments, several new diagnostics were developed to measure the total neutron source strength, the neutron emission profiles, which are a measure of the alpha-particle birth location, and the escaping and confined alpha particles. Since these new measurements are central to the D-T experiments, they are described below.

1. Neutron measurements

The neutron emission rates were measured in JET with silicon surface-barrier diodes and using ^{235}U and ^{238}U fission chambers (which are not capable of discriminating between 2.5-MeV and 14-MeV neutrons). These detectors were calibrated by comparison with the total time-integrated neutron yield measured by the activation of two elemental samples positioned near the vessel. Silicon was used, but since the ^{28}Si (n,p) reaction is not well characterized, it was cross-calibrated against the standard dosimetry reaction of ^{63}Cu $(n,2n)^{62}$Cu and ^{56}Fe $(n,P)^{56}$Mn. The accuracy of the total neutron yield is estimated at $\pm 7\%$. The neutron energy spectrum was measured with a liquid-scintillator spectrometer. Neutron emission profile data were obtained from 19 similar spectrometers arranged in two cameras with orthogonal views (JET Team, 1992; Marcus *et al.*, 1993).

TFTR also has an extensive set of fusion neutron detectors—five fission detectors, two surface-barrier detectors, four activation-foil stations (Barnes *et al.*, 1995), and a ten-channel neutron collimator with 25 detectors (including ^{4}He recoil detectors) to provide time resolution, as well as energy discrimination of the D-T and D-D neutron fluxes. The systems were calibrated *in situ* by positioning an intense neutron source at many locations within the vacuum vessel (Barnes *et al.*, 1990; Hendel *et al.*, 1990; Strachan *et al.*, 1990). The yield mea-

TABLE I. Comparison of JET and TFTR engineering parameters.

	JET	TFTR
Plasma major radius R	2.96 m	2.6 m
Plasma minor radius (horizontal) a	1.25 m	0.9 m
Plasma elongation ratio κ	1.68	1.0
Toroidal magnetic field (plasma center) B_t	3.45 T	5.9 T
Plasma current I_p	7.0 MA	3.0 MA
Neutral beam power P_b	18 MW	40 MW
ICRF power P_{ICRF}	22 MW	11 MW

TABLE II. Diagnostic measurements on TFTR.

Profile Data	Impurity Concentration
$T_e(r)$	Visible bremsstrahlung array
TV Thomson scattering	VUV survey spectrometer
ECE heterodyne radiometer	Multichannel visible spectrometer
ECE Fourier transform spectrometer	X-ray pulse-height analyzer
ECE grating polychromator	Radiated power
$n_e(r)$	Tangential bolometers
TV Thomson scattering	Bolometer arrays
Multichannel far infrared interferometer	Wide-angle bolometers
$T_i(r)$	Fluctuations/Wave Activities
Charge-exchange recombination spectroscopy	Microwave scattering
X-ray crystal spectrometer	X-ray imaging system
$q(r)$	Ion-cyclotron emission/rf probes
Motional stark effect polarimeter	ECE grating polychromator
	Mirnov coils
Fusion Neutrons	Neutron fluctuation detector
Epithermal neutrons	Magnetic Measurement
Neutron activation detectors	Plasma current
14 MeV neutron detectors	Plasma geometry
Collimated neutron spectrometer	Diamagnetic flux
Multichannel neutron collimator	Loop voltage
Fast neutron scintillation counters	Plasma Edge/Wall
Gamma spectrometer	Plasma TV
Alpha-particles	IR camera
Lost alpha/triton array	Filtered diodes (H-alpha)
Pellet-charge-exchange	Filtered diodes (C-II)
Alpha charge-exchange recomb. spectroscopy	Fabry-Perot spectrometer
	Sample exposure probe

sured by the fission, surface-barrier, and ^{4}He recoil detectors is linear, with the yield measured by activation foils over six orders of magnitude. The system of multiple measurements has allowed a $\pm 7\%$ determination of the fusion energy production (Jassby *et al.*, 1995; D. Johnson *et al.*, 1995; Strachan *et al.*, 1995). The neutron profile and hence the alpha birth location is measured with the neutron collimator.

2. Escaping-alpha-particle measurements

Fusion product losses from TFTR plasmas are measured by a poloidal array of detectors just behind the limiter shadow. The detectors are situated at poloidal angles 90°, 60°, 45°, and 20° below the outer midplane. The ion $\nabla \mathbf{B}$ drift direction is toward the 90° detector. The 20° detector is mounted on a movable probe. The detectors are illustrated in Fig. 7. A set of apertures disperses the particles by pitch angle (the escaping particle's angle with respect to the toroidal field) and gyroradius onto a planar scintillator. Light from the scintillator is carried by coherent fiber-optic bundles to remote detectors, which record the two-dimensional position on the detector surface and the total scintillation light versus time (Darrow *et al.*, 1995).

An alternative approach to measuring escaping fusion products has been developed by Herrmann *et al.* (1995, 1997) and Chong (1995). Alpha particles escaping from the plasma are implanted in nickel foils located in a series of collimated ports on a vertically-movable probe drive, located at 90° below the midplane. Each port accepts particles with a limited range of pitch angles. The Ni foils with the implanted alpha particles are removed from the vessel and analyzed for He content. The alpha energy distribution is deduced by measuring the depth distribution of He in the Ni foils. This diagnostic has better energy resolution than do scintillator detectors but does not have intrinsic time resolution.

3. Confined-alpha-particle measurements

Measurements of confined alpha particles are especially difficult because of their relatively low concentration, $n_\alpha/n_e \sim 10^{-3}$, and large range in energies, from the birth energy of 3.5 MeV to thermal. Two techniques, pellet charge exchange (PCX) and alpha charge-

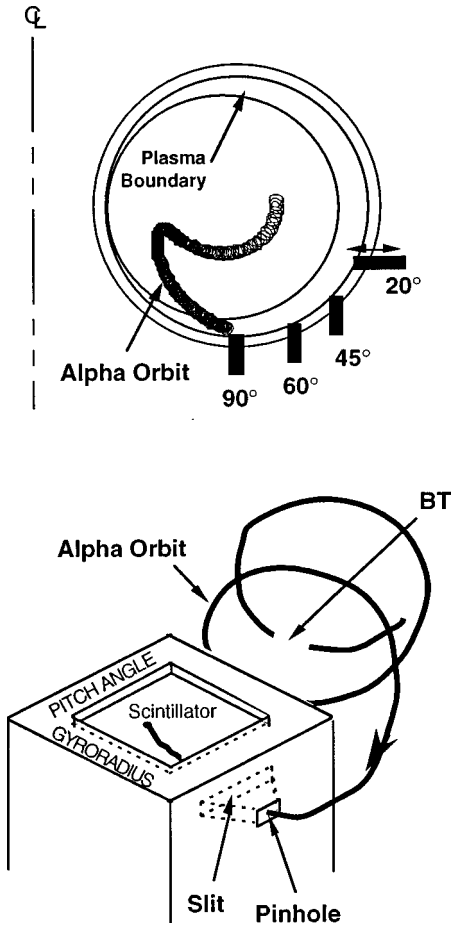

FIG. 7. Schematic diagram of the TFTR lost-alpha detector. Four lost-alpha detectors are located behind the limiter shadow. The escaping alphas enter a pair of apertures that disperse them in pitch angle and gyroradius (Darrow *et al.*, 1996a).

exchange recombination spectroscopy (α-CHERS), have been used on TFTR to study the confinement and thermalization of alpha particles.

In the pellet charge-exchange diagnostic, small lithium or boron pellets ($\sim 7\,\mathrm{mm}^3$) are injected radially into TFTR. Upon entering the plasma, the pellets ablate, surrounding themselves with a dense localized cloud of ionized lithium as they travel through the plasma. This cloud is sufficiently dense that a small fraction of the alpha particles incident on the cloud are neutralized by sequential single-electron capture,

$$\mathrm{He}^{2+}+\mathrm{Li}^{+}\rightarrow\mathrm{He}^{+}+\mathrm{Li}^{2+},$$

$$\mathrm{He}^{+}+\mathrm{Li}^{+}\rightarrow\mathrm{He}^{0}+\mathrm{Li}^{2+},$$

and also double capture,

$$\mathrm{He}^{2+}+\mathrm{Li}^{+}\rightarrow\mathrm{He}^{0}+\mathrm{Li}^{2+}.$$

By measuring the energy distribution of the resultant helium neutrals escaping from the plasma using a mass- and energy-resolved neutral-particle analyzer, one can determine the energy distribution of the confined alphas by modeling the fraction of alpha particles that are neutralized in the cloud as a function of alpha energy

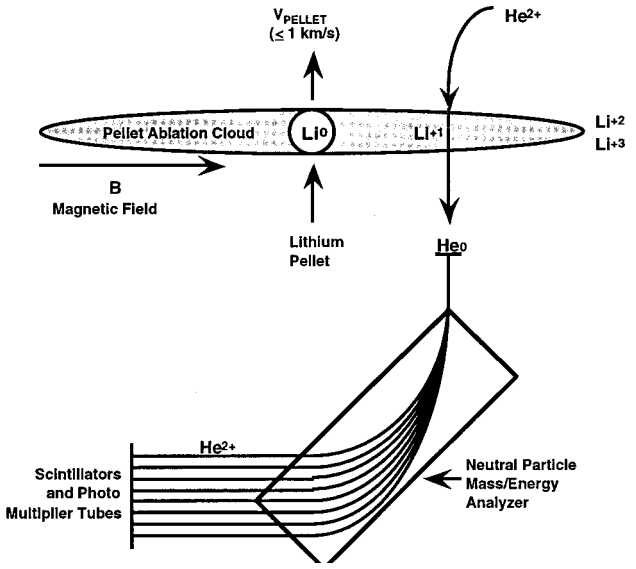

FIG. 8. Illustration of the pellet charge-exchange diagnostic for measuring confined alpha particles (Medley *et al.*, 1996b).

(Fisher *et al.*, 1995; Medley *et al.*, 1996b). This diagnostic technique is illustrated in Fig. 8. The technique has successfully measured confined alpha particles from 0.5 to 3.5 MeV with good signal-to-background ratio. When the radial position of the pellet was measured as a function of time, using a linear photodiode array situated on the top of the vacuum vessel and the time-dependent flux to the neutral-particle analyzer, good radial resolution of ~ 5 cm was obtained (Fisher *et al.*, 1995; Medley *et al.*, 1995, 1996a; Petrov *et al.*, 1995, 1997). The principal limitations of the PCX approach are that it provides a measurement at only one time in the discharge due to the large increase in density resulting from the Li pellet, which impacts on the evolution of the discharge, and that its use is typically restricted to the period after high-power heating in order to achieve adequate pellet penetration. Because of the viewing angle of the detector, only near-perpendicular energetic ions with $v_{\parallel}/v=-0.048$ are detected. This could, in principle, be changed.

α-CHERS, a charge-exchange recombination spectroscopy diagnostic, is designed to observe confined alphas with energies in the range from thermal to ~ 700 keV. A schematic illustration of the diagnostic is shown in Fig. 9 (McKee *et al.*, 1995a). Alpha particles are observed by measuring the Doppler shifted $n=4$ to 3 transition of He^{+1} near 468.6 nm, which is excited by electron exchange reactions between the injected neutral-beam atoms and alpha particles. Analysis of the spectrum yields the spatial density profile and the low-energy distribution. This is a very challenging measurement due to the relatively low signal level compared with the background light from bremsstrahlung and impurity lines emitted by low charge states of carbon. A very high light-throughput system was developed employing a moderate resolution spectrometer and low-noise, high-quantum-efficiency, high-dynamic-range detectors to improve the photon-counting statistics.

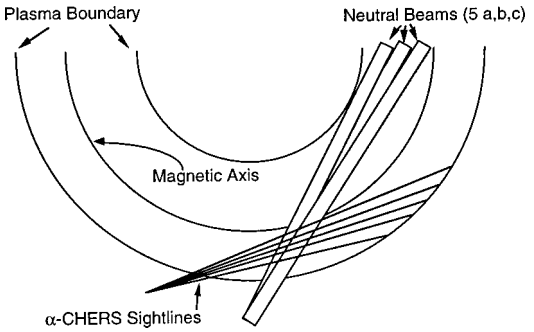

FIG. 9. Alpha charge-exchange recombination spectroscopy (α-CHERS) sightlines and beam viewing geometry (McKee *et al.*, 1995a, 1997).

The background light is carefully subtracted from the measured spectrum to give the contribution attributed to alpha particles. During the high-power phase, neutron-induced fluorescence in the optical fiber also contributes to the observed signals. As a result, the data are typically taken after the high-power phase when the population of alpha particles is still high, but the neutron flux has decreased substantially. The advantages of this technique are that it can provide time-dependent measurements at several radial locations, and furthermore, the intensity measurements are absolutely calibrated, which allows direct comparison with simulation codes.

III. REGIMES OF OPERATION

Both JET and TFTR operate in a variety of regimes, which span a wide range of plasma parameters and are characterized by differences in plasma transport and stability. The underlying physics responsible for the transport variability will be briefly described, although a comprehensive discussion of this extensive literature is beyond the scope of this paper. Fortunately, there are several papers that provide a good background to these issues, which remain under active study in the worldwide program. In this paper, only the regimes of operation that have been studied on JET and TFTR with D-T plasmas will be presented to provide a background to the results in the following sections.

A. L mode

The most easily obtained operating regime is called L mode because it is characterized by comparatively low confinement and can be reliably achieved. In this regime, there is a substantial influx of hydrogen and carbon at the limiters and/or divertors. The resulting density profiles are broad and edge-ion temperature is low. The electron and ion temperatures are typically comparable, especially at high density. An empirical relationship (Yushmanov *et al.*, 1990) has been derived from the worldwide database, which describes the confinement time for L-mode plasmas,

$$\tau_E^{\text{ITER-89P}} = 0.048 I_P^{0.85} R^{1.2} a^{0.3} n_e^{0.1} B_t^{0.2} (A_{\text{HYD}} \kappa / P)^{0.5}.$$

Here A_{HYD} is the mass of the hydrogenic species, P is the total heating power in MW, I_P is the plasma current in MA, R and a are the major and minor radii in meters, n is the line-averaged plasma density in units of 10^{20} m^{-3}, and B_t is the toroidal field in T. The confinement increases with mass of the hydrogenic species A_{HYD} and with plasma current and degrades with increasing auxiliary heating power. This regime of operation has been studied on TFTR briefly in D-T, but extensively in D.

The empirical observation of transport in TFTR L-mode discharges (Hawryluk *et al.*, 1991 and references therein) has revealed the following features:

(a) Radial transport is governed by turbulent processes such that the electron and ion heat, particle, and momentum transport are much larger than predicted by collisional transport theories.
(b) The degradation of thermal confinement with power, $\tau_E^{\text{th}} \sim P^{-0.7}$, is even stronger than that given by the global scaling relationship (Scott *et al.*, 1997).
(c) Local transport coefficients [electron heat diffusivity (χ_e), ion heat diffusivity (χ_i), and toroidal momentum diffusivity (χ_ϕ)] increase strongly with power or temperature (Scott *et al.*, 1990b).
(d) $\chi_i \approx \chi_\phi$ as expected from microturbulence theories.
(e) Degradation is not caused by anomalous loss of fast ions. For a comprehensive review see Heidbrink and Sadler (1994).
(f) Perturbative measurements of the electron particle transport indicate an adverse temperature scaling.
(g) Toroidal velocity profile measurements following off-axis neutral-beam injection can be modeled without introducing an inward momentum pinch.

Progress has been made in the understanding of transport processes in the core of L-mode discharges. Kotschenreuther *et al.* (1995), utilizing gyrofluid and gyrokinetic nonlinear simulations of the plasma turbulence, reproduced the observed variation of the confinement time and ion and electron temperature profiles with plasma current and neutral-beam power. The gyrokinetic equation is derived by averaging the Vlasov-Boltzmann kinetic equation to eliminate the fast time scales associated with the gyrating cyclotron motion of the particles, while retaining the essential nonlinear physics associated with slower processes involved in the MHD phenomenon and fine-scale instabilities and turbulence related to drift waves. Gyro-Landau-fluid equations are derived by integrating the gyrokinetic equation over all particle velocities, obtaining fluid conservation laws for particle density, momentum, pressure, etc.; they differ from regular fluid or MHD equations by including particle gyration effects and adding models of wave-particle resonances important in the low-collisionality and long-mean-free-path regimes of hot plasmas. (Regular fluid equations are derived in high-collisionality regimes.) The principal transport mechanism in these simulations is low-frequency electrostatic turbulence driven by ion temperature gradients. Over

most of the plasma, the ion temperature profile is near marginal stability to the mode responsible for the turbulence. Although quite successful for L-mode plasmas, the model used by Kotschenreuther *et al.* (1995) has some important limitations, especially when applied to enhanced confinement regimes. First, the model is not applicable to the edge region (roughly $r/a>0.85$), and experimental measurements are required to set the boundary conditions. Particle transport (and hence the heat transport by convection) is known to be important in regimes of operation in which the turbulence driven by the ion temperature gradient is suppressed and remains to be incorporated into the model. The effect of shear in the poloidal and toroidal flow velocities is treated in an approximate fashion. This is an especially important mechanism in turbulence suppression, and the formation of transport barriers is discussed further below. Despite these caveats, this model provides a satisfactory description of the performance of L-mode discharges within its domain of applicability and does not require any adjustable parameters.

Another approach has been pursued by Bateman *et al.* (1995, 1997), Kinsey and Bateman (1996), and Kinsey *et al.* (1996) using a multimode model in which analytic expressions describe the dependence of plasma energy and particle transport in TFTR, JET, and DIII-D discharges. In this approach, the numerical factor setting the transport level for each model is obtained by fitting the experimental data and evaluating the overall fit to the data (Kinsey *et al.*, 1995). The edge conditions are not taken from experimental data; however, the influx of neutrals from the edge is adjusted to obtain agreement with the measured density. The transport is predicted to be governed by electrostatic drift-wave turbulence and ballooning modes. The agreement between theory and experiment is satisfactory for a broad range of conditions. Further tests of the model employing both a wider range of data and responses to plasma perturbations, are required to evaluate the range of validity of the multimode model.

B. Enhanced confinement regimes

The experimental programs on JET and TFTR have focused on operating conditions that produce substantial fusion power and hence can be used to study alpha and other D-T-related issues in reactor-relevant conditions. Due to the low confinement in the L-mode discharges, creating reactor-relevant conditions would require heating powers beyond those available. Thus nearly all experiments have been conducted in enhanced confinement regimes: H-mode, supershot, high-ℓ_i, and, most recently, enhanced reverse-shear discharges.

1. H mode

Since the discovery on the ASDEX diverted tokamak of an enhanced confinement regime known as the H mode (for its high confinement time) by Wagner *et al.* (1982), a great deal of research has been conducted on the physics of this regime (ASDEX Team, 1989). In it a transport barrier (i.e., a thermally insulating layer) is established at the edge of the plasma, resulting in reduced particle outflux, broader density profiles, and improved global energy confinement time. A further difference between L- and H-mode discharges is that the core transport is reduced in H modes. Furthermore, the global empirical scaling relationships for the energy confinement time for H-mode discharges has an unfavorable scaling with power, implying an unfavorable temperature scaling and a favorable scaling with plasma current. H-mode operation has been extended to limiter discharges, albeit under more restrictive conditions.

Particles that are transported out of the plasma impinge upon plasma facing components, typically the limiter or divertor. Some of the particles are trapped on the surfaces or are neutralized and pumped; however, typically many of the particles either reenter the plasma after striking the plasma facing components or create an efflux of particles from the surface due to heating or physical or chemical sputtering. This "recycling" of particles from the edge is an important parameter in the degree of confinement improvement, with lower recycling yielding improved confinement. Various wall-coating and vessel-conditioning processes, as well as techniques to reduce the neutral influx from the divertors, are used to decrease the edge recycling in the main plasma chamber. On JET, beryllium evaporation was extensively used to coat the walls to decrease recycling and the influx of impurities. Depending upon the density and the heating technique, it is possible to operate in the H mode with $T_i>T_e$; the term hot-ion H mode is commonly used for this operating regime.

The transport barrier in the edge can suddenly collapse momentarily as a result of MHD instabilities called edge-localized modes (ELMs). The transport barrier then can be reestablished (or not, depending upon the plasma parameters). This ELM phenomenon is an important consideration for reactor designs because the heat loss to the divertor plates or limiter is suddenly and significantly increased during the relaxation. Under some conditions it is possible to operate without these relaxation events, and the discharges are called ELM-free. ELM-free discharges have even better energy confinement, though they are transient. The high-performance JET D-T experiments were conducted in ELM-free hot-ion H-mode discharges. The plasma parameters for discharges from the JET Preliminary Tritium experiment, which achieved the highest fusion power and triple product, are shown in Table III, and the density and temperature profiles are shown in Fig. 10. H-mode transitions have also been observed in limiter high-ℓ_i discharges on TFTR and are discussed in Secs. III.B.3 and V.A.

Table III introduces several important parameters that will be used in this paper. The plasma purity is an important consideration for several reasons. Impurities dilute the plasma and reduce the plasma reactivity. Also, radiation from impurity ions in the plasma core can be an energy-loss mechanism, reducing the confinement of the plasma. In the present experiments, this problem has

TABLE III. Summary of JET experimental parameters comparing a high-performance D and D-T discharge from the Preliminary Tritium Experiment (JET Team, 1992).

Parameters	Units	26087	26148
Plasma current (I_p)	MA	3.1	3.1
Toroidal field (B_t)	T	2.8	2.8
NB power (P_b)	MW	14.9	14.3
Central electron density [$(n_e(0)]$	10^{19} m^{-3}	5.1	3.6
Central (D+T) density [$(n_p(0)+n_T(0)]$	10^{19} m^{-3}	4.1	2.4
$Z_{\rm eff}$		1.8	2.4
$T_e(0)$	keV	10.5	9.9
$T_i(0)$	keV	18.6	18.8
Plasma diamagnetic energy ($W_{\rm dia}$)	MJ	11.6	9.1
$dW_{\rm dia}/dt$	MW	6.0	4.7
$\tau_E = W_{\rm dia}/(P_{\rm tot} - dW_{\rm dia}/dt)$	s	1.2	0.9
$[n_D(0)+n_T(0)]T_i(0)\tau_E$	10^{20} m^{-3} keV s	9.0	3.8
$[n_D(0)+n_T(0)]T_i(0)\tau_E^*$	10^{20} m^{-3} keV s	5.4	2.5
Ratio of average T to (D+T) density		0	0.11
Maximum fusion power	MW	0.05	1.7
β_N		2.2	1.7

been alleviated by the choice of materials and wall coatings and by the design of divertor and limiter. Impurity radiation in the edge of the plasma can be beneficial by reducing the heat flux to the divertor or limiter. The parameter $Z_{\rm eff} = \Sigma n_i Z_i^2/n_e$ is used to characterize the plasma purity, though for detailed analysis the composition of the ion species must be included.

The ratio of the plasma pressure to the toroidal field pressure, $\beta_t = p/(B_t^2/2\mu_0)$, where $\langle p\rangle$ is the volume-averaged plasma kinetic pressure, is cutomarily used to characterize the performance of a magnetic confinement system. The parameter of relevance for fusion yields, which is approximately weighted to take into account the plasma reactivity, is $\beta_t^* = \langle\langle p\rangle\rangle/(B_t^2/2\mu_0)$, where $\langle\langle p\rangle\rangle$ is the root-mean-square pressure, $\langle\langle p\rangle\rangle = [\int p^2 dV/\int dV]^{0.5}$. In a tokamak with typical current profiles, the MHD stability limit was described by Troyon *et al.* (1984) in terms of $\beta_N = \beta_t(\%)a(m)B_t(\mathrm{T})/I_p(\mathrm{MA})$ and the corresponding fusion reactivity weighted parameter is $\beta_N^* = \beta_N\langle\langle p\rangle\rangle/p$.

The plasma stored energy in the experiments summarized in Table III was measured using a diamagnetic loop.

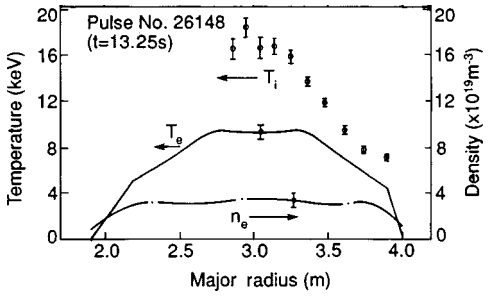

FIG. 10. Radial profiles of the ion and electron temperature and electron density for JET pulse No. 26148 (JET Team, 1992).

The mechanisms responsible for the formation of a transport barrier in the edge region have been reviewed by Burrell (1994), Itoh (1994), Carlstrom (1996), and Ward (1996). The basic model underlying many theories concerning the H mode is that a large radial electric field or electric-field gradient is formed in the edge region, which reduces the amplitude of the turbulent fluctuations or the correlation between the pressure and potential fluctuations. The parameter of importance in many theoretical studies is the shearing rate, which is the rate at which an ordered structure in the turbulence is pulled apart by **E×B** rotation shear. Though a comprehensive model of the H mode has not been established, there is growing agreement on the importance of shear in the radial electric field.

In the core region, the temperature profiles of H-mode plasmas in JET have been successfully simulated by Bateman *et al.* (1997) with the same multimode model that describes L-mode plasmas. In these simulations, the measured edge parameters are used as boundary conditions because this model does not simulate the development of the edge transport barrier. The inference from these simulations is that the underlying transport mechanisms within the core are the same in H- and L-mode discharges. In these simulations, the higher edge temperatures resulting from the transport barrier reduce the core transport because the turbulence is near a condition of marginal stability and attempts to maintain the ion temperature gradient. The reduction in transport in the edge permits the attainment of high confinement times, plasma stored energy, and, consequently, fusion power. This analysis, along with the large experimental literature, indicates the importance of edge conditions in plasma confinement.

Transient changes to the transport barrier in the edge by the occurrence of edge-localized modes provide interesting tests of transport models. Cordey *et al.* (1995)

and Bak *et al.* (1996) analyzed the rapid increase of electron temperature throughout the plasma cross section following the occurrence of an L→H transition and concluded that on JET the transition cannot be explained by a sudden reduction in transport in just the edge region. Much better agreement is obtained by a model in which there is a sudden reduction in transport *everywhere* outside the $q=1$ region after the L→H transition. [The safety factor q is defined as the ratio of the number of toroidal transits of the field line to the number of poloidal transits of the field line. For circular low-β plasmas, $q=rB_t/RB_p(r)$]. Whether the changes in plasma transport results can be adequately described by the models of Bateman *et al.* (1997) or Kotchenreuther *et al.* (1995) is not known. Bak *et al.* (1996) have also shown that there are three phases in JET H-mode discharges with ELMs. During the ELM ($\leqslant$1 ms), the MHD event modifies the electron temperature, not only near the plasma edge, but also far inside the plasma volume. Afterwards, the transport remains large and exceeds the L-mode value for 10–30 ms, and then the transport is reduced to the low H-mode level. Thus, in understanding and interpreting H-mode discharges, it is necessary to know the frequency and amplitude of the ELMs as a result of the complex interplay between MHD instabilities at the edge and core transport. A comprehensive model that covers transport-barrier formation, change in underlying transport, and relaxation of the barriers due to MHD instabilities does not exist. However, major elements of a model are now emerging.

The maximum stored energy in high-performance JET discharges is limited by the occurrence of ''X events.'' The X events involve increased MHD activity, loss of confinement, and influx of impurities which set operational limits on the maximum stored energy. The phenomena responsible for degradation in performance are both complex and varied. The JET Team (presented by Thomas) (1997) identified the importance of, and interaction among, giant ELMs, sawteeth, and outer modes. Sawtooth oscillations are a common MHD instability in tokamak discharges and are characterized by a periodic collapse of the pressure of the plasma core and a redistribution of the particles and energy. The so-called outer modes have been identified as saturated low-m/n external kinks. The kink mode is an ideal MHD instability. It is so named because it leads to a kinking of the magnetic surface and the plasma boundary. The driving force comes from the radial gradient in the plasma current (Bateman, 1978; Freidberg, 1982; Wesson, 1987). The giant ELMs occur when the plasma is calculated to be unstable against kinks and ballooning modes simultaneously. The ballooning modes are another MHD instability caused by large plasma pressure gradients. They are located in the region of destabilizing magnetic-field-line curvature, which in a tokamak is typically in the low-field side. The occurrence of MHD instabilities for a duration short compared with τ_E, and the subsequent degradation of the energy confinement time and fusion performance, is believed to be associated with the modification of edge conditions, due to the onset of MHD instabilities and possible interaction with the plasma facing components. After the initial onset of MHD instabilities, the plasma does not, in general, regain the high-performance condition it had prior to degradation, even if the activity subsides and remains quiescent for a period longer than the energy confinement time. Recently, Wesson and Balet (1996) inferred an abrupt change in the underlying core transport after the occurrence of these instabilities and prior to a significant change in the plasma parameters. Further work is in progress to understand this seemingly irreversible and rapid degradation in confinement in the highest-performance discharges.

2. Supershot

Strachan *et al.* (1987) demonstrated that by extensively conditioning the limiters to decrease the influx of deuterium and carbon, one can obtain enhanced confinement limiter discharges. These enhanced confinement discharges are characterized by peaked density profiles, hot-ion regimes characterized by $T_i(0)/T_e(0)\sim 2-4$, high edge-ion temperature, and strong-beam particle fueling. These discharges are commonly referred to as supershots and have been extensively studied on TFTR. Recently more effective conditioning techniques involving lithium coating of the limiter have been used to further suppress the influx of deuterium and carbon and extend the range of operation (Mansfield *et al.*, 1995, 1996). Table IV provides a summary of parameters from high-performance deuterium-tritium supershot discharges on TFTR. The density and temperature profiles are shown in Fig. 11 for the discharge with the largest triple product and are contrasted with an L-mode discharge.

In TFTR high-performance supershot discharges, the sawtooth instability is typically stabilized even when the central safety factor $q(0)$ is less than one. Levinton *et al.* (1994) showed that, when the pressure and density profiles are sufficiently peaked compared with the shear in the q profile, stabilization occurs as predicted by a two-fluid MHD model (Zakharov and Rogers, 1992; Zakharov, Rogers, and Migliuolo, 1993; Rogers and Zakharov, 1995).

Core transport in supershot discharges is substantially reduced compared with L-mode discharges. The global parametric confinement scalings which characterize L-mode discharges do not describe the trends in supershot discharges (Bell *et al.*, 1988). In supershots, the confinement time remains approximately constant with both neutral-beam heating power and the plasma current, whereas in L- and H-mode discharges the confinement is observed to decrease with power and increase with current. Regressions on the supershot database, as well as dedicated experiments, reveal a strong adverse dependence of confinement upon the influx rates of carbon and deuterium measured spectroscopically (Strachan, 1994). One consequence of an increased influx of carbon and deuterium is a broadened density profile and reduced depth of penetration by the neutral beam. Park

TABLE IV. Summary of TFTR experimental parameters achieved in high-performance supershot discharges (Hawryluk *et al.*, 1995; McGuire *et al.*, 1996).

Parameters	Units	68522	76778	80539	83546
Plasma current (I_p)	MA	2.0	2.5	2.7	2.3
Toroidal field (B_t)	T	5.0	5.1	5.6	5.5
NB power (P_b)	MW	30.8	33.7	39.6	17.4
Tritium NB power	MW	0	20.0	25.5	17.4
Central electron density [$n_e(0)$]	10^{19} m^{-3}	9.6	8.5	10.2	8.5
Central hydrogenic density $n_{\mathrm{HYD}}(0)=[n_{\mathrm{H}}(0)+n_{\mathrm{D}}(0)+n_{\mathrm{T}}(0)]$	10^{19} m^{-3}	6.8	6.3	6.7	6.6
Z_{eff}		2.6	2.2	2.4	2.0
$\mathrm{T}_e(0)$	keV	11.7	11.5	13	12.0
$\mathrm{T}_i(0)$	keV	29.0	44	36	43
Plasma energy (W_{tot})	MJ	5.4	6.5	6.9	4.9
dW_{tot}/dt	MW	2.1	7.5	0	3.0
$\tau_E=W_{\mathrm{tot}}/(P_{\mathrm{tot}}-dW/dt)$	s	0.19	0.24	0.18	0.34
$n_{\mathrm{HYD}}(0)\mathrm{T}_i(0)\tau_E$	10^{20} m^{-3} keV	3.9	7.1	4.3	9.6
$n_{\mathrm{HYD}}(0)\mathrm{T}_i(0)\tau_E^*$	10^{20} m^{-3} keV	3.6	5.5	4.2	8.0
Ratio of average T to (D+T) density		0	0.5	0.47	0.58
Maximum fusion power	MW	0.065	9.3	10.7	2.8
β_{N}		2.1	2.0	1.8	1.5
β_{N}^*		3.5	3.1	3.0	3.0

(1997) has shown that the energy confinement time is also correlated with central-beam fueling.

Local transport studies of supershots indicate that most of the improvement in confinement is associated with the reduction of ion heat conduction (Scott *et al.*, 1990a, 1990b; Zarnstorff *et al.*, 1989a, 1989b) and ion particle transport (Synakowski *et al.*, 1993). Though in L-mode discharges the ion heat conduction is typically much larger than ion heat convection, in the core of supershots the upper bound for the ratio of Q_i to $\Gamma_i \mathrm{T}_i$, where Q_i is the total ion heat transport and Γ_i is the ion particle flux, is only $\sim$ 3/2 with balanced injection, indicating that conduction is relatively small. In the electron channel, the ratio of Q_e to $\Gamma_e \mathrm{T}_e$ is 2. Perturbation experiments by Kissick *et al.* (1993) also have demonstrated that convective heat transport is dominant in the core of supershots. As noted by Zarnstorff *et al.* (1988a, 1989a), this implies that electron heat transport is not consistent with a strong stochastic particle loss and lends support for the contention that the transport is caused by electrostatic-driven turbulence. The transport studies also indicate a very different scaling of χ_i and χ_ϕ with T_i. Meade *et al.* (1991) and Scott *et al.* (1990b) have observed that χ_i and χ_ϕ decrease with T_i in supershot discharges.

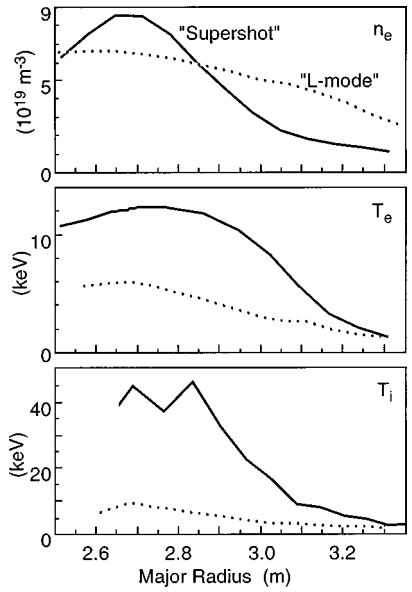

FIG. 11. Radial profiles of the electron density and electron and ion temperature for TFTR pulse No. 83546, a high-performance supershot, contrasted with a comparable L-mode discharge with similar plasma current and heating power.

An analysis by Kotschenreuther *et al.* (1995), using the gyrofluid and gyrokinetic models, indicates that reduction in transport is associated with the suppression of ion-temperature-gradient-driven modes due to large values of T_i to T_e which, at least in part, are made possible by the high edge-ion temperature and peaked density profiles. However, as noted above, this model did not have a comprehensive treatment of the particle dynamics and, in particular, of convective heat transport in the core or the effect of radial electric-field shear stabilization. Thus these results, while suggestive and supportive, are not conclusive. One would qualitatively expect as a general consequence of ion-temperature-gradient models that if the edge temperature were reduced, the ion transport would rapidly increase and that such an edge perturbation would propagate into the plasma. Experiments have been reported by Zarnstorff *et al.* (1990, 1991) and Scott *et al.* (1990b) in which either a helium

gas puff or a deuterium pellet was injected into the plasma. The resulting change in ion temperature and energy confinement did not show evidence for a rapidly propagating wave of enhanced transport, indicating either that the ion profiles were not marginally stable or that the mode was too weak to enforce marginal stability. Theoretical analysis of these experiments by Horton *et al.* (1992) indicates that enforcement of marginal stability should not be expected.

As in the case of H-mode transport-barrier formation, another mechanism that can be important is electric-field shear stabilization of the turbulence. Bush *et al.* (1996) have observed a correlation between Li conditioning and the development of steep ion temperature and toroidal velocity gradients. Ernst *et al.* (1995, 1996) have recently calculated that the reduction in transport in supershot discharges may be due, in part, to the large pressure gradients, which in turn generate gradients in the radial electric field. The experimental observation that optimal global confinement is obtained with slightly co-dominated injection is another suggestion that the radial electric field affects confinement. Though the present theory of electrostatic turbulence provides an overall description of the mechanisms for improved confinement in supershots, key elements in the model require further validation.

At modest auxiliary heating power (20 MW), the duration of supershot discharges in TFTR can exceed ten energy confinement times, and a quasi-steady-state condition can be achieved by operating away from the β limits. In the highest-performance discharges in which the operating boundaries are being challenged, β limits and/or increased influx of carbon and hydrogen from the limiters limit the duration of the high-performance phase.

Two different mechanisms appear to be responsible for the β limit in supershot discharges on TFTR: neoclassical tearing modes and intermediate-n ballooning instabilities coupled to a lower-n kink mode. The onset of tearing modes (Chang *et al.*, 1994, 1995a) is found to degrade the confinement, the plasma stored energy, and the neutron emission in the discharges, but does not typically result in an abrupt termination of the discharge, a "disruption." The tearing instability is driven by the radial gradient in the equilibrium current density. The tearing and reconnection of magnetic field lines which occur during the instability are a consequence of finite resistivity. These modes appear spontaneously and have low frequencies (<50 kHz) and low poloidal and toroidal wave numbers, $m/n=3/2$, 4/3, and 5/4. The 2/1 mode is rarely observed but is particularly detrimental to confinement. The nonlinear evolution of these modes agrees well with the predictions of neoclassical pressure-gradient-driven tearing-mode theory. The predicted evolution of the island width is found to be in reasonable agreement with measurements, as shown in Fig. 12. In the comparison with experiment, the simulation is initialized to the experimentally measured island width, and the constant factor in the neoclassical driving terms is chosen to match the saturated island width. Though

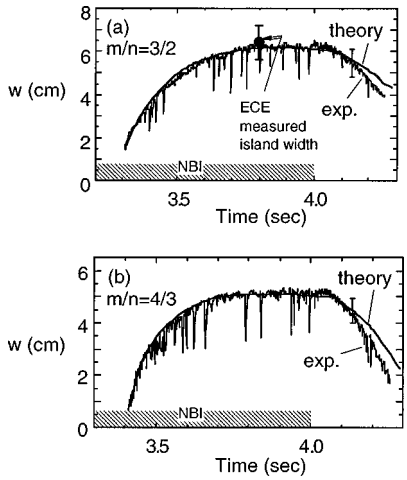

FIG. 12. Comparison of the measured magnetic island evolution with the nonlinear, neoclassical, pressure-driven tearing mode theory for (a) the $m/n=3/2$ mode case and (b) the 4/3 mode case (Chang *et al.*, 1994).

the present theory predicts several important trends in the data, it does not predict a threshold island width and therefore when and which modes should grow.

The degradation in stored energy δW can be quantitatively attributed to the width of saturated magnetic islands, as shown in Fig. 13. In the theoretical simulation of the degradation of the stored energy, the island width is calculated from magnetic-field fluctuation measurements. The theory of Chang *et al.* (1994) assumes that magnetic islands introduce a large transport region in their vicinity. Therefore it is expected and observed that $\delta W/W \propto w/a$, as can be seen in Fig. 13(b). Thus it is

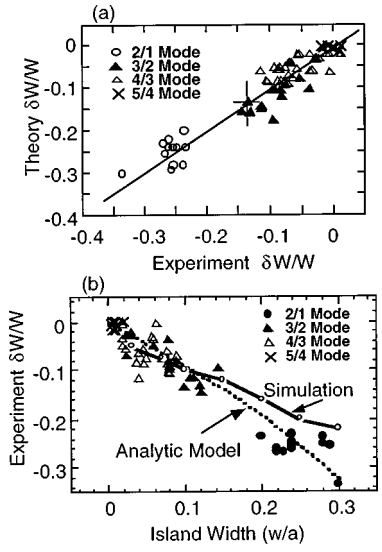

FIG. 13. Stored energy deterioration due to neoclassical tearing modes: (a) Comparison of stored-energy deterioration ($\delta W/W$) theory and experiment due to neoclassical tearing modes; (b) energy deterioration proportional to the island width as predicted by the theory and simulation, in agreement with simple analytic estimates, as well as a time-dependent transport simulation (Chang *et al.*, 1994).

possible to reproduce successfully the confinement degradation and plasma profile evolution due to neoclassical tearing modes (Chang *et al.*, 1994).

In discharges on TFTR with high toroidal field and plasma current, the neoclassical tearing modes do not appear to be a significant limitation. In these discharges, the maximum stored plasma energy is limited by the onset of a rapidly growing intermediate-n ballooning instability ($n=10-20$) coupled to a low-n ideal kink mode (Nagayama *et al.*, 1993; Fredrickson *et al.*, 1995a, 1996). The distortions to the plasma caused by the large low-n ideal mode appear to push the plasma over the ballooning-mode stability boundary. The ballooning-mode precursor to the disruption was studied using two grating polychromators separated toroidally by 126° to measure the electron temperature, as shown in Fig. 14. From these data, it is possible to deduce that the ballooning mode is both toroidally and poloidally localized on the outboard midplane. Park *et al.* (1995), using a three-dimensional nonlinear MHD code, successfully modeled the observed electron temperature fluctuations, as shown in Fig. 15. These simulations indicate that the high-n mode becomes even more localized, producing a strong pressure bulge that destroys the flux surfaces and resulting in a thermal quench. This instability limits the maximum fusion power achieved in supershots on TFTR and can result in a plasma disruption.

Operational experience has developed well-defined guidelines for regimes in which the probability of disruption is small. Mueller *et al.* (1996b) have characterized the operation regime of supershots in terms of the parameter β_N and the density peaking parameter $n_e(0)/\langle n_e\rangle$. The likelihood of disruption increases with increased values of both β_N and $n_e(0)/\langle n_e\rangle$. In TFTR, as a result of aggressive wall conditioning, which enables the limiter to pump (absorb) escaping particles, and strong central-beam fueling, values of $n_e(0)/\langle n_e\rangle$ up to 4.6 have been attained. Since the variation in the temperature profile is much less, $n_e(0)/\langle n_e\rangle$ is a useful indicator of the peaking of the pressure profile. (Another important parameter in the MHD stability is the current profile shape, as will be discussed below.) By restricting the operating range of β_N and $n_e(0)/\langle n_e\rangle$, it is possible to operate with an acceptably low probability of disruption ($\sim 10^{-2}$) for discharges with fusion power at about half of the highest achievable.

In high-power, neutral-beam-heated discharges, the stored energy and neutron flux are observed to decrease with an increase in the influx of hydrogenic and carbon impurities. At the highest power (>30 MW), rapid influxes of carbon sometimes occur. This phenomenon, which has been observed on both JET and TFTR, is called a "carbon bloom." The influx is attributed to overheating in localized regions of the divertor or limiter (Ulrickson *et al.*, 1990). A more common occurrence at lower power is the gradual increase in both deuterium and carbon recycling during neutral-beam injection. Li wall conditioning by means of pellet injection is found to reduce carbon and deuterium recycling significantly and improve confinement (Terry *et al.*, 1991; Strachan *et al.*, 1992, 1994c; Mansfield *et al.*, 1995, 1996). By means of extensive Li pellet conditioning, the energy confinement time has been increased to 340 ms; the highest fusion triple product of $n_{HYD}(0)T_i(0)\tau_E^*=8.0\times10^{20}$ m^{-3} s keV, where n_{HYD} is the sum of hydrogenic ion densities, has been achieved for the condition shown (shot 83546) in Table IV. However, for heating pulse durations significantly greater than τ_E and at high power (>30 MW), the favorable confinement is observed to decrease during the high-power phase. Techniques need to be further developed to extend the duration of the high-power enhanced confinement regime.

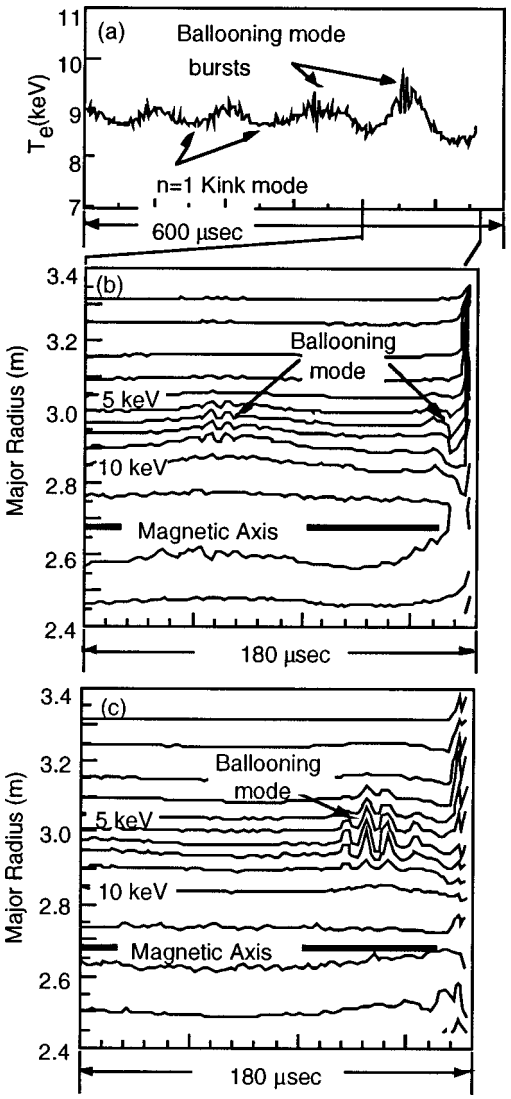

FIG. 14. Growth of a ballooning mode prior to a plasma description. (a) Electron-cyclotron emission measurements of the evolution of the electron temperature prior to a disruption. An $n=1$ kink mode is observed to precede the destabilization of a ballooning mode (Fredrickson *et al.*, 1995a, 1996); (b) Contours of the electron temperature evolution at one toroidal location. The ballooning mode is observed on the outer midplane; (c) Contours of the electron temperature evolution toroidally separated by 126° from the previous set of measurements.

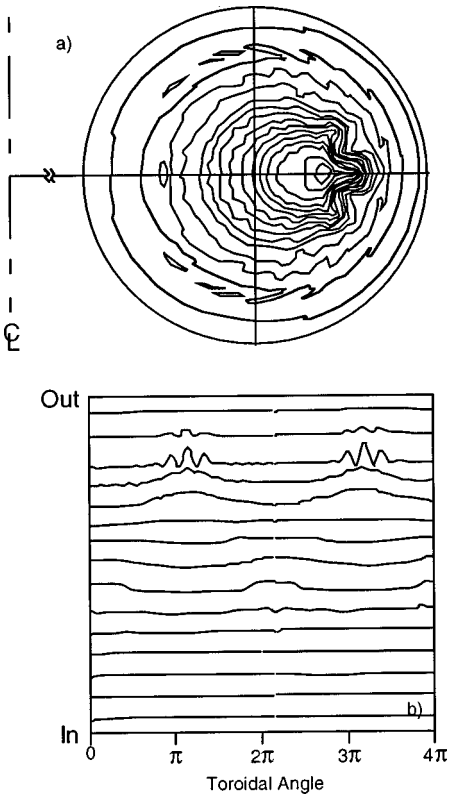

FIG. 15. Modeling of the ballooning mode. (a) Three-dimensional nonlinear simulation of equipressure contours of the MHD instability. (b) Simulations of the electron-cyclotron emission measurements of the electron temperature reproduce the observation of the ballooning mode shown in Fig. 14 being destabilized by a low-n kink mode, with the largest displacement on the outboard side of the plasmas (Park *et al.*, 1995). Since the plasma rotates toroidally, the calculations vs toroidal angle are related to the measurements vs time.

3. High ℓ_i

Since MHD stability at present limits the maximum fusion power attainable in TFTR supershots, current profile modification has been explored to increase the operational parameter range. Two different operating regimes, high ℓ_i and reversed shear, have been studied. In high-ℓ_i discharges, the current profile is peaked, increasing the plasma internal inductance ℓ_i, which for low-β circular plasmas is given by

$$\ell_i = \frac{\int_0^a (B_p^2/2\mu_0) 2\pi r \, dr}{[B_p^2(a)/2\mu_0]\pi a^2}$$

whereas in reverse-shear discharges, the current profile is broader and the value of ℓ_i is decreased.

In the present high-performance plasmas, the discharge duration is less than the current relaxation time. Thus, by varying the time evolution of the plasma current, it is possible to change the current profile within the plasma and experimentally evaluate the effect of the current profile on confinement and stability. On TFTR, two approaches have been used to obtain high-ℓ_i discharges: (1) rapidly decreasing the plasma current or (2) using a novel growth technique to alter the current profile at constant plasma current. When the plasma current is ramped down, the peakedness of the current profile, and thus the plasma internal inductance, is transiently increased. Using this technique, the energy confinement and plasma stability are increased relative to a discharge with a relaxed (broad) current profile at the same total plasma current. This regime of operation on TFTR is called the high-ℓ_i (or high-β_p) regime and has been studied in D (Navratil *et al.*, 1991; Sabbagh *et al.*, 1991; Zarnstorff *et al.*, 1991), and D-T (Sabbagh *et al.*, 1995a, 1995b; 1997) discharges. In recent rampdown experiments, H-mode transitions were frequently observed, permitting the effects of tritium on H-mode physics to be studied.

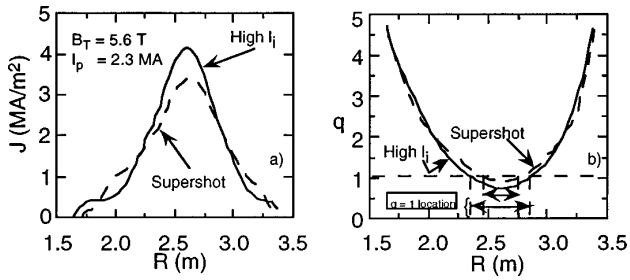

FIG. 16. Motional Stark effect measurements of the $j(r)$ and $q(r)$ profiles in a high-ℓ_i discharge, contrasted with a supershot discharge (Sabbagh *et al.*, 1997).

More recently, another method has been developed to produce high-ℓ_i plasmas at high current (Sabbagh *et al.*, 1997; Fredrickson *et al.*, 1997). The method involves starting the discharge at very low edge q, $q_a \sim 2.5$, by reducing the minor radius, increasing the current to its final level at constant q_a, and then expanding the minor radius rapidly to a near-full-aperture discharge. This is conceptually similar to the technique of expanding the plasma elongation developed on DIII-D, in which the plasma shape is suddenly changed to alter the current profile distribution (Lao *et al.*, 1993). Since the current profile expands relatively slowly after the plasma motion, the internal inductance is transiently higher. Motional Stark-effect measurements of the current profile show that the high-ℓ_i plasmas have an increased core current density and an increased radius of the $q=1$ surface compared with supershot plasmas, as shown in Fig. 16. This technique has the advantage that it is not necessary to achieve currents substantially greater than the final current to attain higher values of the internal inductance.

A summary of parameters for the high-ℓ_i discharge that achieved the highest fusion power is given in Table V. In terms of the normalized parameters β_N and $H \equiv \tau_E / \tau_E^{\text{ITER89-P}}$, these discharges have a much broader range of operating space, as shown in Fig. 17, than supershots. At present, the maximum fusion power produced in the high-ℓ_i regime is 8.7 MW with a stored energy of 6 MJ, which is comparable to that achieved in supershots with similar neutral-beam powers (Sabbagh *et al.*, 1997) but at higher current and field. The maxi-

TABLE V. Summary of TFTR experimental parameters achieved in high-ℓ_i and enhanced reverse-shear discharges by means of current profile modification (McGuire *et al.*, 1996).

Parameters	Units	High ℓ_i 95603	ERS 88170
Plasma current (I_p)	MA	2.0	1.6
Toroidal field (B_t)	T	4.8	4.6
NB power (P_b)	MW	35.5	28.1
Central electron density [$n_e(0)$]	10^{19} m^{-3}	6.9	9.0
Central hydrogenic density $[n_H(0)+n_D(0)+n_T(0)]$	10^{19} m^{-3}	6.0	7.0
Z_{eff}		1.6	2.1
$T_e(0)$	keV	8.0	8.0
$T_i(0)$	keV	45	25
Plasma energy (W_{tot})	MJ	5.7	3.9
dW_{tot}/dt	MW	11.0	3.0
$\tau_E = W_{tot}/(P_{tot} - dW_{tot}/dt)$	s	0.23	0.15
$n_{HYD}(0)\mathrm{Ti}(0)\tau_E$	10^{20} m^{-3} keV	6.2	2.6
$n_{HYD}(0)\mathrm{Ti}(0)\tau_E^*$	10^{20} m^{-3} keV	4.3	2.4
Ratio of average T to (D-T) density		0.42	0
Maximum fusion	MW	8.7	
β_N		2.4	1.95
β_N^*		3.9	3.7

mum performance in high-ℓ_i discharges was not limited by MHD stability, but by the confinement time and the occurrence of carbon blooms at high heating power. Further development of limiter wall coatings and power handling techniques is required to evaluate the potential of this regime.

4. Reverse shear

Theoretical MHD stability studies (Ozeki *et al.*, 1993; Kessel *et al.*, 1994; Turnbull *et al.*, 1995) predicted that by creating a plasma core with reversed magnetic shear, i.e., $dq/dr<0$ over some region of the profile, it would be possible to increase MHD stability. In addition, experimental work on a number of devices indicated a reduction of core transport that was possibly associated with the formation of regions of reversed shear (Lazarus *et al.*, 1991; 1992; Hugon *et al.*, 1992; Goldston *et al.*, 1994; Hoang *et al.*, 1994; Kamada *et al.*, 1994). These initial experimental observations were further encouraged by the theoretical work of Kessel *et al.* (1994), who predicted that plasma transport could be reduced in discharges with reversed magnetic shear. The recent development of operational techniques to create this magnetic configuration reliably, coupled with new diagnostics for measuring the pitch of the magnetic field on TFTR (Batha *et al.*, 1995b; Levinton *et al.*, 1995), DIII-D (Strait *et al.*, 1995), and JT-60U (Fujita *et al.*, 1997), have resulted in rapid progress and exciting new results. Recent and significant work on the effect of modifying the core current profile has been reported by the DIII-D group (Lazarus *et al.*, 1996, 1997), JT-60U group (Ushigusa *et al.*, 1997), JET Team (1997) presented by Gormezano, TFTR (Levinton *et al.*, 1997; Synakowski *et al.*, 1997a), and Tore Supra group (Equipe Tore Supra, 1997).

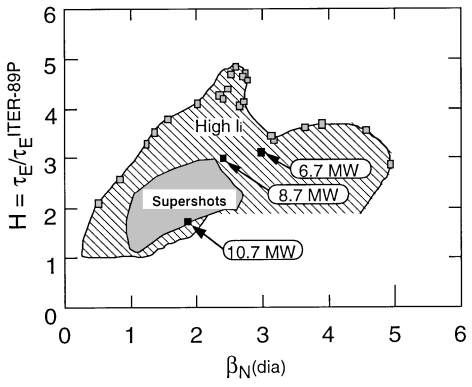

FIG. 17. Operating range of high-ℓ_i discharges in terms of the enhancement in energy confinement time, $H=\tau_E/\tau_E^{TER89\text{-}P}$, and β_N is compared with the operating range of supershot discharges (Sabbagh *et al.*, 1995b, 1996).

To create a reverse magnetic shear configuration, the plasma is typically started at full size and the current is ramped up rapidly. Since the current diffusion time is slower than the rise time of the total plasma current, the current-density profile $j(r)$ is hollow during, and for some time after, the ramp. Low-power auxiliary heating is frequently applied during the current ramp, which raises the electron temperature, decreasing the plasma resistivity and slowing the inward diffusion of current. This prelude heating is followed by the main heating phase of beam injection, as shown for a TFTR discharge in Fig. 18. With variations of beam timing and total current, a range of q profiles has been produced, with $q(0)$ in the range from 2 to 5 and q_{min} from 1.8 to 3, according

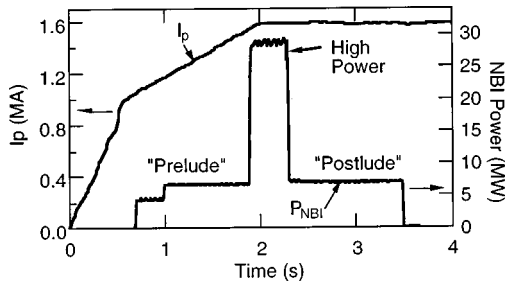

FIG. 18. Hollow current profiles are achieved by rapidly ramping the plasma current and heating the plasma in the "prelude" phase prior to the "high-power" heating phase. Subsequently, the power is decreased in the "postlude" phase to study the evolution of the plasma transport (Levinton *et al.*, 1997).

to motional Stark-effect measurements. This is shown in Fig. 19 (Batha *et al.*, 1995b).

The confinement characteristics of reverse-shear shots on TFTR in the main heating phase resemble those of supershots with the same machine parameters. In particular, the global confinement time is enhanced relative to L-mode scaling, and convection is important in the core power balance. However, above a power threshold (which depends on machine conditioning and the q profile), the core transport changes abruptly at 0.2–0.3 s into the main heating phase within the region of reversed shear. In TFTR discharges, the effect is most clearly seen in the evolution of the central density, which can rise by more than a factor of 2 in 0.3 s as shown in Fig. 20. Since the density outside the reversed-shear region changes little, the density profile following the transition becomes very peaked, reaching values of $n_e(0)/\langle n_e\rangle \sim 5$. This state of improved confinement in the core of reverse-shear plasmas is known as enhanced reverse shear in TFTR. Similar improvements in confinement have been observed in reverse-shear plasmas in DIII-D, JET, JT-60U, and Tore-Supra.

At the transition, the inferred electron particle diffusivity in the region of the steepest gradient drops by a

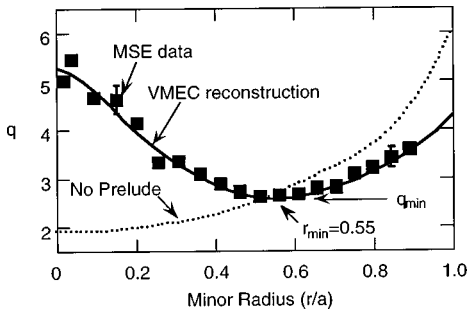

FIG. 19. Motional Stark-effect measurements of the safety factor q, which illustrate the effect of applying heating power during the "prelude" phase. The magnetic equilibrium reconstruction analysis is shown for comparison. The normalized minor radius of the minimum of the safety factor is denoted $r_{\min}$, and the corresponding value of the safety factor is denoted $q_{\min}$ (Levinton *et al.*, 1996).

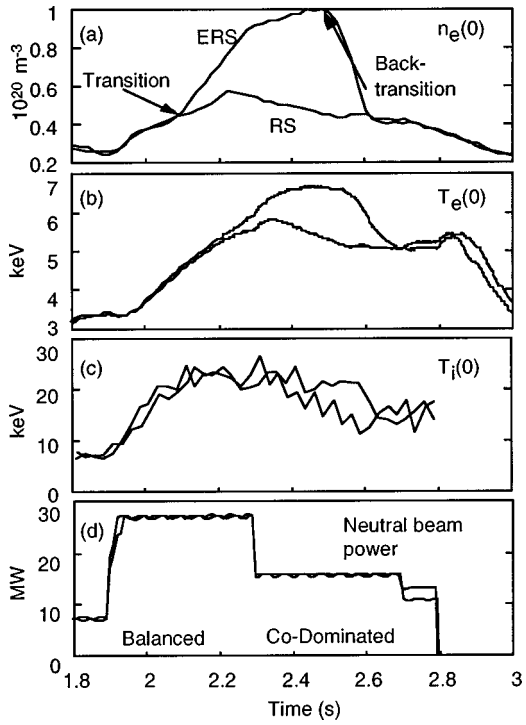

FIG. 20. Comparison of the evolution of two reverse-shear discharges near the threshold power for a transition: (a) central electron density; (b) central electron temperature; (c) central ion temperature; (d) total neutral-beam power waveform. In the enhanced reverse-shear discharge, the development of an internal transport barrier and reduced core transport result in a large increase in the central density and core pressure. In this enhanced reverse-shear plasma, the loss of good core confinement in the 14-MW "postlude" period of injection is correlated with a reduction in the $\mathbf{E}\times\mathbf{B}$ shearing rate γ_s, induced by opposing contributions from corotation and plasma pressure. After the back transition, the plasma confinement properties return to those in the reverse-shear discharge without the transport barrier (Synakowski *et al.*, 1997a).

factor of 10–50 to near neoclassical levels, while the ion thermal diffusivity falls to levels well below predictions from conventional neoclassical theory (Levinton *et al.*, 1995), as shown in Fig. 21. Similar improvements in the ion momentum diffusivity have also been observed. The region of steepest pressure gradients and where the transport coefficients drop is where a transport barrier is assumed to form. Relatively small changes are observed in the electron heat conductivity. Similar behavior of the transport coefficients in reverse-shear plasmas is seen on DIII-D as well, but both JT-60U (Fujita *et al.*, 1997) and Tore Supra (Hoang *et al.*, 1994) have reported significant decreases in χ_e, and DIII-D in rf-heated plasmas (Forest *et al.*, 1996). Possible explanations for the apparent sub-neoclassical ion thermal diffusivity are the violation of the assumptions of standard neoclassical theory, the presence of anomalous electron-ion coupling, or a thermal pinch. Recent calculations by Lin *et al.* (1997) indicate that a more comprehensive analysis of neoclassical transport, which considers orbit dimensions comparable with pressure scale lengths, is in better

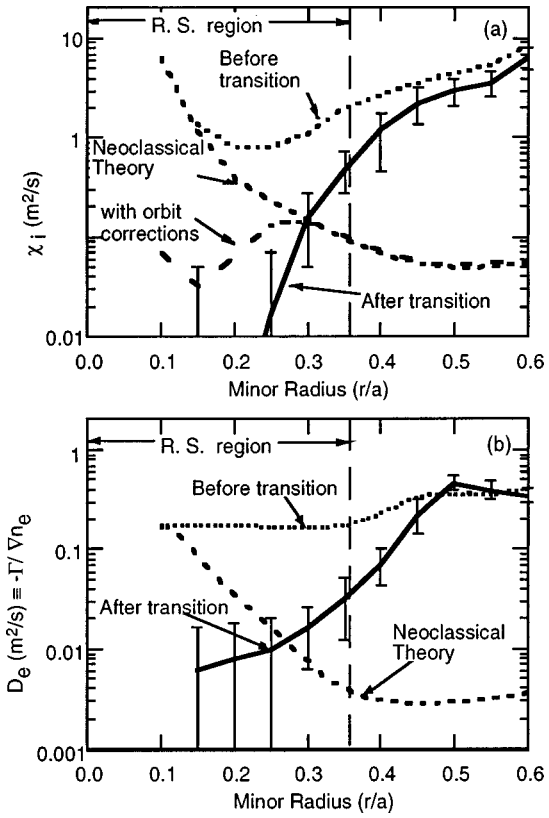

FIG. 21. Enhanced reverse-shear discharges: (a) the inferred ion thermal diffusivity and (b) particle diffusivity are observed to decrease dramatically (Levinton *et al.*, 1995). For comparison, the standard calculation of neoclassical ion heat conductivity is shown, as well as the recent calculations by Lin *et al.* (1997).

agreement with the data in the enhanced confinement regime. Inasmuch as neoclassical transport is usually thought to be the minimum transport possible, these results represent a dramatic improvement in confinement and performance.

Theories developed to explain the formation of transport barriers in H-mode discharges (Biglari, Diamond, and Terry, 1990; Shaing, *et al.*, 1990; Hahm, 1994; Hahm and Burrell, 1995; Burrell, 1997, and references therein) are being investigated in an effort to understand the formation of the transport barrier in enhanced reverse-shear discharges (Hahm *et al.*, 1997; Diamond *et al.*, 1997). In TFTR, the inferred shear in the radial electric field increases in the region of the transport barrier after the transitions. This growth in the shear is driven by the increasing pressure gradient in TFTR discharges, though in experiments with unidirectional beam injection such as DIII-D toroidal velocity gradients appear to be important. A model for enhanced core confinement is being investigated (Diamond *et al.*, 1997). The model's central features are positive feedback between increased pressure gradients, the accompanying growth in electric-field shear, and subsequent turbulence decorrelation and confinement improvement. In addition, gradients in the shift of the center of the magnetic flux surfaces with minor radius (Shafranov shift) of reverse-shear plasmas lead to favorable drift precession of trapped electrons and subsequent reduction of turbulence-induced flows (Beer *et al.*, 1997). Recently, Drake *et al.* (1996) suggested that local negative shear may be important in the formation of a transport barrier, though the particular instability (drift-resistive ballooning modes) is believed to be stable in the core. The enhanced reverse-shear transition has been correlated with the suppression of turbulence by the **E×B** shear flow, that is, when the shearing rate $\gamma_s \equiv |(RB_p/B)d/dr(E_r/RB_p)|$ exceeds the plasma turbulence decorrelation rate, which is estimated to be about the linear growth rate of the turbulence. After the enhanced reverse-shear transition, the fluctuation level in the core is dramatically suppressed according to reflectometer measurements (Mazzucato *et al.*, 1997). Experiments on TFTR indicate that **E×B** shear is necessary to achieve an internal barrier, and that the gradient in the Shafranov shift is not sufficient to maintain the barrier (Levinton *et al.*, 1997; Synakowski *et al.*, 1997a, 1997b). Though the agreement between theory and experiment is promising, further work is required to understand why the present models do not adequately describe the dependence of the power threshold on the toroidal field and neutral-beam-induced rotation. It is also unclear whether the higher power threshold for enhanced reverse-shear discharges in T versus D can be readily reconciled with simple **E×B** mechanisms (Scott *et al.*, 1997). Another topic requiring further investigation is the apparent decoupling of the electron and ion heat diffusivity, suggesting that perhaps more than one mechanism is important in core transport.

MHD stability in enhanced reverse-shear discharges is an active area of investigation due to the potential for increased performance. In the region of reversed shear, MHD activity is absent in enhanced reverse-shear discharges as measured by the four-channel reflectometer, suggesting that, as predicted by theory, reversed-shear plasmas may indeed have greater local MHD stability. The local pressure gradient in flux coordinates in enhanced reversed-shear discharges on TFTR is larger, by a factor of 3–5, than in typical supershots with monotonic q profiles, which very often have low-n MHD modes in the core. However, as the transport barrier moves into the weak- or positive-shear region, and as the radius of the minimum value of $q(r_{\min})$ moves to the core region, a rapidly growing MHD instability is observed. The maximum pressure appears to be limited in this region by the ideal infernal mode. Comparison of the structure of the observed and calculated modes (see Fig. 22) is in good agreement, and the threshold is in reasonable agreement (Hender *et al.*, 1996; Manickam *et al.*, 1997). In at least one case, the infernal mode was coupled to a moderate-n, toroidally localized ballooning mode, similar to what occurs in supershot disruption (Park *et al.*, 1997). MHD behavior in both prelude and postlude phases is even more complex, with the occurrence of double tearing modes, which can also disrupt the plasma (Chang *et al.*, 1996a).

In most of the present experiments, the current and pressure profiles are not actively controlled but evolve

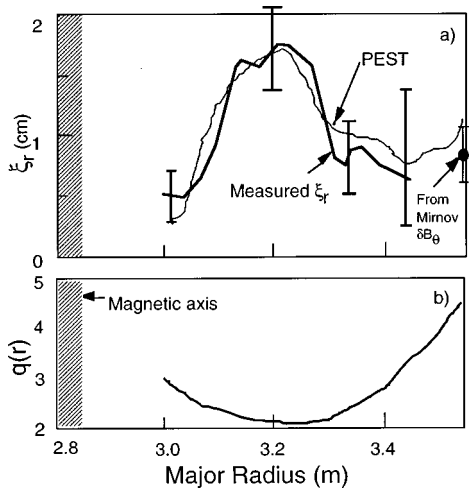

FIG. 22. Simulation of the ideal MHD instability prior to a dissipation in reversed sheer discharges. (a) Electron-cyclotron-emission measurements of the displacement of the magnetic surfaces are in good agreement with the predictions of ideal MHD theory for reverse-shear TFTR discharges (Manickam *et al.*, 1997). (b) The corresponding q profile.

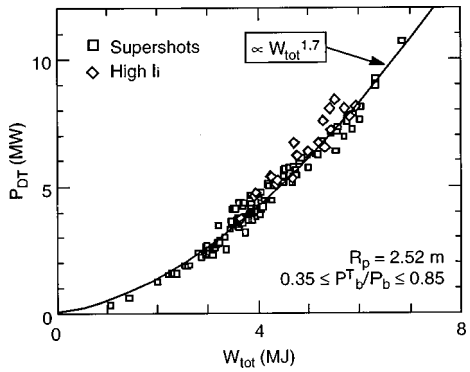

FIG. 23. Dependence of the peak D-T fusion power (averaged over a 40-ms interval) on total plasma energy in high-current ($\geqslant$2.0 MA) supershots [squares] and high-ℓ_i plasmas at 2.0–2.3 MA produced by cross-section expansion of low-q ($q_a \approx 2.5$) discharges [diamonds]. All plasmas have approximately the same volume ($\sim 38\ m^3$) and a nearly optimal mixture of D and T in the reactive region produced by neutral-beam injection. P_b^T is the tritium neutral-beam power injected, and P_b is the total beam power. The ratio has been constrained to correspond to the near-optimal mix for fusion power production (Bell *et al.*, 1997).

toward a resistive equilibrium. The evolution of the current profile is due not only to the formation technique, which creates an initially hollow current profile, but also to the generation of bootstrap currents, which are driven by the strong pressure and density gradients caused by improved confinement. Kikuchi and Azumi (1995) recently reviewed the work on bootstrap currents. Bootstrap currents were first theoretically predicted by Galeev (1970) and Bickerton *et al.* (1971) and experimentally inferred to exist on a tokamak (TFTR) by Zarnstorff *et al.* (1988b), and subsequently on JET (Challis *et al.*, 1989) and JT-60 (Kikuchi *et al.*, 1990). A bootstrap current reduces the auxiliary current-drive requirement and facilitates the development of a steady-state reactor concept. In the present experiments, the radial variation of the bootstrap current generated by the pressure profile is different from the current profile required for MHD stability. New techniques (Craddock and Diamond, 1991; Biglari *et al.*, 1992; Craddock *et al.*, 1994), such as the application of ion Bernstein waves to control the internal transport-barrier location and hence the pressure profile, have been demonstrated on the PBX-M tokamak (Ono, 1993) and are under development to control the evolution of the bootstrap current. In lower-β_p discharges, the bootstrap current is smaller and hence less important. Under these conditions, Ide *et al.* (1996) have demonstrated it is possible to sustain the reversed-shear configuration noninductively by using lower hybrid waves. Extension of this technique to higher-β reversed-shear discharges, in which the evolution of the bootstrap current is substantial, is required to combine improved MHD stability and enhanced confinement. Limited control of the evolution of the current profile on TFTR with the available hardware, combined with the development of large pressure gradients due to transport-barrier formation and evolution, has prevented realization of the potential improvement in fusion power production of reverse-shear operation in TFTR.

IV. FUSION POWER PRODUCTION

Fusion power in TFTR D-T and D discharges increases nonlinearly with the plasma stored energy ($P_{\rm fus} \alpha W_{\rm tot}^{1.7}$), as shown in Fig. 23. This illustrates the motivation for developing enhanced confinement regimes with increased MHD stability to increase the plasma stored energy.

The discharges with the highest fusion power produced are shown in Figs. 24 and 25 for JET and TFTR. In both devices, the decrease in fusion power during the high-power heating phase is triggered by MHD instabilities followed by carbon blooms. In the JET D-T experiments, a sawtooth collapse coupled to an edge-localized mode led to a carbon bloom. In the TFTR high-power discharge shown in Fig. 25, a minor disruption terminated the high-performance phase. The total fusion yield from a single plasma pulse reached 6.5 MJ on TFTR. The fusion power densities achieved at the center of high-performance TFTR supershots, up to $2.8\ MW\ m^{-3}$, are comparable to, or greater than, those expected in ITER. The fusion power density in the JET discharges was $0.08\ MW\ m^{-3}$. The value of $P_{\rm fus}/P_{\rm aux}$ reached 0.12 in JET and 0.27 in TFTR. The fusion power density in the JET discharges was suppressed by the relatively low concentration of tritium compared with deuterium in their initial experiments. The JET Team (1992) has projected that, for the parameters of their D-T discharges, the fusion power would have in-

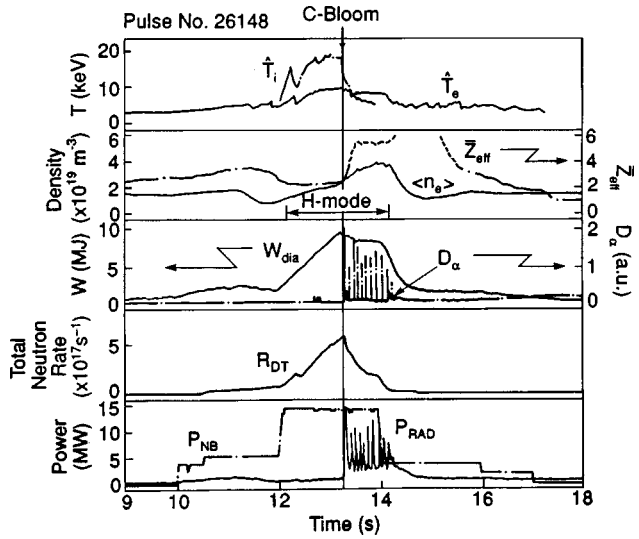

FIG. 24. Time dependence of the central electron and ion temperatures, the volume-averaged electron density, the line average $Z_{\rm eff}$, the plasma diamagnetic energy, the D_α emission, the total neutron rate, and the neutral beam and radiated power for pulse No. 26148 (JET Team, 1992).

creased from 1.7 MW to 4.6 MW with an optimum fuel mix, and the ratio of $P_{\rm fus}/P_{\rm aux}$ would have increased to 0.32.

In the literature, the quantity $Q_{\rm DT}$ which in steady-state discharges is defined as $Q_{\rm DT}=P_{\rm fus}/P_{\rm aux}$, where $P_{\rm aux}=P_\Omega+P_b+P_{\rm rf}$, P_Ω is the ohmic heating power, P_b the neutral-beam heating, and $P_{\rm rf}$ the rf heating power, is often used to describe the fusion performance of plasma discharges. Though $Q_{\rm DT}$ has very limited engineering usefulness *per se*, it is commonly used as a figure of merit to illustrate technical progress. In discharges in which there are significant effects associated with the time variation in stored energy or heating power, several

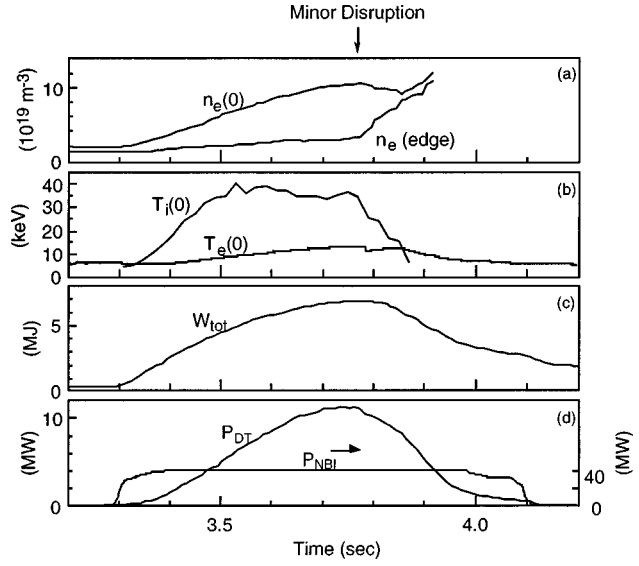

FIG. 25. Evolution of TFTR shot No. 80539: (a) central electron density; (b) ion temperature and electron temperature; (c) stored energy; (d) fusion power.

different definitions of $Q_{\rm DT}$ have been used. The TFTR group adopted the convention that $Q_{\rm DT}=P_{\rm fus}/P_{\rm aux}$ during the high-power phase. This definition provides a simple figure of merit for the performance of high-power discharges relative to the auxiliary heating system, but cannot be extended to transient conditions such as when the heating power is turned off or decreased to a lower value. (An example of such an experiment is the postlude phase shown in Fig. 18). The JET Team (1992) defined it as the sum of separate terms arising from thermal-thermal, Q_{tt}, beam-thermal, Q_{bt}, and beam-beam, Q_{bb}, reactions:

$$Q_{\rm DT}=Q_{tt}+Q_{bt}+Q_{bb},$$

where

$$Q_{tt}=P_{tt}/(P_{\rm loss}-0.2P_{tt}),$$

$$Q_{bt}=P_{bt}/(P_b-P_{st}),$$

$$Q_{bb}=P_{bb}/(P_b-P_{st}).$$

Here P_{tt}, P_{bt}, and P_{bb} are the fusion powers, respectively, from thermal-thermal, beam-thermal, and beam-beam reactions, $P_{\rm loss}=P_b+P_\Omega-P_{st}-dW/dt+P_{\alpha i}+P_{\alpha e}$ where $P_{\alpha i}$ and $P_{\alpha e}$ are the alpha heating power to the ions and electrons, and P_{st} is the neutral-beam "shinethru" power, which is not absorbed by the plasma but impinges on the protective armor beyond the plasma. This definition excludes part of the inefficiency associated with the neutral-beam heating system by ignoring the shinethru power. In hot-ion discharges such as those achieved on TFTR (McGuire *et al.*, 1997) and JT-60U (Ushigusa *et al.*, 1997) and to a lesser extent on JET [the JET Team (presented by Jacquinot) 1997], in which the central ion temperature is approaching 2/3 of the mean energy of the beam-injected ions, the distinction between thermal and beam-thermal reactions is somewhat arbitrary and depends on when a thermalized beam ion is considered part of the thermal distribution. However, under the definition used by JET, the value of $Q_{\rm DT}$ does depend upon this distinction, since the term dW/dt is included in the thermal component. Another issue with this definition of $Q_{\rm DT}$ is that it does not take into account the effect of how the heating power affects the plasma transport. This may be especially important if the high-power phase creates a transport barrier (or reduces transport) which cannot be sustained in the lower-power phase for time durations long compared with the core energy and particle confinement time, as in the "postlude" phase. In the literature, factors of 1.6 can be found due to differences in the definition of $Q_{\rm DT}$.

The usefulness of the parameter $Q_{\rm DT}$ is further complicated because, with the exception of the TFTR and JET experiments, measurements are made in D discharges and then extrapolated to what would occur in D-T. In the literature, the term $Q_{\rm DT}^{\rm Equiv}$ is commonly used for such a projection. The extrapolation is typically performed by using computer codes, though both the JET Team (1992) and Jassby *et al.* (1996) have utilized trace tritium experiments in conjunction with computer modeling to extrapolate to an optimum D-T mix. The ex-

trapolation from D to D-T depends on various assumptions, which are discussed later. Only recently have the codes and assumptions been benchmarked in actual D-T conditions. A more consistent technique for comparing the performance of deuterium discharge is to compare the ratio $P_{\rm fus}/P_{\rm aux}$ with the caveats and limitations described above; however, as with the definition of $Q_{\rm DT}$ there are differences in viewpoint within the community.

Simulations of the neutron production on JET and TFTR have been performed using the TRANSP data analysis code (Hawryluk, 1980; Goldston *et al.*, 1981; Budny, 1994; Budny *et al.*, 1995). This code uses the measured electron-density and temperature profiles, ion temperature profile, and visible bremsstrahlung measurements in conjunction with other diagnostic and engineering data, such as the beam heating power and source divergence, to calculate the neutron source rate from thermal, beam-thermal, and beam-beam reactions. Up to five thermal ion species and one impurity species can be modeled simultaneously in TRANSP. The equilibrium magnetic flux surfaces are calculated by solving the fixed-boundary Grad-Shafranov equation using the total pressure. Monte Carlo techniques (Goldston *et al.*, 1981) are used to compute the deposition of the neutral beams and the distribution of the beam ions and fusion ions, such as alpha particles. The beam ions and fusion products are assumed to slow down classically, though the code has provisions to incorporate the effects of anomalous radial diffusivity and stochastic ripple diffusion, which will be discussed in Sec. VIII.B.2. The ratio of thermal reactions to those from beam-thermal and beam-beam reactions depends upon the density, electron temperature, and beam parameters. The overall agreement for both the time dependence of the D-T neutron emission and the neutron emissivity profile is well described by the TRANSP code, as shown in Figs. 26 and 27 for JET (JET Team, 1992) and TFTR supershot (Budny *et al.*, 1995) discharges, respectively. Typical results are shown in Fig. 28 for TFTR supershot discharges for the neutron emissivity profile, and good agreement is found in the radial profile (Budny *et al.*, 1995). Bell *et al.* (1994) noted, however, that despite the reasonable agreement in D-T discharges, there appears to be a small but consistent difference in the TFTR results for similar D-only plasmas. The TRANSP code predicts the neutron emission in deuterium discharges to be lower than the measured values by approximately 20%. The cause for this relatively small discrepancy is not understood. Though the agreement is good in supershot discharges, detailed comparisons of the predicted neutron emission with experiment remain to be performed for the reverse-shear discharges.

Since experiments on most fusion devices use only deuterium fuel, computer codes such as TRANSP are used to extrapolate from deuterium experiments the fusion power in D-T experiments. In these codes, the expected fusion reactivity enhancement in D-T plasma over their deuterium counterparts can be estimated from the ratio of the velocity-weighted fusion cross sections for DT and DD reactions. For fixed fuel density

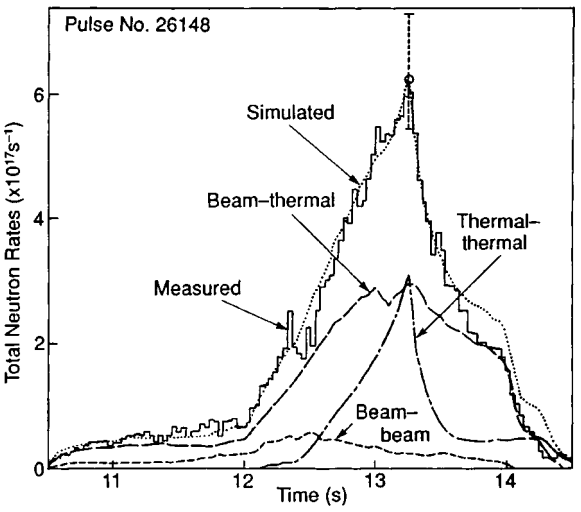

FIG. 26. Neutron source strength measurements and TRANSP simulation of the total neutron rate of JET pulse No. 26148 (JET Team, 1992).

and temperature, the ratio of $P_{\rm DT}$ to $P_{\rm DD}$ from purely thermal reactions reaches an idealized maximum of $\sim$223 for $T_i \sim 12$ keV, but the ratio decreases to $\sim$150 at $T_i = 30$ keV. For discharges in which the reactivity is enhanced due to nonthermal reactions, the ratio of $P_{\rm DT}$ to $P_{\rm DD}$ also decreases for T_i above 15 keV. Experimentally in high-performance supershots on TFTR, the ratio of $P_{\rm DT}$ to $P_{\rm DD}$ is $\sim$115 if plasmas with the same stored energy are compared (Bell *et al.*, 1994; 1997; McGuire *et al.*, 1997). This ratio is especially relevant if the stored energy is constrained by β-limiting disruptions. When one compares plasmas with the same heating power, the stored energy in D-T plasmas is typically higher than that for similar D-only plasmas due to a favorable isotope effect (which is discussed in the next section) and to the increased stored energy from the beam-injected tritons and alpha particles. As a result, the power ratio $P_{\rm DT}/P_{\rm DD}$ is $\sim$ 140 at constant beam power. This value is

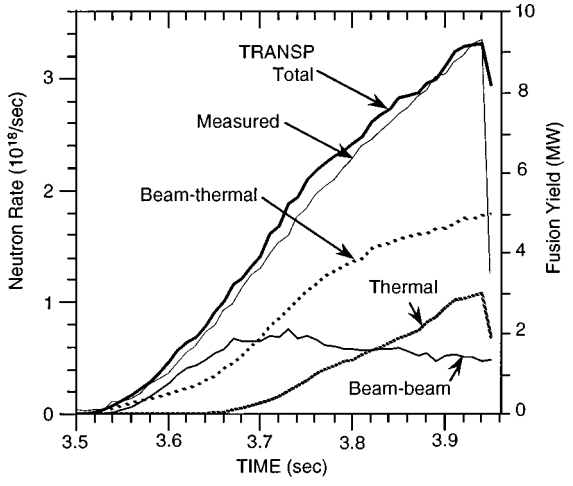

FIG. 27. Neutron source strength measurement and TRANSP simulation of the total neutron rate for TFTR pulse No. 76778 with $P_b = 33.9$ MW (Budny *et al.*, 1995).

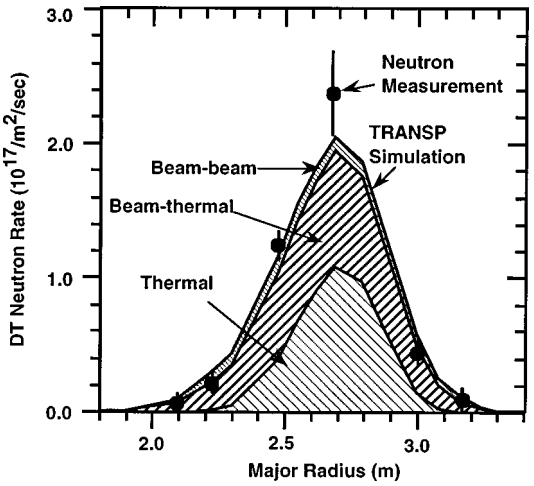

FIG. 28. Neutron emission profile as measured by the neutron collimator, compared with a TRANSP simulation. The contributions from thermal-thermal, beam-thermal, and beam-beam reactions are shown (Budny *et al.*, 1995).

experimentally relevant when, for example, the heat flux to the plasma facing components limits the heating power. On TFTR, it is possible to increase the neutral-beam heating power by operating the beam sources in tritium because of its higher neutralization efficiency. As a result of the increased beam power, the highest fusion power in TFTR D-T discharges is ~165 times greater than in D discharges. This was achieved by increasing the plasma stored energy from 5.6 MJ in the D plasma to 6.9 MJ in the D-T plasma, which required operating at a higher magnetic field and plasma current.

Another practical consideration is that the ratio of n_{D} to n_{T} is determined not only by the ratios of the beam fueling rate, $P_b^{\mathrm{T}}/P_b^{\mathrm{D}}$, but also by the recycling and influx of hydrogenic species from plasma facing components (Bell *et al.*, 1994). A striking result of the TFTR experiments was the low level of tritium recycling at the limiters. Even in hot-ion-mode supershot discharges without supplementary gas injection at the edge of the plasma (gas puffing), wall recycling is an important factor in fueling the plasma. The exchange of hydrogenic species at the limiters and walls is important in determining the mix of deuterium and tritium in the plasma. A Fabry-Perot interferometer was used to measure the Balmer H_α, D_α, and T_α transitions from the plasma edge (Skinner *et al.*, 1995a, 1995b), and Monte Carlo neutral-transport simulation was used to interpret the measured line shapes (Stotler *et al.*, 1996). On a particular day, the T_α fraction was typically undetectable on the first D-T neutral-beam-fueled discharge $[\mathrm{T}_\alpha/(\mathrm{H}_\alpha+\mathrm{D}_\alpha+\mathrm{T}_\alpha) < 2\%]$ and then increased by about 1% per discharge (Skinner *et al.*, 1997a). The maximum was 11% after eight D-T neutral-beam-fueled discharges, indicating that the incident tritium flux is being exchanged with the imbedded deuterium and hydrogenic species in the limiter. Only as a result of extensive gas puffing to fuel the discharge in support of L-mode experiments did the ratio increase to 75% (Skinner *et al.*, 1997b). To compensate for the influx of deuterium from the limiters and walls, the fusion reactivity was optimized in supershot discharges by increasing the tritium beam power (and hence fueling rate) relative to deuterium beam power (Bell *et al.*, 1994).

These practical considerations illustrate some of the issues in projecting from D to D-T operation. In addition, the results depend on the operating density and temperature, as well as the plasma response to changes in isotopic concentration and heating power deposition. For example, since the density in many low recycling conditions such as the supershot regime on TFTR and the hot-ion H-mode on JET is determined largely by beam fueling and wall recycling, it is difficult to optimize the plasma reactivity by independently varying the density because the overall confinement is affected. In principle, such an optimization and projection from one operating point to another is possible, but it requires a detailed understanding of how the underlying transport is affected by changes in the edge conditions associated with the influx of gas to fuel the discharge. As will be discussed in the next section, the confinement changes with isotopic concentration need to be incorporated in the projection. In addition, the tritium neutral beams do not penetrate as well, resulting in slightly broader density profiles. In future long-pulse devices, the accumulation of He ash must also be incorporated into the simulation. The integration of these various issues and operational constraints determines the observed ratio of $P_{\mathrm{DT}}/P_{\mathrm{DD}}$, and differences in assumptions (explicit and implicit) account for the large variation in this parameter in the literature. This discussion also highlights some of the important physics issues of confinement, stability, power handling, and fuel mix associated with projecting the performance of future machines and the need for a detailed characterization and understanding of the underlying physics.

V. CONFINEMENT IN D-T DISCHARGES

Previous experiments on a large number of devices and operating regimes have shown that the confinement in D discharges is different from that in H discharges, as discussed by Bessenrodt-Weberpals *et al.* (1993) and references therein. More recent experiments in the literature have borne this out. The scaling of confinement time with isotopic mass is important, not only for projecting the performance of future devices operating in D-T but also as a test of different transport models. It was immediately apparent in the initial TFTR D-T experiments that the global energy confinement in supershots is significantly better in D-T plasmas than in comparable D plasmas (Hawryluk *et al.*, 1994a). This favorable result was also evident in high-ℓ_i plasmas including those with H-mode transitions. Recent D-T experiments in L-mode plasmas on TFTR have shown that the global and thermal plasma energy confinement scaling is at least as favorable with average ion mass as the $\tau_E \propto \langle A_{HYD} \rangle^{0.5}$ dependence embodied in the ITER-89 L-mode scaling. Most transport theories scale as gyro-Bohm, i.e., $\chi \propto \chi_B \rho^*$, where $\chi_B = cT/eB$, $\rho^* \equiv \rho/a$ and ρ

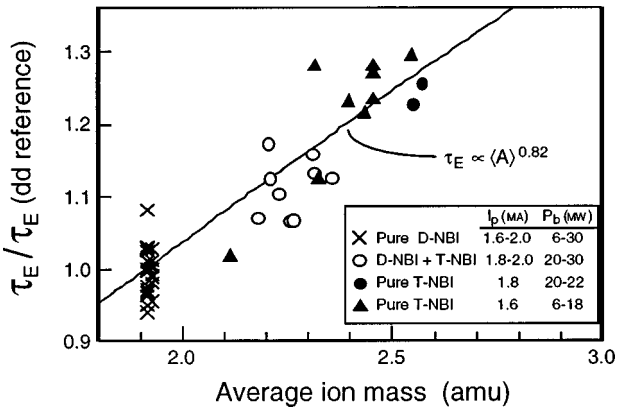

FIG. 29. The ratio of the energy confinement in a D-T discharge compared with that in a companion D discharge vs the average hydrogenic ion mass, $\langle A \rangle = \Sigma n_i A_i / \Sigma n_i$, where n_i is the hydrogenic density (Scott *et al.*, 1995a, 1996b).

is the ion Larmor radius and would predict an unfavorable scaling with ion mass. The favorable dependence of confinement upon ion mass is opposite to the ρ^* scaling predicted theoretically and observed in B-field scans and thus presents fertile ground for benchmarking theoretical models of transport. Due to the low concentration of tritium in the JET experiments, as well as the limited number of shots, no effect in the energy transport could be attributed to the presence of tritium (Balet *et al.*, 1993). The D-T discharges in JET had a higher ion thermal conductivity (poorer confinement) than the D discharge used for comparison but were similar to many other D discharges studied.

A. Isotope effects on energy confinement

The initial D-T experiments in the supershot regime indicated an increase of up to 20% in τ_E between D and 50:50 D-T under identical external conditions (R, B_t, I_p, P_b held constant; Hawryluk *et al.*, 1994a). The increase of global energy confinement time τ_E with average ion mass, including more recent data, is shown in Fig. 29. For higher heating power, 60–80% of the increase in $W_{\rm tot}$ between D and D-T plasmas is due to changes in the thermal plasma. An improvement in thermal energy confinement with ion mass is observed for supershots, limiter H modes, high-ℓ_i, and L-mode plasmas in TFTR.

Ion temperature measurements by charge-exchange recombination spectroscopy show (Fig. 30) that the central ion temperature increased from 30 to 37 keV in going from D to ~50:50 D-T. Since the central electron and ion densities remained approximately constant, $n_i(0)\ T_i(0)\tau_E^*$ increased by about 55% between D and ~50:50 D-T plasmas. In some cases, up to 80% improvement in the triple product was obtained. Detailed profile measurements show (Fig. 31) that the effective ion thermal diffusivity (including conduction and convection) improved throughout the confinement region ($r/a < 0.75$) in a 50:50 D-T plasma relative to a D plasma (Scott *et al.*, 1995a, 1995b).

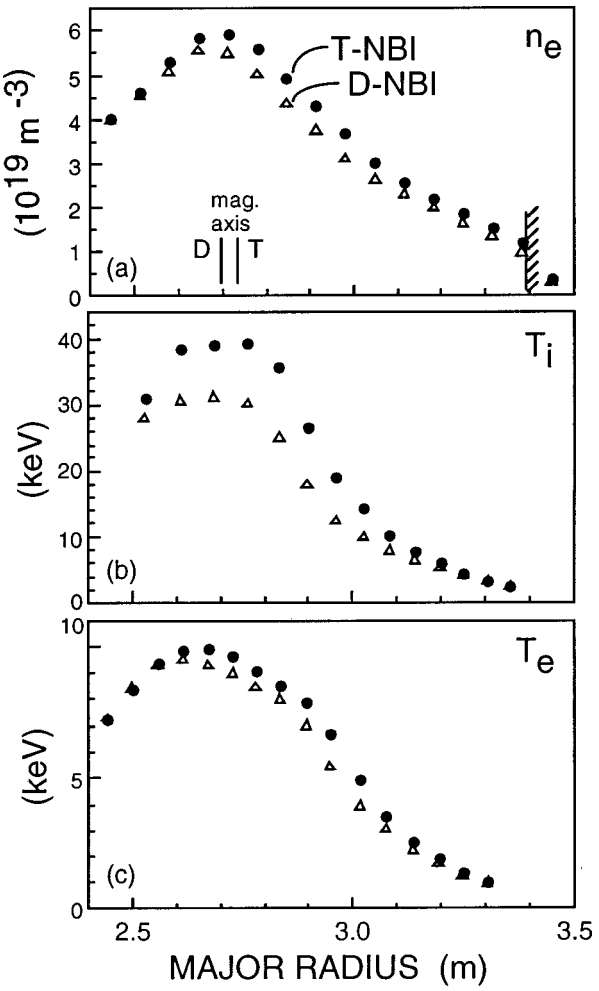

FIG. 30. Comparison of a D and a companion D-T discharge: (a) electron density; (b) ion temperature profiles and electron temperature profiles (Scott *et al.*, 1995b).

The inferred scalings in supershot plasmas with average isotopic mass are quite strong, with $\tau_E \propto \langle A \rangle^{0.82\pm0.06}$, $\tau_E^{\rm thermal} \propto \langle A \rangle^{0.89\pm0.1}$, $\chi_i^{\rm tot} \propto \langle A \rangle^{-2.6\pm0.3}$, $\chi_e^{\rm tot} \propto \langle A \rangle^{-1.2\pm0.4}$, and $D_e \propto \langle A \rangle^{-1.4\pm0.2}$ at fixed P_b. The quoted scaling of χ_e was obtained from electron-cyclotron emission measurements of the electron temperature profile. A significantly weaker dependence ($\chi_e^{\rm tot} \propto \langle A \rangle^{\sim 0}$) is implied by Thomson scattering measurements of the electron temperature. At fixed T_i, $\chi_i^{\rm tot} \propto \langle A \rangle^{-1.8\pm0.2}$ is obtained, so the observed isotopic variation of $\chi_i^{\rm tot}$ cannot be explained by a simple dependence on T_i/T_e or by its previously observed correlation $\chi_i \sim T_i^{-1}$ in the supershot regime. When the isotopic scaling of χ_i is combined with the correlation with T_i^{-1}, this implies roughly $\chi_i \propto A^{-1}\rho_i^{-1}$ (for fixed B) in contrast to the gyro-Bohm dependence (Zarnstorff *et al.*, 1995). In both the supershot (Synakowski *et al.*, 1995b) and L-mode (Scott *et al.*, 1997) regimes, matched density and temperature profiles were obtained with D and D-T plasmas by injection of ~25% less beam power in D-T than in D. The matched pairs thus have the same β and ν^* but different ρ^*, with the larger ρ^* in D-T corresponding to improved confinement, as shown in Fig. 32

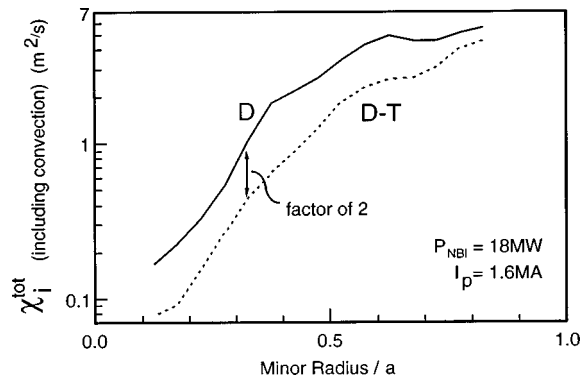

FIG. 31. Comparison of the ion thermal diffusivity in a D-T plasma heated by tritium beams with a companion D discharge. The thermal mix of the background ions is approximately 50:50 D-T (Scott *et al.*, 1995b).

for an L-mode discharge. This trend is opposite to that inferred in ρ^* scans performed with a single isotope by varying the B field.

The energy confinement time in limiter H-mode plasmas on TFTR produced in high-ℓ_i D-T plasmas was significantly greater than in corresponding D plasmas prior to the onset of edge-localized modes, as shown in Fig. 33. In D-T plasmas, energy confinement time >4 relative to the ITER-89P scaling, while corresponding D plasmas had enhancements of ~ 3.2 (Sabbagh *et al.*, 1995a, 1995b; Bush *et al.*, 1994, 1995). The ion heat conductivity was improved across the plasma profile during the D-T H mode, as shown in Fig. 34. The edge-localized modes are much larger and exhibit a lower frequency during the D-T H modes and may suggest that reactor D-T plasmas are more susceptible to giant ELMs than was inferred from D-only experiments. The power threshold for the transition to an H mode is similar in D and D-T TFTR limiter discharges. Due to the limited experimental campaign on JET, isotope scaling in diverted H-mode plasmas has not been established. Further experiments in the divertor JET configuration are planned and necessary to extend the TFTR results.

A number of auxiliary-heating L-mode studies in both small and large tokamaks have demonstrated improved global energy confinement in deuterium versus hydrogen plasmas, typically scaling as $\tau_E \propto \langle A \rangle^{0.3-0.4}$ when neutral beams are used for auxiliary heating. Although some of this improvement can be attributed to purely classical differences in beam stored energy, higher central electron temperatures are consistently observed in the D plasmas, clearly indicating improvement in thermal electron energy confinement. A consensus regarding changes in ion heat and momentum confinement in H versus D L-mode plasmas has not emerged among the various tokamaks. TFTR L-mode experiments in H versus D with $P_b \leqslant 7$ MW (Barnes *et al.*, 1996) observed $\tau_E \propto \langle A \rangle^{0.41\pm0.12}$, $\tau_E^{th} \propto \langle A \rangle^{0.26\pm0.11}$, small increases in $T_e(0)$, and no apparent change in thermal ion heat or momentum transport. Similar experiments in JET H versus D L-mode plasmas obtained results in reasonable agreement with the TFTR experiment, $\tau_E \propto \langle A \rangle^{0.32}$, and $\tau_E^{th} \propto \langle A \rangle^{0.20}$ (Tibone *et al.*, 1993). A fairly weak isotope effect on τ_E was also observed when comparing D and D-T plasmas in TFTR L-mode experiments at low beam power (~ 8 MW). Similar to the experience in D-T supershot plasmas, the isotope effect in the D-T L-mode regime appeared to increase with heating power, and at $P_b = 18$ MW the confinement scaling was somewhat stronger than $\tau_E \propto \langle A \rangle^{0.5}$.

In addition to neutral-beam heating, ICRF hydrogen minority heating in D and D-T L-mode plasmas has been studied (Rogers *et al.*, 1996). The advantage of this technique is that the heating profile does not change. The observed increase in stored energy is consistent with $\tau_E \propto \langle A \rangle^{0.35-0.5}$. In these experiments clear evidence of a favorable scaling of electron heat diffusivity with mass was observed.

The favorable isotope scaling of energy confinement in supershot, H-mode, high-ℓ_i, and L-mode plasmas is a serious constraint to the models used to predict the heat and particle flux and hence the energy confinement time. To resolve this discrepancy, several different effects are being investigated. Scott *et al.* (1997) have shown that the model of shear flow modification to the ion-temperature-gradient turbulence reproduces the observed isotope effect in L-mode plasma. In addition, the role of multi-ion species (D, T, and C) is being invoked as possibly altering the turbulence and giving an apparently favorable scaling with ion mass. This remains an important area of investigation, and the ramifications for the performance of larger devices have not been resolved.

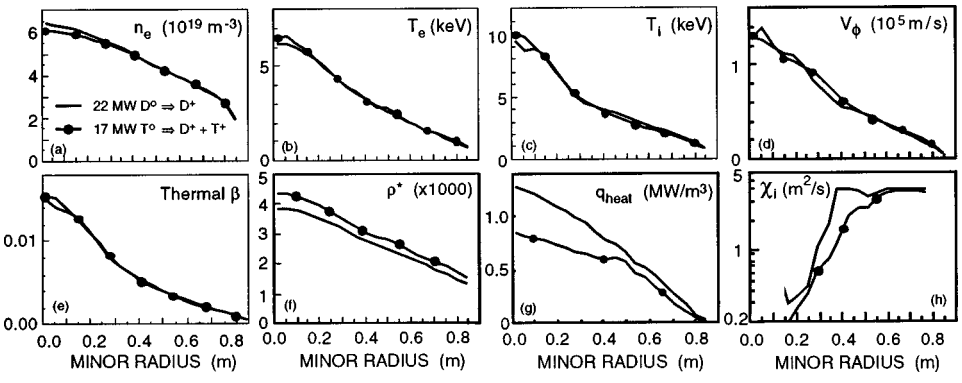

FIG. 32. Kinetic profiles in D and D-T L-mode "isotope ρ^*-scaling" plasmas matched in density, temperature, β, ν^*, B_t, I_p, Z_{eff}, and ν^*_e. Contrary to gyro-Bohm expectations, the D plasma with smaller ρ^* requires $\sim 30\%$ more heating power to sustain the temperature (Scott *et al.*, 1997).

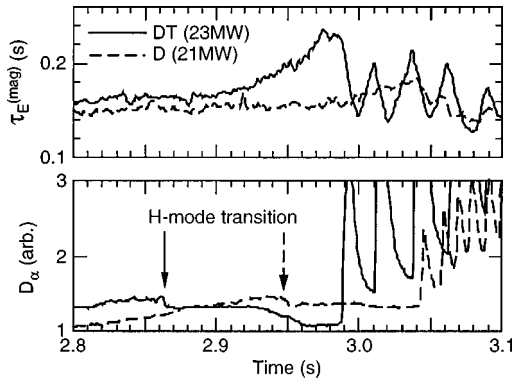

FIG. 33. Evolution of (a) τ_E and (b) D_α (including H_α and T_α) for a D-T discharge and a companion D discharge on TFTR (Bush *et al.*, 1995).

Interestingly, in the TFTR reverse-shear regime, as well as the enhanced reverse shear, there is no isotope scaling with mass (Scott *et al.*, 1997), as shown in Fig. 35. This result is especially surprising in the reversed-shear plasmas, whose temperature and density profiles are similar to those of supershots. Why changes in the current profile should affect the isotope scaling remains to be clarified. In enhanced reverse-shear discharges, the power threshold for the formation of an internal transport barrier was significantly higher in a D-T discharge fueled and heated by tritium neutral beams than it was with a D discharge. Further work is required to assess the implications of this result for the new models of transport-barrier formation.

B. Particle transport

Due to the large differences in the nuclear reaction cross sections between D-D and D-T reactions, tritium transport in a deuterium plasma can be inferred from profile measurements of the 14-MeV neutron source strength using the multichannel neutron collimator (Balet *et al.*, 1993; Johnson *et al.*, 1994). This was proposed by Strachan, Chrien, and Heidbrink (1983) and now provides direct measurements of the transport of the hydrogenic species in a tokamak plasma. Inversion of the neutron source strength provides local measurements of the

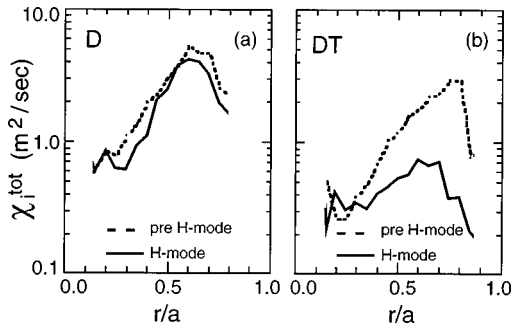

FIG. 34. Comparison of the effect of H-mode transition in (a) D and (b) D-T limiter discharge on TFTR (Bush *et al.*, 1995).

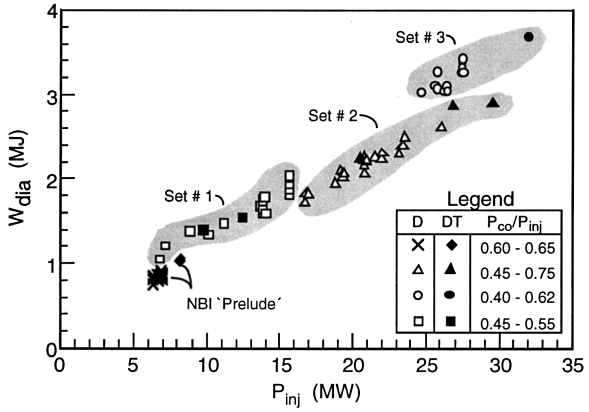

FIG. 35. Stored plasma energy measured by a diamagnetic loop as a function of heating power in reverse-shear plasmas without an enhanced reverse-sheer transport barrier. All shots have $I_p = 1.6$ MA, $B_t = 4.6$ T, $R = 2.59$ m, with identical plasma growth and neutral-beam "prelude" prior to the start of high-power beam heating. For the D-T plasmas, the fraction of beam power in tritium is 100% for the "neutral-beam injection-prelude" discharges, 50–70 % for set 1, 60–100 % for set 2, and 55% for set 3 (Scott *et al.*, 1997).

tritium density, as shown in Fig. 36, following a small gas puff into a supershot discharge on TFTR. Analysis of the evolution of the profile indicates that the trace tritium particle diffusivity in supershot discharges is comparable to the electron diffusivity and to the ion thermal diffusivity, as shown in Fig. 37. The tritium trace-particle convection velocities are found to be small (Efthimion *et al.*, 1995a, 1995b). Similar results were inferred from neutron profile measurements in JET experiments in which the beam was fueled using trace quantities of tritium injected into a deuterium hot-ion mode discharge (Marcus *et al.*, 1993). The evolution of the neutron profile after the turnoff of the beams was simulated using the TRANSP code. Balet *et al.* (1993) concluded that the effective tritium diffusivity is similar to that for deuterium, observed in similar pure-deuterium discharges, and to that for helium, observed during He-beam injection into a deuterium plasma. This approach has been used to exclude various models of particle transport and to place constraints on the models, but it does not determine the diffusivity and convection velocities separately, as can be achieved by gas puffing experiments.

Recently, the transport of tritium has been studied in the steady-state "postlude" phase of enhanced reverse-shear discharges on TFTR. The tritium profile remains hollow for a long time, > 0.15 s, and does not peak on axis. The results are qualitatively different from those in supershot discharges. In comparisons with reverse-shear plasmas with similar q profiles but no transition, the tritium particle diffusivity is nearly one order of magnitude smaller inside the reverse-shear region, while comparable outside the region. In the enhanced reverse-shear case, the diffusivity drops an order of magnitude in going from r/a 0.45 to 0.35, a clear indication of a particle transport barrier. These lower diffusivities within the reverse-shear region are consistent with neoclassical

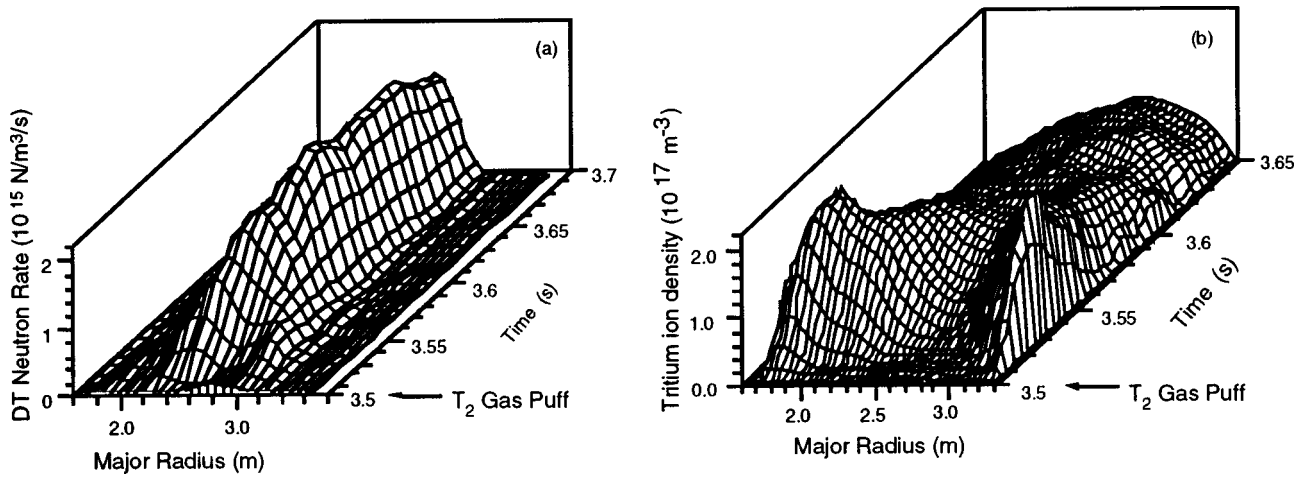

FIG. 36. Aftermath of a small tritium gas puff into a supershot discharge on TFTR: (a) evolution of D-T neutron emissivity; (b) the inferred tritium density profiles (Johnson *et al.*, 1994; Efthimion *et al.*, 1995a).

particle transport predictions for tritium and qualitatively similar to those observed in the study of He transport. He gas puffing studies in the "postlude" phase show a rapid rise in He density up to the barrier and a slow increase within the barrier.

VI. HEATING OF D-T DISCHARGES

Neutral-beam injection is used to heat and fuel JET and TFTR D-T discharges, and rf heating in the ion-cyclotron range of frequencies has been used to heat and drive localized currents on TFTR.

A. Neutral-beam heating

Neutral-beam injection has been extensively studied on a large number of tokamaks and is well understood. By injecting short pulses of high-power D-T beams into TFTR and analyzing the evolution of the neutron profile, Ruskov *et al.* (1995) studied the radial transport of the beam ions in TFTR in a set of 28 D and D-T discharges. Analysis of these discharges (see Fig. 38) indicates that, for 26 of the 28, the radial diffusion coefficient for the fast-beam particles, D_f, is < 0.2 m^2/s, which implies that radial transport for the beam ions is not important. The two exceptions were in discharges with larger major radii, in which the ripple in the toroidal field was greater. Stochastic ripple diffusion, which will be discussed in Sec. VII.B.2, is believed to be responsible for the increased radial transport.

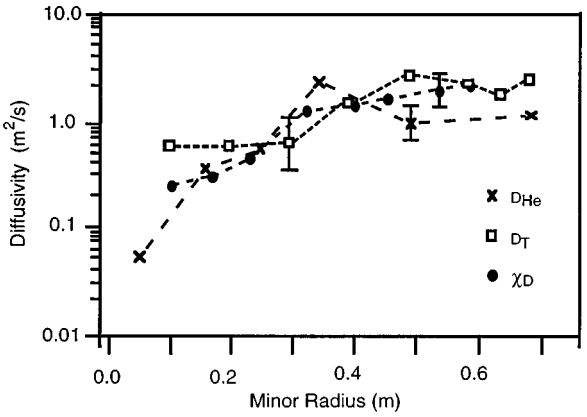

FIG. 37. Tritium particle diffusivity following a small tritium gas puff, compared with the electron particle diffusivity and the He diffusivity (Efthimion *et al.*, 1995a).

B. ICRF heating

ICRF heating and current drive have been studied in D-T plasmas on TFTR. ICRF wave physics in D-T plasmas is complicated by the possibility of multiple, spatially separated resonances and by alpha-particle damping, which can compete with electron absorption in the

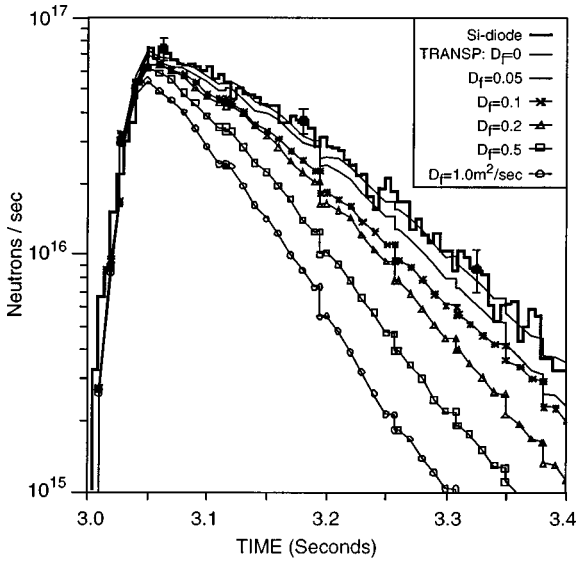

FIG. 38. 14-MeV neutrons as measured by a Si-diode detector caused by a short pulse of high-power neutral-beam injection. The measured neutron source strength is in good agreement with simulations which assume a small radial diffusivity ($D_f < 0.05$ m^2 s) for the beam ions (Ruskov *et al.*, 1995).

fast-wave current-drive regime. A promising scenario for heating D-T plasmas is fast-wave absorption at the second harmonic of the tritium cyclotron frequency, which is degenerate with the ^{3}He fundamental. By selectively heating a majority ion species rather than a minority ion species, one may avoid potential difficulties with ICRF-driven fast-ion excitation of MHD instabilities, such as toroidal Alfvén eigenmodes. In TFTR supershot plasmas, the second-harmonic tritium ($2\Omega_T$) layer is coincident with the magnetic axis at 2.82 m, $B_t = 5.66$ T. Experiments have been performed utilizing combined ICRF heating and neutral-beam injection in D-T plasmas (Taylor *et al.*, 1995, 1996a; Wilson *et al.*, 1995). These experiments have focused on the rf wave coupling and damping physics associated with D-T plasmas. Second-harmonic tritium heating with ~5.5 MW (with a 2% ^{3}He minority) in a plasma with 23.5 MW of neutral-beam injection (60% in T) has resulted in an increase of the ion temperature from 26 to 36 keV, as shown in Fig. 39. The electron temperature increased from 8 to 10.5 keV due to direct electron damping and ^{3}He minority tail heating. Similar results were obtained in discharges in which no ^{3}He was added. Because of significant D (and minimal T) wall recycling, n_T/n_e was only ~25–30% in these plasmas. Despite this relatively low T concentration, as much as 70% of the rf power was absorbed by the ions. In these experiments, the power was modulated and the local heating measured to determine the absorption mechanism. Comparisons with two independent full wave codes, Poloidal Ion Cyclotron Expansion Solution (PICES) and TRANSP, show reasonable agreement with the observed ratio of ion to electron absorption (Fig. 40; Phillips *et al.*, 1995). PICES is a time-independent two-dimensional ICRF wave field and power deposition code similar to the ICRF model in TRANSP. It includes a multiple toroidal wave number spectrum for the launched spectrum, whereas TRANSP retains only the peak value (Jaeger, Batchelor, and Stallings, 1993).

Second-harmonic tritium ICRF heating experiments have also been performed in D-T L-mode plasmas that are not heated by neutral beams. The development of an ion tail has been measured using the pellet charge-exchange diagnostic. A tritium tail temperature of ~350 keV has been obtained and shows localized heating within 0.2 m from the resonance location (Duong *et al.*, 1997a). Despite the initially low single-pass absorption from the low ion temperature, the absorption rate increases substantially with the formation of the tritium tail, thereby demonstrating that second-harmonic tritium heating of an L-mode plasma could be an effective heating technique in the startup phase of ITER. The increase in stored energy is the same as that obtained by injection of neutral beams into comparable plasmas (Rogers *et al.*, 1996).

Majeski *et al.* (1994) have proposed a novel technique using the mode-converted ion Bernstein wave excited at the ion-ion hybrid layer in a multiple-ion-species plasma (such as D-T) for electron heating or for generating localized electron currents. In more conventional ICRF heating schemes, fast magnetosonic waves launched by antennas on the low-field side of the magnetic axis propagate into the core, where absorption by minority and/or majority ions occurs with or without some mode conversion to ion Bernstein waves. In plasmas consisting of a majority ion species plus a low-concentration mi-

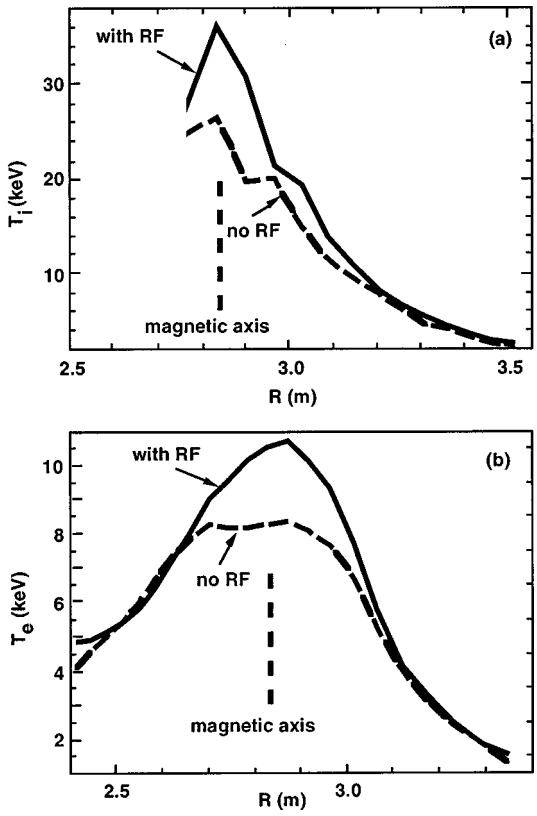

FIG. 39. Ion and electron temperature profiles in a discharge heated with 23.5 MW of neutral-beam heating and in another supplemented by an additional 5.5 MW of ICRF heating (Wilson *et al.*, 1995).

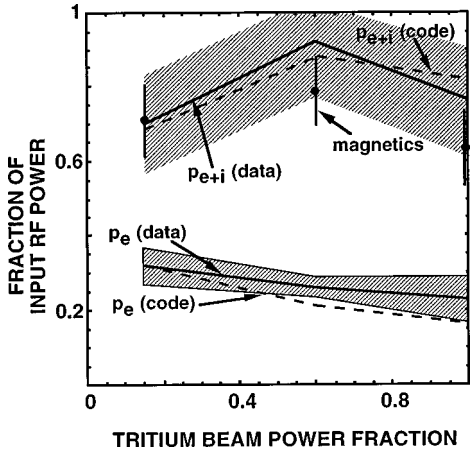

FIG. 40. Measurements and prediction using the PICES and TRANSP codes of the fraction of rf power absorbed by electrons and ions vs the triton-beam power fraction. Modulation of the rf power, together with the evolution of the electron and ion temperature, is used to infer the fraction of power absorbed by ions and electrons (Phillips *et al.*, 1995).

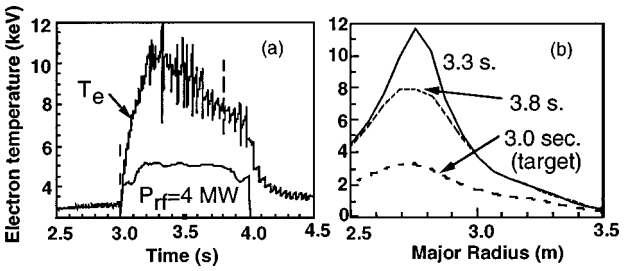

FIG. 41. Mode conversion of the fast-wave results in strong and highly localized electron heating at the ion-ion hybrid layer using (a) time and (b) radius (Majeski *et al.*, 1996).

nority ion species, the rf power absorbed by ions near the cyclotron resonance is enhanced by the presence of the nearby ion-ion hybrid layer. The ion-ion hybrid layer is located approximately where $n_{\|}^2 = S$, where S is the familiar cold-plasma dielectric tensor element and $n_{\|}$ is the parallel component of the wave vector, $k_{\|}$ normalized to the free-space wavelength ω/c, with ω equal to the wave frequency. At sufficiently high minority concentration, the fast wave can be cut off in the narrow region between the cyclotron layer and the hybrid layer, so the incident waves must tunnel through a cutoff region to reach the mode-conversion layer and the high-field side of the discharge. High concentrations of a "minority" ion can be utilized to move the mode-conversion/cutoff region away from the Doppler-broadened ion-cyclotron resonance region so that ion heating is minimized, while mode conversion of the incident fast waves to ion Bernstein waves is maximized. The "minority" species can be D in D-T plasmas, with mode conversion occurring near the D-T ion-ion hybrid layer, or ^{3}He in either D-T-^{3}He or D-^{4}He-^{3}He plasmas, with the mode conversion occurring near the D-^{4}He-^{3}He ion-ion hybrid layer.

For an isolated ion-ion hybrid layer, the maximum mode conversion that can be attained is approximately 25%. However, if the mix of species, plasma density, toroidal magnetic field, and $k_{\|}$ are chosen carefully, then the fast-wave cutoff on the high-toroidal-field side of the

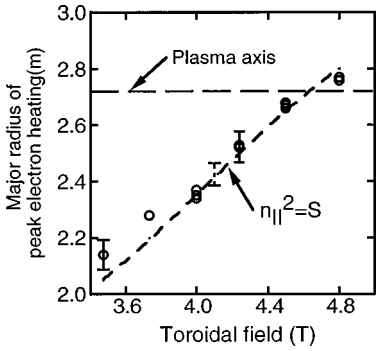

FIG. 42. Observed radius of electron power deposition as a function of toroidal field for constant ^{3}He fraction and density. The open symbols denote the observed location from electron temperature measurement, and the line denotes the location of the mode-conversion layer (Majeski *et al.*, 1996).

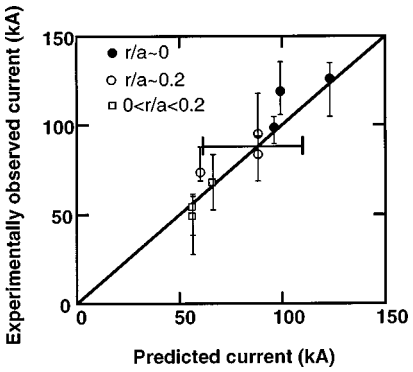

FIG. 43. Measured mode-conversion current drive compared with predicted current drive (Majeski *et al.*, 1996).

plasma (small R), which usually occurs in the low-density edge regions, can be moved into the high-density regions near the mode-conversion/cutoff layers. This leads to a closely spaced "cutoff-resonance-cutoff" triplet. An increase in mode-conversion efficiency by a factor of 4 (i.e., approaching 100%) over the isolated hybrid layer can result from constructive interference effects (Phillips *et al.*, 1995). Experiments on TFTR in D-^{3}He plasmas have demonstrated strong, highly localized electron heating in multiple-ion-species plasmas, as shown in Fig. 41, with greater than 80% of the ICRF power coupled to electrons near the mode-conversion surface achieving temperatures of ~10 keV (Majeski *et al.*, 1995, 1996). The experimentally observed single-pass absorption efficiency for mode-conversion heating can exceed the single-pass absorption for direct fast-wave electron heating by more than an order of magnitude. Efficient heating has been demonstrated at radii over the range $0 < r/a < 0.5$ by changing either the toroidal field or ion-species mix to move the mode-conversion layer, as shown in Fig. 42 (Majeski *et al.*, 1996).

Current drive has been demonstrated as well, using the mode-converted ion Bernstein wave by phasing the antenna. This technique has been used to drive 130 kA of on-axis and off-axis current in a D-^{4}He-^{3}He discharge. The experimentally observed noninductive current (Majeski *et al.*, 1996) is in good agreement with the estimated driven current based on the Ehst and Karney (1991) parametrization, as shown in Fig. 43. The combination of high, single-pass absorption and ability to drive localized off-axis currents may make mode-conversion current drive (MCCD) a potentially attractive current-drive technique.

Recent mode-conversion heating experiments have been performed in D-T plasmas by lowering the source frequency to 30 MHz. The fraction of heating power going to the electrons decreased to less than 30% (Rogers *et al.*, 1996). This low efficiency is believed to be due to competition from ^{7}Li minority heating. ^{7}Li is the most common isotope of Li (92.5% of natural Li) and is used to condition the vessel walls in TFTR. Calculations indicate that a concentration of 0.5% of ^{7}Li would be sufficient to reduce the mode-converted power to the

electrons to the observed level. This could be avoided by using ^{6}Li for wall conditioning or eliminating the use of Li. However, plasma facing components using beryllium would result in a similar problem if the ^{9}Be concentration were more than 0.1% in the plasma. In this case, a suitable alternate isotope does not exist.

VII. ALPHA-PARTICLE CONFINEMENT

The behavior of alpha particles from D-T reactions is a fundamental consideration for the performance of a future D-T reactor. If a significant fraction of the alpha particles is not confined, then the $n\mathrm{T}\tau$ requirements for ignition will increase; however, the confinement of the resultant alpha ash must be sufficiently short to avoid quenching the reaction. Also, if a small unanticipated fraction (a few percent) of the alpha particles is lost in a reactor such as ITER and the resulting heat flux is localized, damage to first-wall components could result. Thus a detailed knowledge of alpha-particle loss processes is vital in designing the plasma facing components to avoid damage by energetic alpha particles. The study of energetic-particle physics in a tokamak is an interesting scientific topic. The alpha transit time in TFTR is $\tau_{\mathrm{trans}} = 2\pi R/V_\alpha \approx 10^{-6}$ s, while the alpha thermalization time ~ 0.3 s with $R = 2.5$ m, $I_P = 2.5$ MA, $\mathrm{T}_e(0) = 10$ keV, and $n_e(0) = 10^{20}$ m^{-3} (Zweben *et al.*, 1997). Since the alpha thermalization time is greater than (or comparable to) the confinement time of the background plasma and much longer than the transit time, it is possible to study the radial confinement of the alpha particles.

In a tokamak, there are two generic classes of particles, those with passing orbits and those with banana orbits that mirror between the high-field portions of the orbit as illustrated in Fig. 44. The loss of alpha particles to the plasma facing components is caused by three generic mechanisms. The first is single-particle effects due to the structure of the confining magnetic field. The main examples of such losses are (a) first-orbit losses, caused by particles born on fat banana orbits which intersect the wall, (b) ripple-trapping losses, in which particles are mirror-trapped between toroidal field coils and drift out of the confinement region, and (c) stochastic toroidal field ripple diffusion, where trapped particles with their banana tips in certain regions can diffuse to the wall because of stochasticity brought on by toroidal field ripple. The second mechanism is alpha-particle interactions with MHD instabilities and radio-frequency waves, and the third is alpha-particle interactions with MHD instabilities that are driven by the presence of alpha particles, which will be discussed in Sec. VIII.

A. Single-particle effects

Since the canonical angular momentum of a collisionless alpha particle is an adiabatic invariant in a toroidally symmetric tokamak, alphas that are confined on their first orbit should remain well confined. Thus the ions are expected to remain within a distance of $\Delta_\alpha \approx q\rho_\alpha (R/a)^{1/2}$ of the field line of their birth, ignoring collisional effects (Furth *et al.*, 1990). For future large machines such as ITER ($q \sim 3$, $R = 8.14$ m, $a = 2.8$ m) the deviation from the birth field line and consequent first-orbit loss should be small with $\Delta_\alpha / a \sim 0.1$. In TFTR, which is both smaller and operates over a large range in plasma current (and hence q), the first-orbit loss can be significant. First-orbit losses can be evaluated by following orbits of individual particles numerically. Monte Carlo techniques are commonly used to calculate orbit trajectories in analysis such as TRANSP, as described in Sec. IV. Recent experiments provide a detailed test of the theoretical models.

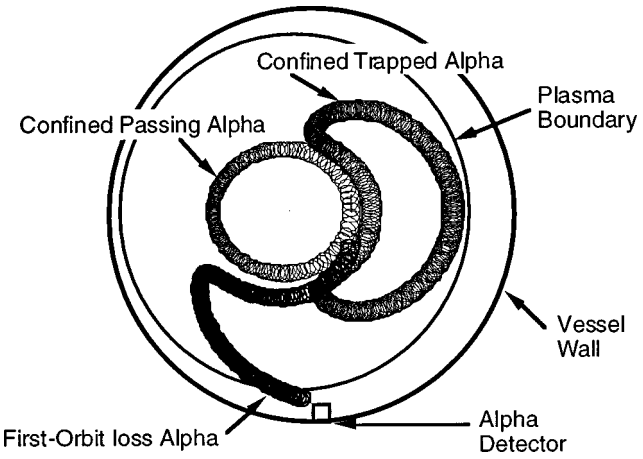

FIG. 44. Illustration of the poloidal projection of confined passing alpha-particle orbits, confined trapped alpha particles on banana orbits, and unconfined trapped alphas.

1. First-orbit loss scaling

An extensive study of fusion product losses in deuterium experiments was conducted on TFTR prior to beginning D-T experiments (Zweben *et al.*, 1990; 1991; 1993a, 1993b; 1994; Boivin *et al.*, 1993). Zweben *et al.* (1995b) summarized the results from the deuterium experiments on TFTR, using the escaping-fusion-product detectors described in Sec. II.B.2:

(a) For MHD-quiescent $R = 2.6$ m plasmas, the loss to the 90° detector was consistent with expected first-orbit loss over the plasma current range $I_p = 0.6 - 2.0$ MA.
(b) An additional anomalous delayed loss was seen at 90° for $R = 2.45$ m plasmas at $I_p = 1.4$–2.5 MA.
(c) During large coherent MHD activity there was an increase up to a factor of 3 in the losses at the 90° and 20° detectors.
(d) The pitch-angle distribution of the loss at 60° and 45° agreed reasonably well with the first-orbit model at $I_p = 1.2$ MA.
(e) There was a large non-first-orbit loss component in the 20° detector, which was consistent with the expected loss due to stochastic toroidal field ripple diffusion.

In the D-T experiments, the alpha flux measured in the 90° detector from quiescent discharges on TFTR is

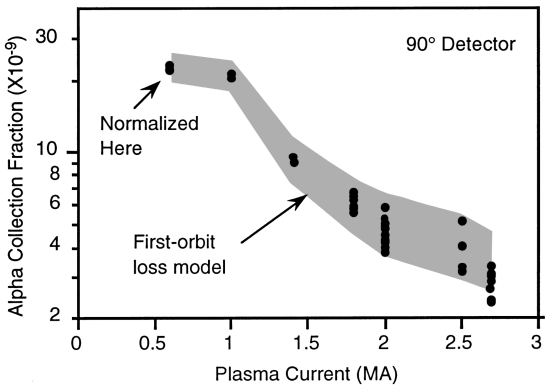

FIG. 45. Fraction of alpha particles collected by a detector located near the bottom of the vessel (90°). The decrease in loss with increasing current is in good agreement with the predictions of the first-orbit loss model. The data is normalized at low currents as indicated (Zweben *et al.*, 1995b).

in good agreement with the first-orbit loss model over the entire range of plasma current, as shown in Fig. 45. Similarly good agreement is found in the pitch-angle variation with current for the 90° detector (Zweben *et al.*, 1995b; Darrow *et al.*, 1996a). Global losses in TFTR are calculated to vary from 3% of the total source rate at $I_p=2.7$ MA to about 50% at $I_p=0.6$ MA. These results set a very low upper limit of $D\leqslant 0.1\ \mathrm{m^2\,s^{-1}}$ for the radial diffusion coefficient of confined passing alphas in the direction counter to the plasma current near the plasma center (Zweben *et al.*, 1997) and are consistent with previous studies of energetic ion transport on many other devices (Heidbrink and Sadler, 1994, and references therein).

In contrast with the deuterium fusion product experiments, no additional delayed loss was observed on the escaping-alpha detector during D-T experiments. Zweben *et al.* (1995b) suggested this might be from the different collisionality of 3.5-MeV alphas and 1-MeV tritons. The tritons from D-D reactions have three times longer slowing-down times, which may make them more susceptible to being scattered into loss orbits either by collisions (pitch-angle scattering) or by MHD effects. Recent foil deposition measurements using an alpha-collector probe by Chong (1995) and Herrmann *et al.* (1997) are in good agreement with the 90° detector measurements at 1.0 MA, but show a significant loss of partially thermalized ions in 1.8-MA plasmas similar to the delayed-loss feature observed in D discharges. The difference between these two measurements has not been fully reconciled; however, the alpha-collector probe indicates that the enhanced loss varies strongly with radial probe position. It is possible that the poloidal limiter in TFTR or other obstacles remove the partially thermalized alpha particles before they strike the scintillator detector. Several possible mechanisms to explain this have been examined by Herrmann *et al.* (1997). One of the more promising is charge-exchange loss, in which the previously confined alpha orbits undergo a transition to prompt-loss orbits as a result of electron capture from H-like carbon impurities. Further work is required to test this hypothesis; however, the observed strong radial dependence does not appear consistent with the large-step-size diffusion that would be associated with this mechanism. Since the mechanism for the delayed loss is not understood, its impact on the design of first-wall components in a reactor cannot be estimated.

2. Stochastic ripple diffusion

Due to the finite number of toroidal field coils ($N=32$ in JET and 20 in TFTR), variation in the magnetic-field strength along a field line is in the range 0.1–1%. Although this ripple is usually too small to cause significant ripple trapping, a more subtle form of "stochastic ripple diffusion" has been predicted by Goldston, White, and Boozer (1981), which can result in rapid energetic-ion loss when the ripple exceeds a threshold γ that is approximately given by

$$\gamma=(r/R\pi \mathrm{N}q)^{3/2}/2\rho q'$$

where q' is the local derivative of the safety factor. The ripple causes radial diffusion of banana orbits whose turning points lie within a certain zone. For alphas in TFTR, that zone is roughly $0.5<r/a<1$. Subsequently, a Hamiltonian coordinate guiding-center code has been developed to simulate the transport of alpha particles in the presence of toroidal field ripple, including collisions and first-orbit loss (Redi *et al.*, 1995a). For TFTR plasmas with $R=2.5$ m, $I_p=2.5$ MA, the calculated stochastic ripple-diffusion loss fraction is $\approx 10\%$ compared with a first-orbit loss of $\sim 3\%$. These guiding-center codes, which take into account the ripple in the toroidal field, are typically relatively time consuming; however, there has been recent progress in developing a more rapid algorithm (White *et al.*, 1996). In the transport interpretative code TRANSP, a simple stochastic domain model for toroidal field ripple loss is used to simulate alpha-particle behavior which has been benchmarked against the more accurate guiding-center model (Redi *et al.*, 1995b). As mentioned above, previous studies of fusion product loss on the 20° detector in TFTR deuterium discharge by Boivin *et al.*, (1993) were at least partially consistent with the predictions of stochastic toroidal field ripple loss.

Measurements of D-T alpha-particle loss near the outer midplane of TFTR are similar to those observed in D discharges (Zweben *et al.*, 1995). Nevertheless, questions remain to be resolved before the midplane measurements can be interpreted by a quantitative model for toroidal field ripple loss of alpha particles (Zweben *et al.*, 1997). One of the main unresolved questions is the role of shadowing effects caused by the outer limiter and the detector itself, which complicates the interpretation of the data and may contribute to the lack of quantitative understanding (Wang and Zweben, 1996).

Recently, sensitive infrared camera measurements on JT-60U have been reported by Ikeda *et al.* (1996). These measurements indicate a localized loss of neutral-beam ions in good agreement with code simulations of the stochastic toroidal field ripple loss. In ICRF discharges on JT-60U, enhanced loss, attributed to stochas-

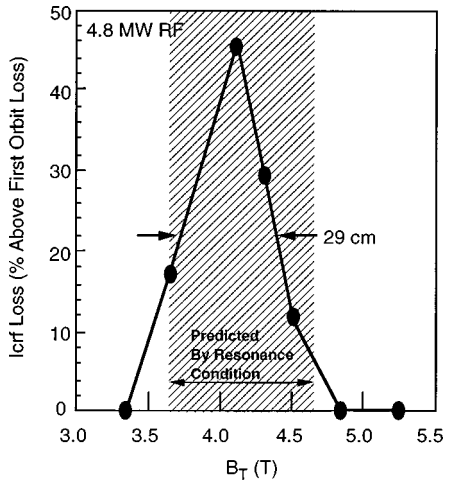

FIG. 46. The increase in alpha loss to the detector at the bottom of the machine resulting from ICRF waves is plotted as a function of toroidal field. The shaded range of toroidal field denotes where marginally passing alpha particles can be in Doppler-shifted resonance with the waves. Loss proceeds by conversion of these marginally passing orbits to lost banana orbits as the alphas are heated.

tic toroidal field ripple diffusion, is also observed; however, a self-consistent simulation of rf heating and orbit trajectories has not been performed.

Tobita *et al.* (1997) studied the confinement of tritium produced by D-D reactions in JT-60U. The subsequent "burnup" of the triton by D-T reactions was measured to evaluate the confinement of tritons in both normal-shear and reversed-shear discharges. The tritons were found not to be so well confined in reversed-shear discharges. The confinement of tritons was well described by Monte Carlo orbit calculations, which include first-orbit and stochastic ripple diffusion as well as collisional ripple loss.

3. Passing-trapped-particle boundary effects due to ICRF

Coupling of the ICRF power to the fusion products has been observed in the TFTR D experiments (Darrow *et al.*, 1996c) and in D-T experiments (Rogers *et al.*, 1994). Figure 46 shows the alpha-particle loss signal from the escaping fast-ion probe at the bottom of the vessel as a function of the toroidal field. The observed gyroradius of the alpha particles ejected during the rf implies energies equal to or slightly greater than the 3.5-MeV birth energy. Radio-frequency heating of the alpha particles increased the perpendicular energy of the alpha particles and caused a fraction of the particles to cross the passing-trapped-particle boundary and go onto loss orbits. When the toroidal magnetic field was below 3.6 T or above 4.5 T no rf-induced losses were seen. The shading in Fig. 46 indicates the range of toroidal field for which marginally passing alpha particles can be in Doppler-shifted resonance with the rf wave, i.e., for which $\Omega_\alpha = \omega - \mathbf{k}_\parallel v_\parallel$. This coincides with the range of fields for which losses are seen, supporting the hypothesis that these losses arise from transforming marginally passing particles to lost banana orbits. Heating of these particles by the rf wave gives them sufficient additional $v_\perp$ that they then mirror on the high-field side of their orbit and are lost. At toroidal fields outside the range shaded, some alpha particles are still being heated but are not being put into loss orbits.

B. Confined alpha particles

The distribution function of the confined alpha particles on TFTR has been measured using pellet charge-exchange diagnostics and charge-exchange recombination measurements, which are described in Sec. II.B.3. The pellet charge-exchange diagnostic obtained data when a boron pellet was fired into a 1.6-MA D-T supershot, 0.2 s after neutral beams were turned off. The measured shape of the energy spectrum of the alphas in the range from 3.5 MeV down to 0.9 MeV is in good agreement with TRANSP-FPPT calculations of the predicted spectrum, as shown in Fig. 47, where the data have been normalized to the TRANSP-FPPT calculations (Fisher *et al.*, 1995; Medley *et al.*, 1995, 1996a; Petrov *et al.*, 1995). The Fokker-Planck Post-TRANSP (FPPT) processor code is based on a numerical solution of the drift-averaged Fokker-Planck equation. The code uses the radial and energy profiles of the pitch-angle-integrated alpha source from TRANSP to calculate the alpha distribution for experimental conditions specific to pellet charge-exchange measurements of the confined alpha particles. The FPPT code is needed to decrease statistical uncertainty in the TRANSP calculations as a result of the limited number of Monte Carlo particles in the appropriate part of phase space corresponding to the pellet charge-exchange measurements. The alpha population in the lower energy range, 0.1–0.6 MeV, has been detected by absolutely calibrated spectrometry of charge-exchange recombination emission (McKee *et al.*, 1995b, 1997). The measured spectrum agrees with TRANSP predictions both in the absolute intensities (within an experimental error of 30%) and the spectral dependence, assuming classical collisional slowing down and neoclassical confinement, as shown in Fig. 48 (McKee *et al.*, 1995b). Measurements of the spatial profile agree with TRANSP and constrain the value of any anomalous radial diffusion coefficient to less than 0.03 m^2 s, in addition to the neoclassical coefficient, which is estimated to be 0.01–0.05 m^2 s.

1. Sawteeth instabilities

The effect of a sawtooth instability on confined alpha particles has been studied on TFTR. As noted before, during the high-performance phase on TFTR, the instability is typically stabilized. Thus the studies of alpha-particle redistribution in TFTR are performed after the neutral-beam heating power is decreased, during which time the density and pressure profile relax and the sawtooth instability reappears. Comparison of pellet charge-exchange measurements in the presence and absence of sawteeth in the period following the D-T heating phase indicate that sawtooth activity transports trapped fast

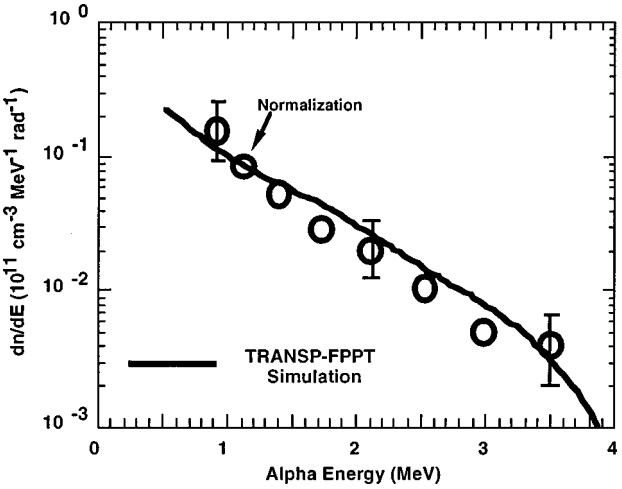

FIG. 47. Measurements of the confined alpha-particle spectrum following neutral-beam heating of a D-T plasma. The TRANSP calculations, which are normalized at one point, are in good agreement with the observed slowing-down spectrum (Fisher *et al.*, 1995; Petrov *et al.*, 1995; Medley *et al.*, 1996a).

alphas radially outward, as shown in Fig. 49 (Petrov *et al.*, 1995, 1997). In these sawtooth cases, no enhanced alpha loss appears on the edge scintillator probes, indicating that redistribution is primarily within the plasma. Gorelenkov *et al.* (1996), Kolesnichenko and Yakovenko (1996), and Zhao and White (1997) have shown that it is necessary to include the helical perturbed perpendicular electric field during a sawtooth crash to understand the rapid radial expulsion of trapped alpha particles and the change in their energy spectrum. The model of Gorelenkov *et al.* (1996) includes the amplitude of the electric field as an adjustable parameter. For reasonable electric-field values, it is in good agreement with pellet charge-exchange measurements of the trapped alpha particles in D-T TFTR plasmas, as shown in Fig. 49. In addition, charge-exchange recombination spectroscopy has been used to measure alpha particles with energies up to 600 keV in a D-T pulse soon after the T-beams have been turned off, but with D-beams remaining on to allow the measurement. As shown in

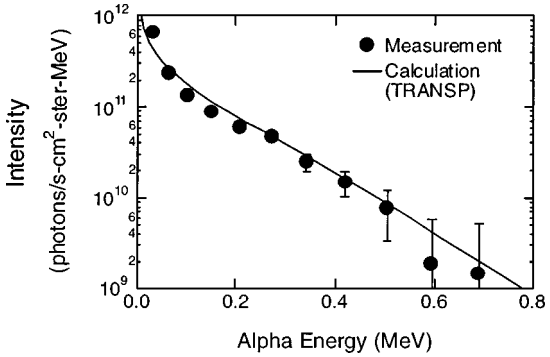

FIG. 48. Measured alpha charge-exchange recombination spectroscopy spectra at $r/a=0.3$ in a nonsawtoothing TFTR D-T supershot vs predictions based on TRANSP calculation of the alpha density (McKee *et al.*, 1995b).

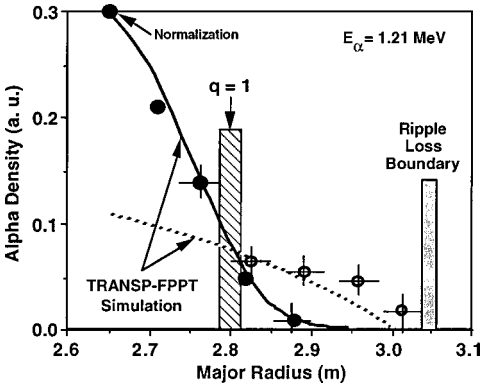

FIG. 49. Pellet charge-exchange measurements of the confined alpha particles prior to (solid points) and after (open points) the sawtooth instability in a companion discharge. The observed redistribution is in reasonable accord with the magnetic reconnection model, which incorporates the effect of the helical electric field. The solid curve corresponds prior to the reconnection and the dashed curve afterwards (Petrov *et al.*, 1996).

Fig. 50, the signal from these intermediate-energy alpha particles is observed to be smaller in a discharge where a sawtooth instability occurred prior to the observation than in one where a sawtooth occurred after the observation period (Stratton *et al.*, 1996). The effect of the sawtooth instability on these lower-energy passing alpha particles has also been modeled and found to be in reasonable agreement with the measurements using the sawtooth model by Kolesnichenko *et al.* (1992), which does not incorporate the helical electric field. For passing alpha particles, the helical electric field would have little effect.

A more internally consistent model of fast-particle redistribution has been developed by Kolesnichenko and Yakovenko (1996) and Zhao and White (1997). A comparison of the data with the model by Kolesnichenko, Lutsenko, and Yakavenko (1996) and Kolesnichenko and Yakovenko (1996) has not as yet been performed. Zhao and White (1997) investigated alpha-particle redistribution during sawtooth crashes by using the Hamiltonian guiding-center model. Once again reasonable agreement with experiment was achieved; however, the simulation corresponding to the trapped alpha particles measured by the pellet charge-exchange analyzer suffered from poor statistics and possibly incorrect treatment of the electric field in the nonlinear stage, indicating the need for perhaps an improved model for sawtooth crashes.

The alpha loss detectors see only a small ($\approx$100 μs) burst of alpha loss at the passing-trapped-particle boundary during a sawtooth crash (Zweben *et al.*, 1997). Thus even in TFTR, the alpha-particle redistribution is predominantly within the plasma. In future large machines such as ITER, the alpha-thermalization time is expected to be less than the time between sawtooth events, enabling the plasma to reheat after a collapse.

2. Stochastic ripple diffusion

The pellet charge-exchange (PCX) diagnostic has also been used to test the predictions of the stochastic ripple-

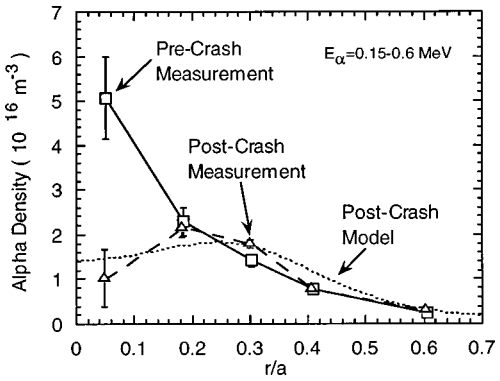

FIG. 50. Alpha charge-exchange recombination spectroscopy measurements of alpha density profiles before and after a sawtooth crash measurements are in good agreement with predictions of the Kolesnichenko *et al.* (1992) sawtooth model (Stratton *et al.*, 1996).

diffusion models, namely, that in certain regions of the plasma the highly trapped alpha particles that PCX measures will be lost. As shown in Fig. 51, PCX results are in reasonable agreement with the energy and q scaling of the simplified Goldston-White-Boozer formalism for the ripple loss threshold (Duong *et al.*, 1997b). Initial modeling of the radial dependence of the alpha-particle density using TRANSP is also in good agreement with PCX data (Redi *et al.*, 1995b). Work is in progress to compare PCX data with the more accurate predictions of orbit-following codes (White *et al.*, 1996) and to extend these studies to reverse-shear discharges.

C. He ash

The production, transport, and removal of helium ash are issues that have a large impact in determining both the size and the cost of a future reactor such as ITER. In previous L-mode and supershot deuterium experiments, helium transport was studied using gas puffing to determine particle diffusivities and convection velocities (Synakowski *et al.*, 1993). These results were compared with transport of trace quantities of tritium in supershot discharges fueled by deuterium (see Sec. V.B). The quantitative results are that the helium and tritium particle confinement times (ignoring recycling) are comparable to the energy confinement time, and that the helium and tritium particle and heat diffusivities are comparable across the profile. The well-conditioned bumper limiter serves as a particle pump in a supershot. The resultant effective helium particle confinement time in previous gas puffing experiments is 5–7 times the energy confinement time, well within the acceptable limits for ITER or for a D-T reactor.

D-T operation provides a unique opportunity to measure alpha ash production and transport. Measurements of radial ash profiles have been made using charge-exchange recombination spectroscopy. Differences between similar D and D-T supershots in the time history and amplitude of the thermal helium spectrum enable the alpha ash profile to be deduced. These measurements have been compared to predictions from the TRANSP code, using transport coefficients for thermal helium from earlier gas puffing experiments in deuterium plasmas and the TRANSP calculation of alpha particle slowing down and transport prior to thermalization. The ash profiles are consistent with the TRANSP modeling, indicating that ash readily transports from the central source region to the plasma edge, as shown in Fig. 52. These results confirm that the thermalization of alpha particles is in agreement with TRANSP modeling. These measurements provide evidence that, even with a central helium-ash source, helium transport from the plasma core will not be a fundamental limiting factor for helium exhaust in a reactor with supershotlike transport (Synakowski *et al.*, 1995a). Further work is required to assess He-ash retention in discharges with internal transport barriers such as the enhanced reverse-shear regime or ELM-free H mode.

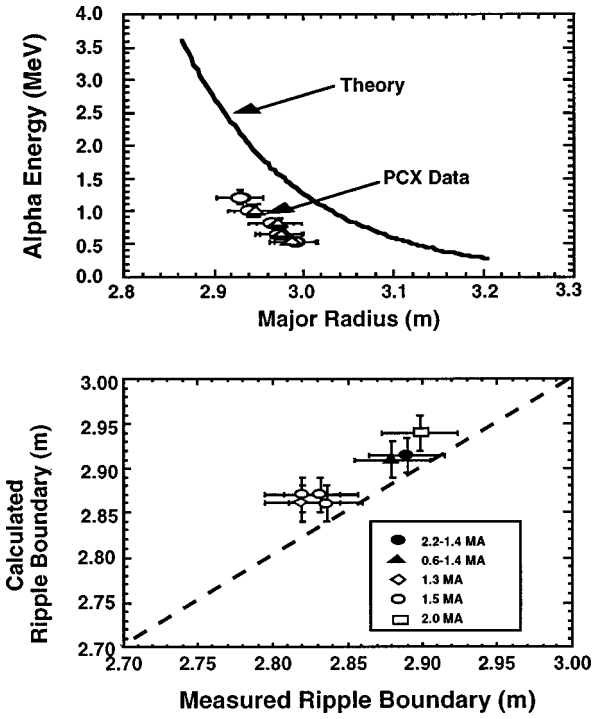

FIG. 51. Ripple boundary for highly trapped alpha particles measured by the pellet charge-exchange diagnostic. The measured boundary is in reasonable accord with a simple estimate of the calculated ripple boundary using the Goldston-White-Boozer formalism (Duong *et al.*, 1997b), in both the observed energy (upper plot) and the q-profile (lower plot) scaling.

D. Interaction with MHD

With the exception of studies of sawtooth instabilities, the above results have been in MHD quiescent discharges. MHD instabilities, as noted earlier, can enhance the transport of the background plasma. Thus the effect of MHD instabilities on alpha particles has been investigated.

1. Disruptions

Both minor and major disruptions produce substantial losses of alpha particles. In major disruptions, losses of

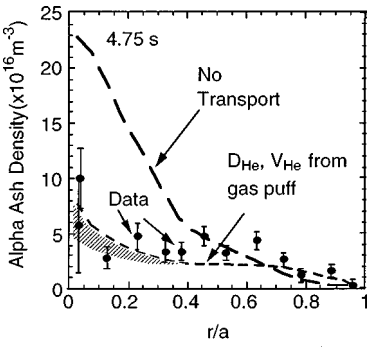

FIG. 52. Measured and modeled ash profile shapes measured 1.95 s after the start of deuterium-tritium beam injection. The errors include uncertainties related to the atomic physics of charge exchange and beam attenuation, as well as photon statistics. The heavy dashed line represents the helium-ash profile shape predicted under the assumption of no radial transport of the thermalized ash. The thinner dashed line represents the predicted profile shape including the effects of radial transport and wall recycling. The shaded region is the difference in the profile shapes that are predicted with and without a central source of thermalizing alpha particles, but with transport in both cases (Synakowski *et al.*, 1995a).

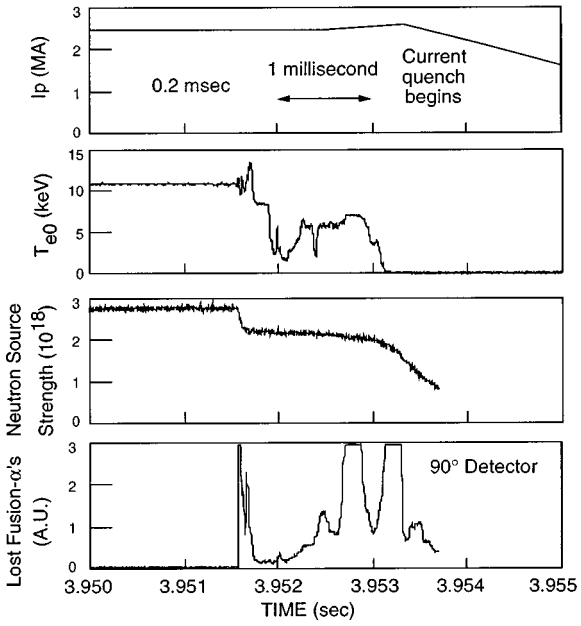

FIG. 53. First burst of alpha particles prior to the detector at 3.9525 s in the bottom of the vessel. This burst precedes the thermal quench of the plasma as measured by the electron temperature diagnostic and is coincident with the MHD activity responsible for the subsequent disruption (Janos *et al.*, 1996).

energetic alphas estimated to be up to 20% of the alpha population have been observed to occur in ~2 ms during the thermal quench phase while the total current is still unperturbed (Janos *et al.*, 1996). The alpha-particle losses are observed to occur prior to the start of the thermal and current quench, as shown in Fig. 53. The start of the alpha losses occurs with the start of the rapid growth of the ballooning mode. Three-dimensional nonlinear MHD simulations predict that the flux surfaces become stochastic from the distortion caused by the ballooning modes. This onset of stochasticity could explain the sudden loss of alpha particles. Such losses, which were observed mainly on the 90° detector and hence localized, could have a serious impact on first-wall components in a reactor. Additional measurements, which view a larger fraction of the first-wall components, are required to assess the degree of localization and reproducibility of the heat flux from alpha particles during disruptions.

2. Low-*m*-*n* modes

In both D and D-T experiments, MHD activity with low toroidal and poloidal mode numbers is observed to increase the loss of fusion products. The alpha-particle loss is sometimes observed to be well correlated with the phase of the modes, as shown in Fig. 54, during the presence of neoclassical tearing modes in a TFTR plasma. Once again, because these modes can persist in the plasma, albeit resulting in a degradation in plasma performance, they can also increase the heat load to first-wall components as a result of localized alpha-particle loss.

3. Kinetic ballooning modes

The first direct evidence of alpha-particle loss induced by an MHD mode was due to a kinetic ballooning mode in TFTR D-T experiments, as shown in Fig. 55 (Chang *et al.*, 1996b). The kinetic ballooning modes are driven by sharp gradients in the plasma pressure profile. These modes are localized near the peak plasma pressure gradient, and the largest amplitude is on the large major radius side of the magnetic axis. In contrast with ideal ballooning modes, which have a small real frequency but large growth rates, the kinetic ballooning mode is predicted to have, due to kinetic effects, $\omega = \omega_i^*/2$ to ω_i^* where ω_i^* is the ion diamagnetic frequency (Tang, Connor, and Hastie, 1980; Biglari and Chen, 1991). These modes are observed on TFTR to often have multiple n (~4–12) numbers, and the frequency in plasma frame is given by $\omega \sim \omega_i^*/2$ (Nazikian *et al.*, 1996). Note that these modes are different from the ideal ballooning modes observed in TFTR before high-β disruptions, which are toroidally localized and have larger radial extents. In general, the kinetic ballooning modes have only a small effect on plasma confinement. Losses induced by these modes are observed in two patterns. One correlates with bursts of multiple n modes with different frequencies, as shown in Fig. 55(a). A factor-of-2-enhancement in lost alpha can be attributed to these modes (Darrow *et al.*, 1996a). Another one is a single bursting ($n=6$) kinetic ballooning mode, shown in Fig. 55(b). It can enhance alpha loss by ~30%. The resonant interaction of the waves with the alpha particles causes increased alpha-particle loss by moving marginally passing alpha par-

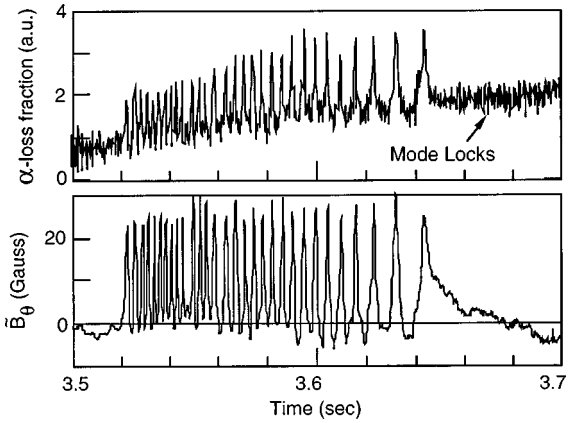

FIG. 54. Alpha-particle loss due to neoclassical tearing modes correlated with fluctuations in the edge magnetic field (McGuire *et al.*, 1997).

ticles into lost banana orbits. This has been simulated using a guiding-center code (Chang *et al.*, 1997). Similar kinetic ballooning modes are observed in D discharges, so the modes are not driven by the alpha particles but by the pressure gradients in the plasma.

E. Overview of alpha-particle confinement

Results from many alpha-particle confinement experiments have been reviewed and summarized in this section. These results will now be discussed in terms of the conventional description of alpha particles typically used in calculating the performance of new devices. In the conventional approach, confinement of alpha particles is described in terms of three mechanisms: neoclassical processes (orbit effects), the transfer of power by Coulomb collisions, and the anomalous transport of the alpha ash from the core. Since the transport of the background plasma is typically more rapid than is predicted by neoclassical theory (see Sec. III and V), it is appropriate to reexamine the recent results with respect to our conventional understanding.

Measurements of confined alpha particles and of loss indicate that in quiescent MHD discharges the radial diffusion coefficient for alpha particles is indeed very small and up to ten times smaller than that of the thermal ions (Zweben *et al.*, 1997). A possible explanation is that "orbit-averaging" effects, which occur when the ion banana width is large compared to the turbulence correlation length, reduce the effect of the underlying background turbulence (Mynick and Duvall, 1989; Myra *et al.*, 1993; Manfredi and Dendy, 1996). The size of the reduction in alpha transport in larger devices may depend on the scaling of the turbulence correlation length with machine size. The good confinement of beam ions in the present machines (Heidbrink and Sadler, 1994), with smaller orbits than those of fusion products, supports the hypothesis that alpha particles should be well confined in larger devices.

As predicted, first-orbit losses are indeed quite small ($\approx 3\%$) at high current in TFTR and should not be important in larger devices. However, the observation

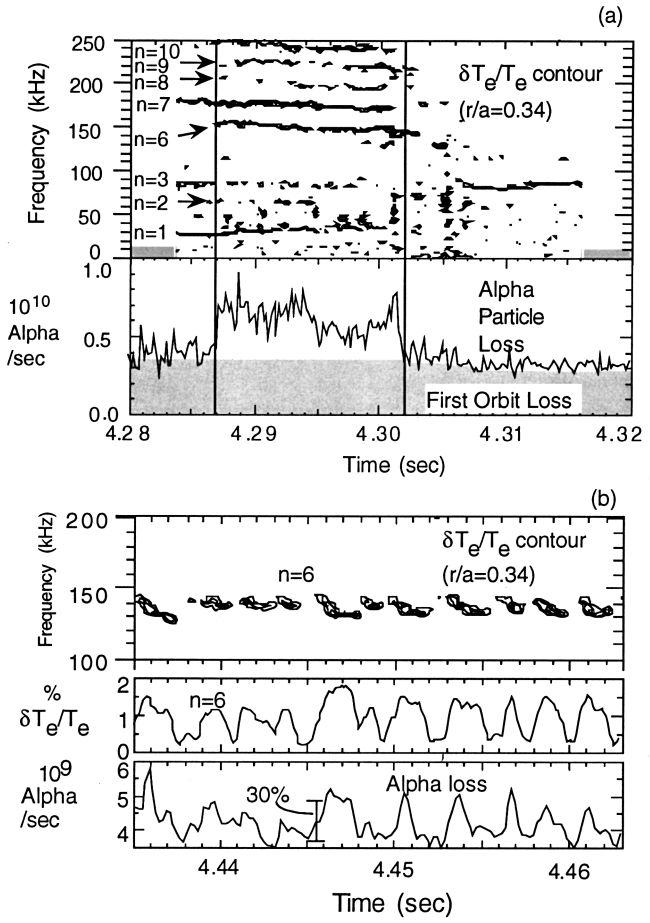

FIG. 55. Alpha-particle loss: (a) correlated with the occurrence of multiple high-n modes; (b) correlated with a single n (=6) mode. Electron-cyclotron emission measurements of electron temperature fluctuations are used to determine the mode frequency and mode number. The corresponding alpha-particle loss is shown. In the absence of fluctuations, the loss corresponds to the first-orbit loss. These modes are identified as kinetic ballooning modes (Chang *et al.*, 1996b).

of partially thermalized alpha-particle loss by Herrmann *et al.* (1997) is not well understood. Measurements of the confined alpha particles, as well as loss measurements indicate the presence of stochastic ripple diffusion, which is predicted to be larger than first-orbit losses. Difficulties in the interpretation of the loss measurements have up til now prevented a quantitative comparison between theory and experiment and highlight the need for further computational improvements to calculate the loss in realistic geometries.

The good agreement between the measured alpha-particle energy spectrum and theory indicates that the transfer of power is well described by Coulomb collisions and orbit effects. These results are also consistent with the observations of beam-ion thermalization on TFTR in D and D-T plasmas as well as in many other devices (Heidbrink and Sadler, 1994). It should be noted that such measurements sample only a small fraction of the alpha distribution function. As will be discussed in

Sec. IX, alpha-particle heating is small in TFTR plasmas and cannot be used to obtain an accurate assessment of the power transferred.

Another confirmation of the conventional model is the He-ash experiment. The modeled helium-ash time evolution indicates that the alpha-particle slowing-down calculations and transport assumptions in supershot discharges are consistent with measurements. Best agreement between the modeling and measurements is obtained using the measured radial particle transport and wall-recycling coefficients for thermal He. When the slowing-down rate is varied by a factor of 2, the data fall within the predicted evolution of the ash density. The time behavior is inconsistent with large anomalous energetic-alpha-particle loss (Synakowski *et al.*, 1995a), but do not exclude the possibility of modest (20–30 %) losses due, for example, to unobserved MHD.

MHD activity is found to affect the confinement of alpha particles. For example, sawteeth can radially redistribute alpha particles. Substantial loss (up to 20%) to the walls occurs during disruptions. Enhanced loss has been observed during the occurrence of neoclassical tearing modes and kinetic ballooning modes. Most of the MHD and rf-induced alpha-particle loss on TFTR occurs at the passing-trapped-particle boundary, at which point alpha particles in the core of TFTR can go into loss orbits. This effect should be smaller in future larger devices such as ITER, with a smaller first-orbit loss region; however, the analogous ripple-loss region could be sensitive to the wave-induced internal diffusion of alpha particles (Zweben *et al.*, 1997).

VIII. COLLECTIVE EFFECTS

The effect of MHD instabilities driven by the background plasma on alpha-particle confinement was discussed in the previous section. Energetic particles such as alphas can also destabilize (or in some cases stabilize) MHD modes. A comprehensive review of this work in H and D discharges is that of Heidbrink and Sadler (1994). This is a potentially important topic because of the coupling between alpha heating and MHD stability in a reactor, as well as the loss of alpha particles to first-wall components caused by induced collective instabilities. Below, the effect of alpha particles on the stability of toroidal Alfvén eigenmodes and Alfvén cyclotron instabilities (also called magnetoacoustic cyclotron instabilities) will be discussed. The alpha parameters achieved in the present experiments on JET and TFTR are summarized in Table VI.

TABLE VI. Alpha-particle parameters for JET and TFTR (Balet *et al.*, 1993 and Budny *et al.*, 1995, respectively).

	JET	TFTR	
	26148	76778	80539
$n_\alpha(0)/n_e(0)$	4.8×10^{-4}	1.5×10^{-3}	1.5×10^{-3}
$\beta_\alpha(0)$	8.0×10^{-4}	2.1×10^{-3}	2.7×10^{-3}
$V_\alpha/V_A(0)$	1.84	1.66	1.70

A. Toroidal Alfvén eigenmodes

Toroidal Alfvén eigenmodes have been shown to exist with discrete frequencies located inside the shear Alfvén continuum gaps created by toroidal coupling of different poloidal harmonics (Cheng, Chen, and Chance, 1985; Cheng and Chance, 1986). These modes were predicted to be driven unstable by energetic particles through wave-particle resonances by tapping the free energy associated with an energetic alpha pressure gradient (Cheng *et al.*, 1989; Fu and Van Dam, 1989; Cheng, 1991). Since this initial theoretical work, a large theoretical literature has developed which includes additional important effects, both in the analysis of instability criteria and in nonlinear saturation mechanisms. Experiments on TFTR (Wong *et al.*, 1991, 1992; Durst *et al.*, 1992; Wilson *et al.*, 1993; Fredrickson, 1995b; Wong *et al.*, 1997), JET [Fasoli *et al.*, 1995a, 1995b, 1996; JET Team (presented by Start), 1997], JT-60U (Saigusa *et al.*, 1995), and DIII-D (Heidbrink *et al.*, 1991; Strait *et al.*, 1993) have shown that the toroidal Alfvén eigenmode could be destabilized by the energetic-ion populations created either by neutral-beam injection or ICRF heating. These instabilities, as shown in Fig. 56, can be sufficiently strong to eject a large fraction of the fast particles (Darrow *et al.*, 1997) and damage first-wall components (White *et al.*, 1995a).

The initial D-T experiments on TFTR in supershot and L-mode discharges, however, showed no signs of alpha-driven instability in the toroidal Alfvén eigenmode frequency range, and the alpha-particle loss rate remained a constant fraction of the alpha production rate as the alpha pressure increased, suggesting that deleterious collective alpha instabilities were not being excited (Batha *et al.*, 1995a; Chang *et al.*, 1995b; Zweben *et al.*, 1996). Theory has since shown that, although TFTR achieves levels of alpha-particle driving terms nearly comparable to those of a reactor, the damping of the mode in TFTR is generally stronger than the alpha-particle drive (Cheng *et al.*, 1995; Fu *et al.*, 1995). Two approaches have been successfully used to study the role of alpha particles in exciting the toroidal Alfvén eigenmodes. The first was to destabilize the plasmas using ICRF heated minority ions, and the second was to alter the magnetic configuration to decrease the threshold requirements. Experiments with ICRF heating of minority ions have found that the rf power threshold for the toroidal Alfvén eigenmode instability is 20% lower in D-T plasmas than in similar D shots, as shown in Fig. 57 (Wong *et al.*, 1996). Calculations indicate that the reduction in threshold power is consistent with the alpha particles' contributing 10–30 % of the total drive in a D-T plasma with 3 MW of peak fusion power.

Recent theoretical calculations have shown that the predicted alpha-driven toroidal Alfvén eigenmode threshold is sensitive to the q profile (Spong *et al.*, 1995; Fu *et al.*, 1996, 1997; Berk *et al.*, 1997). This is potentially important in advanced tokamak configurations in which the current profile is modified to achieve higher

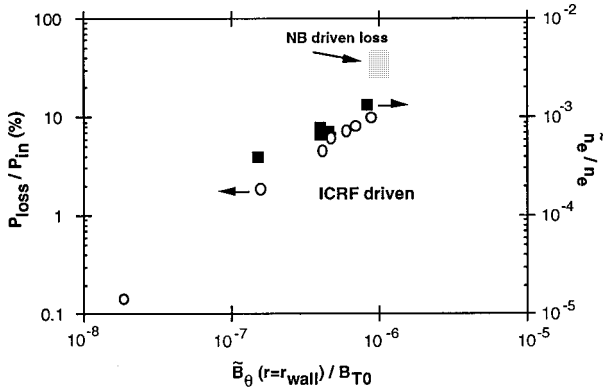

FIG. 56. Fraction of energetic-particle power lost from the plasma and the toroidal Alfvén eigenmode amplitude vs the heating power in TFTR discharges. Energetic-particle loss resulted from toroidal Alfvén eigenmode instabilities driven by neutral-beam injection and ICRF heating but not by alpha particles (Darrow *et al.*, 1997a).

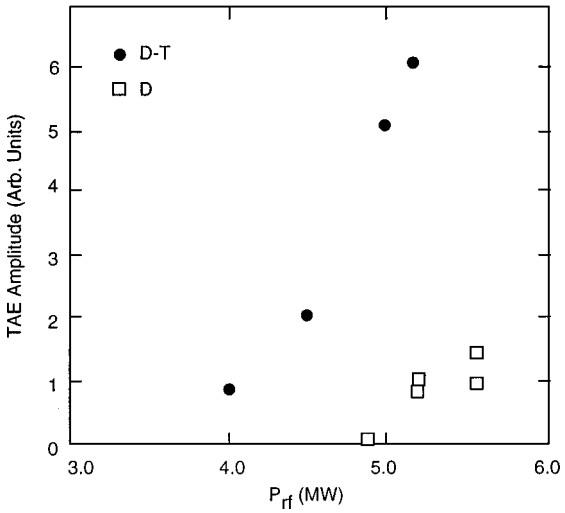

FIG. 57. Toroidal Alfvén eigenmode amplitude in D-T plasmas. Amplitudes are higher than in companion D shots with the same ICRF heating power used to generate the energetic tail of H minority particles (Wong *et al.*, 1996).

stability. In experiments with weak magnetic shear on TFTR, toroidal Alfvén eigenmodes driven by energetic alpha particles have been observed in D-T plasmas (Nazikian *et al.*, 1997a, 1997b; Chang *et al.*, 1997). These modes are observed only after the end of the high-power heating phase, when the beam ion density and plasma pressure are decaying more rapidly than the alpha pressure, as shown in Fig. 58. The fusion power threshold is ~ 1.0 MW with $\beta_\alpha(0) \sim 10^{-4}$ for $q(0) \simeq 2.4$, which is much lower than the value of β_α achieved in high-powered supershot discharges with $q(0) \leqslant 1$ monotonically increasing q profile. As discussed above, the supershot discharges were stable. The onset of mode activity is generally consistent with NOVA-K linear stability calculations (Fu *et al.*, 1997), though the poloidal mode structure remains to be clarified (Chang *et al.*, 1997). The mode amplitude increases with increasing fusion power, as shown in Fig. 59.

So far, the amplitude of this mode is very small, and no loss of alpha particles has been detected. This is consistent with the general arguments presented by White (1995b), which indicate that little radial transport would occur due to a weak single mode. In larger machines, higher values of the mode number could be excited and overlapping modes might result in stochastic diffusion and perhaps increased transport. These recent experimental results have clarified the threshold criteria for alpha-driven toroidal Alfvén eigenmodes instability; however, further experimental work is required, with larger-amplitude modes and perhaps with overlapping modes, to test the nonlinear saturation mechanisms and alpha transport physics due to these instabilities.

B. Ion-cyclotron instabilities

In both JET (Cottrell *et al.*, 1993) and TFTR (Arunsalam and Greene, 1993; Cauffman *et al.*, 1995) experiments, ion-cyclotron emission has been observed during both D and D-T discharges. On JET, ion-cyclotron emission is detected using ICRF antennas, and on TFTR by rf probes located near the top and bottom of the machine. The ion-cyclotron emission spectrum contains superthermal, narrow, equally spaced emission lines, which correspond to successive cyclotron harmonics of deuterium or alpha particles at the outer midplane near the last closed-flux surface. The emission is inferred to arise from alpha particles that are born in the core but whose large orbits intersect the edge of the plasma. As a result, the alpha-particle distribution function in the plasma edge is very anisotropic and provides the free

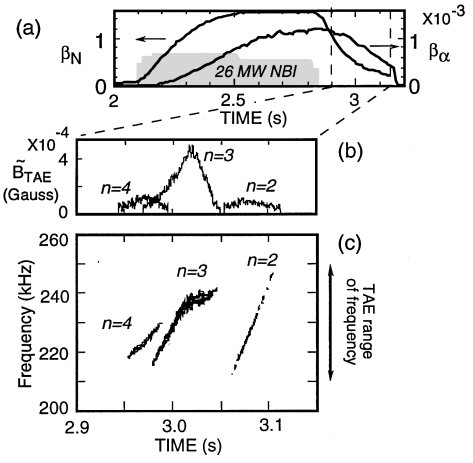

FIG. 58. Alpha-driven toroidal Alfvén eigenmode in TFTR occurring ≈ 0.1 s after neutral-beam injection in a D-T discharge with weak central magnetic shear: (a) the evolution of β_N and β_α; (b) the occurrence of magnetic fluctuations with different toroidal mode numbers; (c) the evolution of the frequency of the magnetic fluctuations. The frequency is consistent with the density-dependent toroidal Alfvén eigenmode frequency, and mode timing is in reasonable agreement with the theoretical prediction based on beam ion damping (Nazikian *et al.*, 1997a).

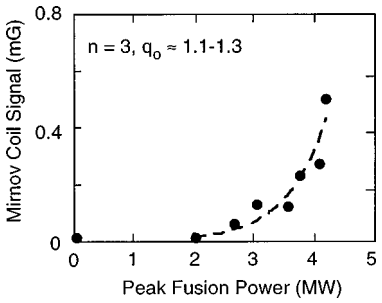

FIG. 59. Toroidal Alfvén eigenmode amplitude measurements using a magnetic pickup coil at the edge. Amplitude increases with fusion power, as expected for alpha-driven toroidal Alfvén eigenmodes near the threshold condition for instability. Modes are observed with $\beta_\alpha(0)>0.03\%$ in weak central shear discharge with $q_0 \sim 1.1-1.3$ (Nazikian *et al.*, 1997a).

energy required to drive the instability. In pure D and mixed D-T JET discharges, the time-averaged ion-cyclotron emission power increases linearly with the total neutron flux over a wide range of six decades in signal intensity, as shown in Fig. 60. The emission is strongly affected by edge-localized modes in the plasma edge. The results on TFTR are similar to those on JET but also have some striking differences. In TFTR supershot discharges, emission at the alpha cyclotron harmonic is observed only for approximately 100–250 ms. However, in discharges with broad density profiles, the emission is observed to persist.

The emission has been studied theoretically by several groups (Coppi, 1993; Arunasalam and Greene, 1993; Arunasalam, Greene, and Young, 1994; Dendy *et al.*, 1994, 1995; Gorlenkov and Cheng 1995a, 1995b; Arunasalam, 1997a, 1997b, McClements *et al.*, 1996; Kolesnichenko *et al.*, 1997). The Alfvén cyclotron instability is driven by the anisotropic alpha distribution function. The results on JET and TFTR are in qualitative agreement with numerical calculations of growth rates due to the magnetoacoustic cyclotron instability (Cauffman *et al.*, 1995). Furthermore, the theory predicts that the instability is sensitive to the ratio of n_α/n_e, the anisotropy in the distribution function, and $V_{\alpha 0}/V_A$ in the edge region, where $V_{\alpha 0}$ is the alpha birth velocity and V_A is the Alfvén velocity. Thus in TFTR supershot discharges with low edge density, $V_{\alpha 0}/V_A$ is <1, and the growth rate is reduced. By contrast, in JET H-mode and TFTR L-mode discharges with broader density profiles, $V_{\alpha 0}/V_A$ is >1, which results in a larger growth rate.

Cottrell *et al.* (1993) suggested that, due to the strong correlation between fusion power and ion-cyclotron emission, this approach could be used as an alpha particle diagnostic. The results on TFTR indicate that the interpretation of the emission depends upon the details of the edge parameters, as well as on the alpha particle density, which will hamper the use of this interesting observation as a diagnostic technique.

IX. ALPHA HEATING EXPERIMENTS

In the highest-performance D-T discharges produced so far, alpha-particle heating is a relatively small fraction

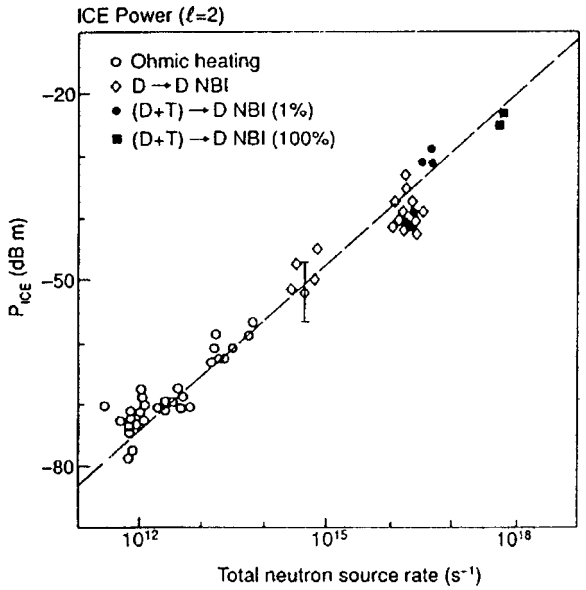

FIG. 60. Correlation between ion-cyclotron emission intensity, $P_{\rm ICE}$, and total neutron emission rate for ohmic and neutral-beam heating in both D and D-T discharges on JET (Cottrell *et al.*, 1993).

of the total power heating the plasma, making its detection difficult. Nevertheless, the electron temperature rise in TFTR D-T shots during beam injection is greater than in D-only or T-only shots (Hawryluk *et al.*, 1994a; Budny *et al.*, 1994; Taylor *et al.*, 1996b). During the initial TFTR D-T experiments, Hawryluk *et al.* (1994a) reported that within $r/a<0.25$, the ratio of the alpha heating power $P_{\alpha e}$ to the total heating power to the electrons $P_{\alpha e}/(P_{\alpha e}+P_{\rm be}+P_{\rm ie}+P_{\rm oh})$, was less than 15%. However, in these experiments there were similar changes in the ion-electron coupling, $P_{\rm ie}$ and collisional beam heating, $P_{\rm be}$. The observed increase of T_e measured by electron-cyclotron emission was roughly twice that expected from alpha heating or the changes in $P_{\rm be}$ and $P_{\rm ie}$ assuming fixed electron thermal diffusivity, suggesting that both alpha heating and other isotope effects were important.

Recent analysis based on a larger data set confirms that the change in electron temperature requires the inclusion of both alpha heating and isotope effects (Taylor *et al.*, 1996b). When the database is constrained to take into account the change in electron temperature associated with confinement, the residual change has been determined to be in reasonable agreement with the predicted alpha heating, as shown in Fig. 61. Further experiments with a higher ratio of alpha heating to beam heating power will be required to evaluate the efficiency of alpha heating.

X. FUTURE DIRECTIONS

In this section, future research opportunities motivated by the results from the JET and TFTR experiments, as well as the accompanying theoretical work in support of those experiments, will be discussed. As with

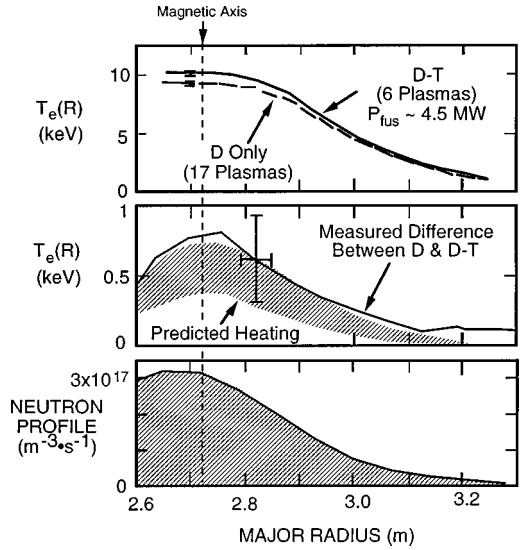

FIG. 61. Comparison of the electron temperature profile for a set of similar D-T and D discharges with comparable energy confinement times and neutral-beam heating power. The measured difference in electron temperature is consistent with the predicted change due to alpha heating. The neutron profile, which is a measure of the alpha-particle birth profile, is shown for comparison (Taylor *et al.*, 1996b).

any active areas of research, future opportunities will largely be defined by theoretical and experimental insights yet to be identified.

A. Alpha heating

Experimental determination of the alpha heating effectiveness remains an important topic due to its crucial importance for reactor design. Though a great deal has been learned about both confined and escaping alpha particles, it must be kept in mind that the present diagnostics sample only part of the distribution function (Zweben *et al.*, 1997). Thus direct measurements of alpha-particle heating effectiveness are important to check the validity of the computational modeling. As discussed in the previous section, although the TFTR experiments have shown that alpha heating is in reasonable accord with expectations, the observed heating is small, and hence the uncertainty in the heating effectiveness is large. To obtain a clearer demonstration requires larger values of $P_{\alpha e}/P_{\mathrm{heat},e}$ and $P_{\alpha e}/P_{\mathrm{ie}}$. The JET Team (1992) has projected higher values of $P_{\mathrm{fus}}/P_{\mathrm{heat}}$ than have been achieved to date on TFTR, albeit in transient discharges with relatively large values of $(dW/dt)/P_{\mathrm{heat}}$. Higher values of $P_{\mathrm{fus}}/P_{\mathrm{heat}}$ offer the possibility of reducing the experimental uncertainty in the alpha heating efficiency, though the interpretation may be complicated due to transient behavior and possible changes in the underlying transport coefficients.

B. Alpha channeling

Several techniques have been proposed for using alpha particle-wave interactions to more effectively utilize the alpha particles in a reactor (Fisch and Rax, 1992; Fisch *et al.*, 1994, Hsu *et al.*, 1994; Mynick and Pomphrey, 1994; Fisch, 1995; Fisch and Herrmann, 1995; Herrmann and Fisch, 1997; Fisch *et al.*, 1997). By coupling the alpha-particle energy to a plasma wave, which then deposits its energy in the plasma, it is theoretically possible to (1) transfer the energy of alpha particles preferentially to the ions and thereby increase the plasma reactivity and reduce the alpha pressure; (2) radially redistribute the alpha particles for alpha ash control; (3) control the alpha heating profile, which may enable pressure profile control in a tokamak; (4) control the alpha pressure profile, which may further reduce the drive for adverse alpha-particle instabilities; (5) transfer momentum to the electrons for current drive. While it may not be possible to achieve all of these objectives simultaneously in a reactor, this concept offers additional flexibility, which may be important to the operation of an advanced tokamak reactor that utilizes self-sustaining pressure and current profile control while requiring as little auxiliary power as possible.

Experiments on TFTR have focused on understanding the physics of energetic-particle interaction with plasma waves, which is a central issue for these approaches. The experiments have utilized a mode-converted fast wave to interact with the energetic ions. In D-^{3}He plasmas, strong interaction between the mode-converted wave and beam ions has resulted in strong beam-ion heating. The escaping energetic ions, shown in Fig. 62, are in reasonable agreement with the alpha particle-wave model when applied to fast beam ions (Fisch *et al.*, 1997).

Radio-frequency-induced alpha-particle cooling, in which the energy in the alpha particle is transferred to the wave, has been predicted for a specific phasing between alphas and high-k_θ ion Bernstein waves, which could then damp on the ions (Valeo and Fisch, 1994). The value of $k_\parallel$ of the fast wave is predicted to change sign after undergoing mode conversion for waves either above or below the midplane. Experiments on TFTR have demonstrated that, in D-^{3}He plasmas, the loss of deuterium-beam ions is correlated with the direction of the rf wave and is in agreement with the rf model, which predicts a dependence on the direction of the wave, thus confirming an important element of the theory (Fisch *et al.*, 1997).

The experimental results (Darrow *et al.*, 1996b) to date support some of the underlying assumptions in the models which predict the feasibility of alpha channeling; however, much more experimental and theoretical work is required to establish this novel approach. In particular, one major element that remains is to establish the transfer of power from the alpha particles to the rf wave. Numerical simulations indicate that for a reactor-size plasma, it will be necessary to excite both toroidal Alfvén eigenmodes and mode-converted ion Bernstein wave to extract more than half the energy from the alpha particles (Fisch and Herrmann, 1995; Herrmann and Fisch, 1997). Evaluation of the interaction of energetic particles with toroidal Alfvén eigenmodes, which have

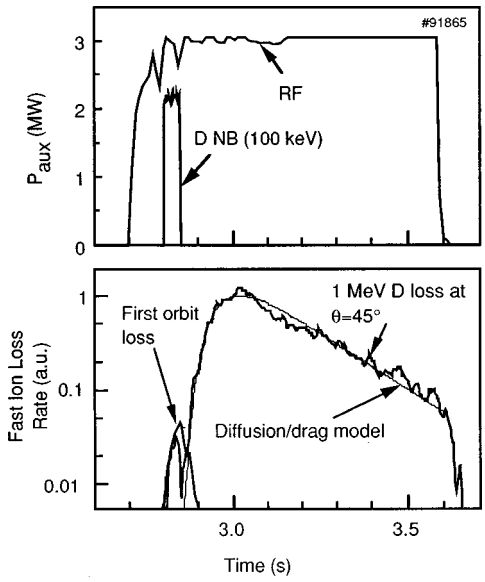

FIG. 62. Fast-ion loss as measured by the 45° detector in the TFTR vessel indicates the loss of deuterium-beam ions heated by mode-converted ion Bernstein waves. The flux of particles is in accord with a simple model of fast-ion heating by the mode-converted wave.

been directly driven by beat waves launched by the ICRF antenna or by a lower-frequency coil antenna [Fasoli *et al.*, 1995a, 1995b, 1995c, 1996; The JET Team (presented by Start), 1997] is an important element in establishing the underlying physics. Ultimately, combining the two waves and demonstrating energy transfer from the alpha particles to the waves, and then damping of the waves, will be required to evaluate this concept.

In the theoretical work by Fisch and Rax (1992), stochastic wave-particle interactions diffuse the particle orbits in a preferred direction by the appropriate choice of wave numbers and wave direction. Another approach, relying upon frequency sweeping of the wave, has been proposed by Mynick and Pomphrey (1994) and Hsu *et al.* (1994). This mechanism can move particles with a selected parallel velocity in a nondiffusive fashion from one specified radius to another. A perturbed single-harmonic wave induces an island in the particle drift surfaces having the same m,n number as the wave. As the wave frequency is slowly varied, a particle starts inside a drift island called a "bucket" and moves adiabatically with that island. By varying the frequency of the wave, it is possible to transport part of the alpha distribution consecutively with the wave. This technique may be used to control the density of He ash, especially in regimes of operation such as the enhanced reverse shear in which the alpha ash accumulation may be important inside the transport barrier. This technique also requires experimental tests to evaluate the efficiency of removing a significant part of the distribution function.

C. Isotope effects in diverted H-mode plasma

The isotope effect has been studied in a wide range of plasma operating regimes on TFTR, as discussed in Sec. V. However, one important operating regime, diverted H modes, which is the planned operating mode for ITER, has not been explored. Isotopic scaling of the energy confinement time and the threshold power for the transition from L and H mode remain to be established. The results from limiter H modes on TFTR indicate that the confinement time has a favorable isotope scaling but the threshold power for the transition is unchanged. In enhanced reverse-shear discharges with an internal transport barrier on TFTR, the confinement time does not exhibit a favorable isotope scaling, and the threshold power appears to be higher in D-T discharges. These differences motivate a thorough study of isotope scaling in diverted H-mode plasmas like those that are planned on JET.

Particle and heat removal is an important issue for future devices operating at much higher powers and for longer pulse durations. In this regard, the ITER device will employ a divertor. Fueling of a diverted tokamak plasma, including control of the ratio of n_T/n_D while minimizing tritium inventory is an operation remaining to be studied. The use of pellet injection and advanced fueling techniques, such as a compact toroid injection, is under study.

D. Ignition devices

In the present experiments, the pressure profile, current profile, and rotation profile are largely determined by the application of auxiliary heating, inductive and noninductive current drive, and applied torque. The current profile is largely determined by the applied external flux and the plasma conductivity. The internally driven bootstrap currents can be significant and can affect the current profile and the plasma stability, although most present high-performance experiments are performed in regimes with small bootstrap current fractions or with heating pulse durations that are short compared with the current diffusion time. Thus the current profile is largely (externally) inductively driven. In current experiments, the rotation profile and the accompanying radial electric-field profile is controlled by the external application of torque (almost always by neutral-beam injection). In the enhanced reverse-shear regime, as well as in the supershot regime on TFTR, the pressure gradient, as a result of intense heating, has become sufficiently large in the plasma core to change the radial electric-field shear significantly. In the present D-T experiments, alpha heating has had a small effect on the pressure profile. While this external control of profiles has facilitated the study of the underlying transport and plasma stability in present-day experiments, it is not representative of conditions in an ignited plasma.

In an ignition device, the operating temperature cannot be simply controlled because the heating power cannot be controlled externally. Simple consideration of the energy balance equation and the temperature dependence of the rate coefficients indicates that ignition at low temperatures can be thermally unstable, but that at high temperature a thermally stable operating point ex-

ists (Borrass *et al.*, 1986). Thus it may be necessary to introduce additional loss mechanisms to obtain a stable operating point.

The problem becomes more complex when one considers the constraints on an economically attractive tokamak device operating in steady state. The self-generated internal processes become dominant for $P_\alpha \sim P_{\rm loss} \gg P_{\rm aux}$. The alpha heating profile is then a sensitive function of the ion pressure profile. In a steady-state machine, the fraction of bootstrap current is expected to be large, otherwise the power required for external current drive using present-day techniques would be too large (Ozeki *et al.*, 1993). [An alternative approach is to design a pulsed device similar in concept to the present machines; however, as discussed by Bathke *et al.* (1994), this may be more expensive]. The rotation profile, and hence the radial electric field, would be largely defined by the plasma pressure gradients because, to drive significant plasma flows, the power required would be too large using neutral-beam injection. In future ignited machines, the role of external heating and current drive, as well as applied torque, will be to control and modify the plasma either through the alpha particles, for example, by alpha channeling, or by altering the underlying transport mechanisms. In addition, the interaction among the pressure, current, and rotation profiles can become much greater, especially in regimes with higher values of β. A couple of examples will be given for illustration. In an ignited plasma, the pressure profile will determine the heating profile, the bootstrap current, and a significant component of the radial electric field. The bootstrap current modifies the current profile, which in turn modifies the radial electric-field shear due to change in the poloidal magnetic field. The radial electric-field shear may decrease radial transport, increasing the plasma pressure, which in turn increases the alpha heating. Hence it is not certain that a self-consistent stable operating point exists, for the processes are highly nonlinear and require a detailed knowledge of the underlying transport mechanisms beyond what has so far been developed. Furthermore, the problem becomes even more complex when MHD stability, which is sensitive to the current and pressure profiles, is taken into account. Controlling the operating point of a burning plasma with a minimum of auxiliary power for the control systems (such as local fueling or heating or momentum input) is a major scientific and technological challenge.

Though the control of a burning plasma is a significant issue, the evolving understanding of the underlying transport mechanisms, MHD stability, and wave-particle interactions in both D and D-T experiments is providing the tools necessary for this task. Advanced computational techniques are being developed and benchmarked on present experiments both to evaluate these problems and to develop new approaches to controlling a burning plasma. Throughout this paper, the results of the D-T experiments have been placed in the context of this evolving understanding of plasma science because this not only has made possible the successful execution of the present experiments but also provides a basis for designing future experiments. With increased understanding, new concepts have emerged, ranging from reverse-shear magnetic configurations to more efficient use of the alpha particles by means of alpha channeling, to the formation of internal transport barriers by use of IBW. Further experimental and theoretical work will determine the viability of these new concepts.

XI. CONCLUSIONS

The first series of high-power D-T experiments on JET and TFTR have provided important new information in fusion technology and science. This is a significant step toward the development of higher-power and higher-performance fusion devices. As discussed in the Appendix, in support of fusion technology development, safe and extended operation of a deuterium-tritium facility has been demonstrated. Tritium handling and processing, tritium retention in plasma facing components, and neutron shielding have been successfully accomplished. Remote handling, use of low-activation materials, and large-scale tritium processing remain to be demonstrated in future facilities. In addition to the large increase in fusion power which occurred with the introduction of D-T fuels, several important scientific issues associated with the use of tritium and the production of alpha particles from D-T reactions have been studied.

The energy confinement time in D-T plasmas has been compared systematically with that in D plasmas in a number of plasma regimes. A significant enhancement in plasma confinement in D-T relative to D has been observed in TFTR L-mode discharges, which at least superficially resemble the proposed ITER plasma conditions of broad density profiles and equilibrated ion/electron temperatures. A somewhat stronger D-T isotope effect on confinement has been obtained in enhanced confinement regimes, including the supershot, H-mode, and high-ℓ_i regimes, all of which typically have peaked density profiles and $T_i > T_e$. On a purely empirical basis, these results provide experimental support for the assumption used in the design of ITER that τ_E would be larger in D-T discharges than in D by the approximate scaling $\tau_E \propto \langle A \rangle^{0.5}$. There is considerable variability in the strength of the confinement enhancement due to isotopes among plasma regimes and as a function of power within a single regime. A negligible isotope effect on energy confinement was observed in discharges with a reverse-shear q profile (including "enhanced" reverse-shear discharges) despite the similarity of their density and temperature profiles to those of the supershot and high-ℓ_i plasmas. This suggests that the isotope effect depends on the current profile. In addition, the power required to obtain an internal transport barrier is greater in TFTR D-T discharges fueled and heated by tritium neutral beams. By contrast, the power threshold for generating a limiter H mode was comparable in D and D-T discharges.

A comprehensive understanding of isotope scaling is still evolving. The favorable scaling with isotopic mass observed in most TFTR plasma regimes imposes a sig-

nificant constraint on proposed transport models based on electrostatic microturbulence, which typically predict an adverse scaling of confinement as ρ^* increases. In particular, the TFTR experiments clearly indicate that confinement *improves* in both supershot and L-mode plasmas if ρ^* is increased by changing the isotope at fixed beta and collisionality. To reconcile this behavior with theory, and with previous scaling experiments in D plasmas which vary ρ^* by varying the magnetic field (Perkins *et al.*, 1992), one is led to conclude that the isotope effect is governed by a fairly powerful effect that leads to reduced transport for heavier isotopes despite their larger gyroradius. Shear-flow modifications to the ion temperature-gradient turbulence model is one such model which would have such an intrinsic effect. As Scott *et al.* (1997) have pointed out, it is intriguing that in both L-mode and supershot regimes the isotope effect appears to be strongest at high power and high temperature, and the effects of shear-flow modifications appear to be sufficiently large even in L-mode discharges to alter the energy confinement time. Projections of the scaling to ITER would be less favorable if isotope scaling in TFTR were caused by sheared-flow effects, which are weaker in larger machines.

The use of tritium permits direct measurement of the transport of hydrogenic species in a plasma. The transport of tritium is comparable to that of electrons and helium gas injected at the edge. More importantly, the transport of particles is comparable in radial dependence and magnitude to the transport of heat and toroidal momentum, placing an important constraint on turbulent transport models for the plasmas. The transport of tritium in enhanced reverse-shear plasmas is much less within the internal transport barrier, qualitatively similar to the changes observed in ion heat transport.

The physics associated with the two principal heating techniques used in the D-T experiments, neutral-beam injection and ICRF heating, was studied. The thermalization rate of tritium- and deuterium-beam ions is in good agreement with classical calculations in discharges with small stochastic ripple diffusion of the beam ions. The introduction of a second ion resonance into the plasma with D-T fuels provides additional flexibility in heating a plasma with ICRF waves. Second-harmonic tritium absorption has successfully been used to heat the plasma in accordance with expectations. In D-^{3}He plasmas, mode conversion was found to heat the electrons locally with high efficiency, and effective current drive was demonstrated. However, when this approach was applied to D-T plasmas on TFTR, the heating efficiency was decreased due to direct absorption by ^{7}Li impurities. This may be especially important in future experiments in which ^{9}Be from the plasma facing components could provide a competing resonance. Further experiments in which the concentration of ^{7}Li impurities is decreased by replacement with ^{6}Li are required to confirm the role of ^{7}Li absorption and evaluate mode-conversion heating and current-drive efficiency in a D-T plasma.

Because of the low concentration of alpha particles, $n_\alpha/n_e \sim 10^{-3}$, and their large energy range, diagnosis of alpha particles, especially in a high-radiation environment, is a formidable challenge. The study of the confinement and loss of alpha particles has been made possible by the successful development of new diagnostic techniques, namely, pellet charge-exchange analysis, charge-exchange recombination spectroscopy, and collector probes. The confined alpha particles behave classically in quiescent MHD plasmas. The study of confined alpha particles has been conducted principally in discharges with monotonic q profiles. Further work is required to evaluate the confinement and transport in reverse-shear discharges. In quiescent discharges, the loss of alpha particles to the collectors near the bottom of the vessel is generally in good agreement with first-orbit loss calculation. Loss of alpha particles caused by stochastic ripple diffusion has been observed, and further work is in progress to obtain a quantitative evaluation of this loss. Loss of alpha particles because of sawtooth events, low-m-n MHD instabilities, plasma disruptions, and rf waves has also been observed. These losses may be an important design consideration in future devices due to the localized heat loss to plasma facing components. Sawtooth instabilities have been observed to redistribute alpha particles in the plasma core. Thermalized alpha particles from fusion reactions have been detected. The radial transport of the alpha ash is comparable to that of the electrons and ions, so accumulation of alpha ash should not be a problem in discharges with supershotlike transport properties. However, the transport of alpha ash has not been studied in discharges with internal transport barriers, and the need for active techniques to remove the ash remains to be determined.

Alpha particles have been seen to initiate MHD instabilities, including the toroidal Alfvén eigenmodes and Alfvén cyclotron instabilities. The stability of the toroidal Alfvén eigenmode has been found to be sensitive to the current profiles, as predicted by theory. In TFTR discharges with monotonic q profiles, the mode was observed to be stable. Only in discharges with weak shear and higher values of $q(0)$ was the mode found to be weakly unstable after the termination of the high-power phase, when beam-ion Landau damping and continuum damping of the mode was decreased. Further experiments with larger-amplitude instabilities are required to evaluate the effect of these instabilities on alpha-particle confinement. The Alfvén cyclotron instability is found to interact with alpha particles in the edge of the plasma by creating ion-cyclotron emission. Good agreement between theory and experiment is found. The impact of this instability, unlike that of the toroidal Alfvén eigenmode, which can theoretically eject significant fractions of alpha particles, appears to be small.

In TFTR experiments, small temperature excursions have been identified as caused by alpha heating. Further experiments in which the alpha heating power approaches the loss power are required to establish the

efficiency of alpha heating and the effect, if any, of alpha heating on plasma transport.

Recent theoretical work on alpha-particle wave interactions, aimed at using the confined particles more effectively to heat the plasma and drive the current, has stimulated basic experiments. These experiments lend support to the underlying physics of alpha-particle wave interactions; however, further work is required to establish this concept.

As with all active research, despite the rapid progress during the past three years of D-T experiments on TFTR, many questions remain. Some of these will be addressed in the current generation of facilities, but others will only be answered on a burning-plasma device operating near ignition conditions.

Note added in proof. Since the submission of this paper, two events have taken place. The first was the completion of the TFTR experimental program in April 1997 followed by the shutdown of the device. The second was the very successful execution of a series of high power D-T experiments on JET. Preliminary results from this campaign (JET Team, presented by Gibson, 1998) included the achievement of 16 MW of fusion power in a hot-ion ELM free H-mode discharge with $P_{\text{fujs}}/P_{\text{abs}}=0.66$ and the production of 21.7 MJ of fusion energy per pulse in an ELMy H-mode discharge.

ACKNOWLEDGMENTS

This work is the product of a great deal of effort by scientists, engineers, and technical staff on both TFTR and JET and is but a brief summary of their work and accomplishments. I should like to express my appreciation to R. Davidson, H. P. Furth, and D. Meade for their steadfast support for and encouragement of the TFTR D-T experiments. I should also like to thank M. Bell, R. Budny, C. Bush, Z. Chang, C. Z. Cheng, G. Cottrell, D. Darrow, P. Efthimion, N. Fisch, E. Fredrickson, G. Y. Fu, A. Gibson, L. Grisham, G. Hammett, J. Hosea, D. Johnson, F. Levinton, K. McGuire, R. Majeski, S. Medley, D. Mueller, R. Nazikian, M. Petrov, C. K. Phillips, G. Rewoldt, E. Ruskov, S. Sabbagh, S. Scott, C. Skinner, E. Synakowski, J. Strachan, B. Stratton, W. Tang, G. Taylor, A. von Halle, M. Williams, J. R. Wilson, K. L. Wong, K. Young, M. Zarnstorff, and S. Zweben for providing figures and valuable input to this paper. The preparation of this manuscript would not have been completed without the help of P. Shangle and C. Such. This work was performed under U.S. DOE Contract No. DE-AC02-76-CH03073.

APPENDIX: TRITIUM AND ACTIVATION CONSIDERATIONS

Deuterium-tritium experiments impose additional requirements on the facility to accommodate the use of tritium, which is radioactive, and the higher level of activation from the D-T reactions (Huguet *et al.*, 1992; Hawryluk *et al.*, 1994b).

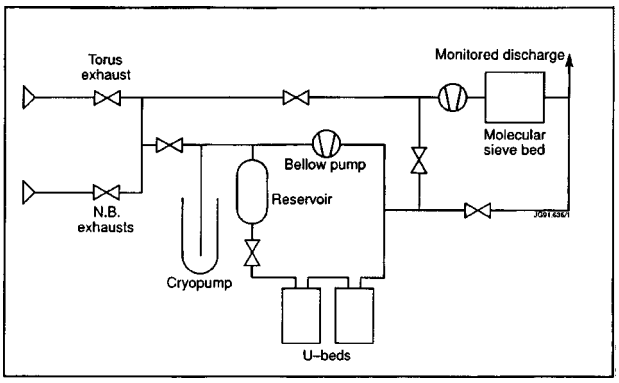

FIG. 63. The JET tritium gas collection system (JET Team, 1992).

1. Tritium systems

The full JET tritium system was not available for the initial D-T experiments (Hemmerich *et al.*, 1992). To collect and measure the injected tritium, the normal torus pumping system was replaced by a cryogenic gas collection system, shown in Fig. 63. During operation, the gas flow from the torus or neutral beamlines condensed on a tubular cryopanel containing activated charcoal at liquid-helium temperature. Subsequently, the condensed tritium, together with larger amounts of deuterium, was transferred to uranium storage beds. Approximately 7.4×10^{13} Bq (2 kCi) of tritium were used in the JET initial D-T experiments.

The TFTR tritium gas handling system is restricted to 1.85×10^{15} Bq (50 kCi) in-process tritium (Hawryluk *et al.*, 1994b; Anderson *et al.*, 1995a, 1995b). By restricting the tritium inventory, the accident potential to personnel working on site, as well as to the general public, is reduced. The tritium gas is brought on site in a shipping canister and is transferred to a uranium bed, where it is stored as shown in Fig. 64. The uranium bed is heated to transfer the gas to the neutral beam or torus injection systems. The gas is then injected into the torus or neutral beams and pumped by the cryopanels in the beam boxes. During plasma operation, some of the gas is retained in the graphite limiter in the vacuum vessel. Outgasing of tritium from the vacuum vessel walls and limiters is pumped by a combination of neutral-beamline cryopanels and a dedicated vessel pumping system. The gas on the cryopanels and from the pumping system is transferred to the Gas Holding Tank, where it is oxidized by the Torus Cleanup System and absorbed onto molecular sieve beds. These beds are shipped off site for reprocessing. More than 3.2×10^{16} Bq (860 kCi) of tritium have been processed from November, 1993 to August, 1996. Since initial operation, a low-inventory cryodistillation system (Busigin *et al.*, 1995; Raftopoulos *et al.*, 1995) has been developed to repurify the tritium on site and decrease the number of off-site shipments of oxidized tritium. This system has been successfully commissioned. In future larger D-T experiments, on-site reprocessing will be required.

Tritium retention. Some of the tritium introduced into the vacuum vessel is retained on the graphite limiter and

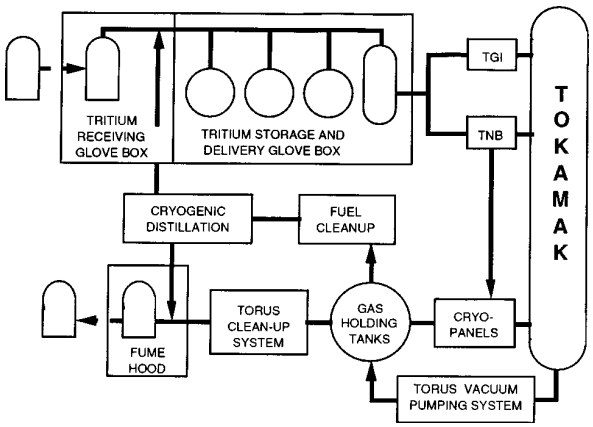

FIG. 64. The TFTR tritium gas fuel cycle (Williams *et al.*, 1997).

co-deposited in layers on the walls. Retention of tritium in the vacuum vessel walls and components is important for two reasons. The first is regulatory (Bell *et al.*, 1992; DeLooper, 1994). The quantity of tritium retained must be accounted for, since special controls are imposed on the handling of tritium (LaMarche *et al.*, 1994; Nagy *et al.*, 1995; Saville *et al.*, 1995). On TFTR, the quantity of tritium permitted in the vessel is restricted to $<7.4\times10^{14}$ Bq (20 kCi) to limit release to the environment in the event of a major vacuum leak and simultaneous failure of tritium containment systems. The second reason is that the interaction of the plasma with the limiter and walls results in the exchange of hydrogenic species between the plasma and the limiters and walls. This can affect the concentration of tritium and deuterium in the discharge, as discussed in Sec. IV.

Saibene *et al.* (1992) and Andrew *et al.* (1993) reported that by a combination of extensive JET operation in deuterium high-power discharges (>1000 shots with and without auxiliary heating), disruptive discharges, glow discharge cleaning, and a deuterium soak of the limiters, it was possible to reduce the tritium in the vessel to as little as 3% of the injected tritium of 2×10^{12} Bq or 54 Ci. A study of the effectiveness of the different techniques was performed. This was aided by having a short concentrated operating phase with tritium followed by an extensive campaign in deuterium to study the evolution of the tritium in the discharge. In TFTR, operations with D-T and D discharges were interspersed for a longer period of time (over two years) and with a larger number of high-power D-T shots (>841) and D shots (>19 700). Two dedicated campaigns were performed on TFTR to remove the retained tritium in October, 1995 and August, 1996. The following are results from the first campaign (Skinner *et al.*, 1996, 1997b; Mueller *et al.*, 1996a). At the start of the removal effort, which followed a series of experiments in which large quantities of T gas were puffed into the plasma, about 50–75 % of the injected tritium (6×10^{14} Bq or 16 kCi) was retained in the vessel. This was in general agreement with the results of previous deuterium retention studies on TFTR and is in contrast with a smaller retention fraction on JET of about 16% (Coad, 1995) in deuterium discharges. Removal of tritium from the TFTR vessel was accomplished by glow discharge cleaning with deuterium and He-O_2 mixtures, followed by a moist-air purge of the vessel. The tritium retention was reduced from 16 kCi to about 8 kCi. It would have been possible to reduce the tritium further with additional time. One difference between the two devices is that JET operates with the vacuum vessel walls at about 300 °C whereas TFTR operates at room temperature. In addition, both devices use wall coatings, Be in JET and Li in TFTR, to reduce the influx of impurities.

The release of tritium caused by the vessel's exposure to air was studied in both devices. In JET, with the walls initially at 300 °C Andrew *et al.* (1993) reported that an air leak liberated about 10% of the tritium in the vessel, 7×10^9 Bq (0.2 Ci). In a planned moist-air purge experiment on TFTR, about 15% of the tritium was released from the vessel surfaces, 7.8×10^{13} Bq (2.1 kCi), and subsequently processed by the cleanup system (Skinner *et al.*, 1997b). The experience on TFTR has shown that it is possible to control the quantity of tritium in the vessel within stringent regulatory requirements; however, the retention of tritium may impose severe operational constraits on future machines using graphite in-vessel components.

2. D-T neutronics

The production of D-T neutrons has been used to study the effectiveness of shielding and machine activation. Apart from its practical importance to present day operations, this is important to the design of future D-T tokamak reactors.

a. Shielding

Due to the complexity of the tokamak structure and the surrounding hardware, including the neutral beamlines and diagnostics, accurate simulations of the effectiveness of machine shielding are difficult to perform. The approach taken on TFTR was to augment the shielding calculations with an extensive set of real-time measurements during deuterium operation, to characterize the shielding and the consequent dose both within the facility and at the site boundary (Kugel *et al.*, 1994, 1995). The results were then compared with existing shielding calculations, assuming a relatively simple model for the machine structure, which was then revised to take into account the additional equipment in the Test Cell. The comparison of the original neutronics modeling with the experimental measurements indicated that the calculations were conservative (Ku and Liew, 1994). Prior to the D-T experiments, supplementary local shielding (especially for sensitive diagnostic equipment) was installed; however, the installation of a complex "igloo" shield around the tokamak was found to be unnecessary, resulting in significant cost savings as well as facilitating maintenance of the machine. The requirement for the design of the shielding for TFTR is that the dose at the site boundary from all sources (direct dose due to gammas and neutrons, as well as from tritium and

activated air) be less than 100 μSv mrem per year. The dose from all pathways has been <5 μSv mrem per year. For the JET experiments, the results from passive dosimetry outside of the biological shield were generally indistinguishable from background (Caldwell-Nichols *et al.*, 1992).

b. Machine activation

Activation of the machine by high-energy neutrons imposes operational constraints in the present machines on maintenance and machine modification (Caldwell-Nichols *et al.*, 1992; Stencel *et al.*, 1994; Kugel *et al.*, 1996). The scope of the JET D-T experiments was limited to permit subsequent hands-on modifications of the components within the vessel (Huguet *et al.*, 1992). In TFTR, the radiation level decreases rapidly with distance from the vacuum vessel, enabling routine hands-on maintenance on nearly all components in the Test Cell except those very close to the vessel. From November, 1993 to August, 1996, 4.8×10^{20} D-T neutrons were produced on TFTR, resulting in an integrated yield of 1.4 GJ. After a week of cooldown for the short-lived isotopes in the stainless steel vessel, the contact dose of the vacuum vessel decreased to 1–2 mSv/hour. Neutronics simulations of the activation of the vessel were benchmarked on TFTR. They are in agreement (within a factor of 2) with the measured activation level and have provided a reliable guide for planning and design. This level of machine activation in TFTR experiments has enabled limited hands-on maintenance of components on the vessel with considerable attention given to reducing the duration of the tasks and providing local shielding. By limiting the scope of the activities and by careful planning, the personnel exposure due to maintenance and modification of the TFTR device was similar during D and D-T operations, despite the factor-of-20 increase in contact dose. In the future, one of the main technological tasks will be to develop remote handling techniques for a fusion reactor. For the next series of D-T experiments on JET, remote handling tools have been developed to remove the divertor cassettes (Pick *et al.*, 1996).

For the long term, one of the most challenging tasks for fusion energy development will be to develop low-activation materials for a reactor. The use of either stainless steel or Inconel alloys, which are used extensively in the present experiments (including TFTR and JET), would create a large waste disposal problem for a fusion reactor. At present, it is difficult to obtain reliable calculations of the nuclear cross sections for reactions producing long half-lives due to large uncertainties on fitted nuclear model parameters. Experiments on TFTR have benchmarked the codes used to predict the level of activation, and specific experiments have been performed to document the activation of other possibly lower-activation materials for the future (Kumar *et al.*, 1996, 1997; Kugel *et al.*, 1996).

In summary, the JET and TFTR D-T experiments have demonstrated it is possible to operate these facilities safely with tritium. Whereas these experiments provide valuable technical data for the design of the next generation of D-T reactors, those machines will encounter much more challenging requirements because of higher neutron fluences and tritium inventory.

REFERENCES

Adler, H. G., K. W. Hill, A. T. Ramsey, and W. Tighe, 1995, Rev. Sci. Instrum. , **66**, 904.

Anderson, J. L., *et al.*, 1995a, Third International Symposium on Fusion Nuclear Technology, Los Angeles, Fusion Eng. Des. **28**, 209.

Anderson, J. L., *et al.*, 1995b, in *Plasma Physics and Controlled Nuclear Fusion Research: Proceedings of the 15th International Conference*, Seville, Spain, 1994 (IAEA, Vienna), Vol. 2, p. 681.

Andrew, P., *et al.*, 1993, Nucl. Fusion **33**, 1389.

Artsimovich, L. A., 1972, Nucl. Fusion **12**, 215.

Arunasalam, V., 1997a, J. Plasma Phys. **58**, 287.

Arunasalam, V., 1997b, J. Plasma Phys. **57**, 523.

Arunasalam, V., and G. J. Greene, 1993, Phys. Rev. Lett. **71**, 3119.

Arunasalam, V., G. J. Greene, and K. M. Young, 1994, Nucl. Fusion **34**, 927.

ASDEX Team, 1959, Nucl. Fusion **29**, 1959.

Aymar, R., *et al.*, 1997, in *Fusion Energy: Proceedings of the Sixteenth IAEA Fusion Energy Conference*, Montreal, 1996 (IAEA, Vienna), Vol. 1, p. 3.

Bak, P., B. Balet, A. Cherubini, J. G. Cordey, N. Deliyankis, M. Erba, V. V. Parail, L. Porte, E. M. Springmann, A. Taroni, and G. Vayakis, 1996, Nucl. Fusion **36**, 321

Balet, B., *et al.*, 1993, Nucl. Fusion **33**, 1345.

Barnes, C. W., M. G. Bell, H. W. Hendel, D. L. Jassby, D. Mikkelsen, A. L. Roquemore, S. D. Scott, J. S. Strachan, and M. C. Zarnstorff, 1990, Rev. Sci. Instrum. **61**, 3151.

Barnes, C. W., A. R. Larson, G. LeMunyan, and M. J. Loughlin, 1995, Rev. Sci. Instrum. **66**, 888.

Barnes, C. W., *et al.*, 1996, Phys. Plasmas **3**, 4521.

Bateman, G., 1978, *MHD Instabilities* (MIT, Cambridge, Massachusetts).

Bateman, G., J. E. Kinsey, A. H. Kritz, A. J. Redd, and J. Weiland, 1997, in *Fusion Energy: Proceedings of the Sixteenth Fusion Energy Conference*, Montreal, 1996 (IAEA, Vienna), Vol. 2, p. 559

Bateman, G., J. Weiland, H. Nordman, J. Kinsey, and C. Singer, 1995, Phys. Scr. **51**, 597.

Batha, S. H., F. M. Levinton, D. A. Spong, R. V. Budny, Z. Y. Chang, D. S. Darrow, E. D. Fredrickson, G. Y. Fu, E. Mazzucato, R. Nazikian, and S. J. Zweben, 1995a, Nucl. Fusion **35**, 1463.

Batha, S. H., F. M. Levinton, M. C. Zarnstorff, and G. L. Schmidt, 1995b, in *22nd European Physical Society Conference on Controlled Fusion and Plasma Heating*, Bournemouth, UK (European Physical Society, Petit-Lancy, Switzerland), Part II, p. 113.

Bathke, C. G., and the Aries Research Team 1994, Fusion Technol. **26**, 1163.

Beer, M., *et al.*, 1997, Phys. Plasmas **4**, 1792.

Bell, A. C., M. Wykes, and B. J. Green, 1992, Fusion Eng. Des. **19**, 169.

Bell, M. G., *et al.*, 1988, in *Plasma Physics and Controlled Nuclear Fusion Research: Proceedings of the Twelfth International Conference*, Nice, 1989 (IAEA, Vienna), Vol. 1, p. 27.

Bell, M. G., *et al.*, 1994, in *Plasma Physics and Controlled Nuclear Fusion Research: Proceedings of the 15th International Conference*, Seville, Spain, 1994 (IAEA, Vienna), Vol. 1, p. 171.
Bell, M. G., *et al.*, 1995, Nucl. Fusion **35**, 1429.
Bell, M. G., 1997, Phys. Plasmas **4**, 1714.
Berk, H. L., *et al.*, 1997, in *Fusion Energy: Proceedings of the Sixteenth IAEA Fusion Energy Conference*, Montreal, 1996 (IAEA, Vienna), Vol. 2. p. 439.
Bessenrodt-Weberpals, M., *et al.*, 1993, Nucl. Fusion **33**, 1205.
Bickerton, R. J., *et al.*, 1971, Nature (London), Phys. Sci. **224**, 110.
Biglari, H., and L. Chen, 1991, Phys. Rev. Lett. **67**, 3681.
Biglari, H., P. Diamond, and P. Terry, 1990, Phys. Fluids B **2**, 1.
Biglari, H., M. Ono, P. H. Diamond, and G. G. Craddock, 1992, in *Proceedings of the Ninth Topical Conference on Radio-Frequency Power in Plasmas*, Charleston, AIP Conf. Proc. No. 244 (AIP, New York), p. 376.
Boivin, R. L., *et al.*, 1993, Nucl. Fusion **33**, 449.
Borrass, K., 1986, Phys. Scr. **T16**, 107.
Bosch, Hans-Stephan, and G. M. Hale, 1992, Nucl. Fusion **32**, 611.
Budny, R. V., 1994, Nucl. Fusion **34**, 1247.
Budny R. V., *et al.*, 1994, in *Proceedings of the 21st EPS Conference on Controlled Fusion and Plasma Physics*, Montpellier, VT, edited by E. Joffrin, P. Platz, and P. E. Stott (European Physical Society, Petit Lancy), Vol. 1, p. 82.
Budny, R. V., *et al.*, 1995, Nucl. Fusion **35**, 1497.
Burrell, K. H., 1994, Plasma Phys. Controlled Fusion **36**, A291.
Burrell, K. H., 1997, Phys. Plasmas, **4** 1499.
Bush, C. E., *et al.*, 1994, in *Proceedings of the 21st EPS Conference on Controlled Fusion and Plasma Physics*, Montpellier, VT, edited by E. Joffrin, P. Platz, and P. E. Stott (European Physical Society, Petit Lancy), Vol. 18B, p. 354.
Bush, C. E., *et al.*, 1995, Phys. Plasmas **2**, 2366.
Bush, C. E., *et al.*, 1996, in *Proceedings of the Plasma Surface Interaction Conference*, 1996, PPPL Report 3207.
Busigin, A., C. J. Busigin, J. R. Robins, K. B. Woodall, D. G. Bellamy, C. Fong, K. Kalyanam, and S. K. Sood, 1995, Fusion Technol. **28**, 1312.
Caldwell-Nichols, C. J., R. Russ, A. C. Bell, N. Davies, A. D. Haigh, H. D. Jones, and L. Serio, 1992, Fusion Eng. Des. **19**, 149.
Carlstrom, T. N., 1996, Plasma Phys. Controlled Fusion **38**, 1149.
Cauffman, S., R. Majeski, K. G. McClements, and R. O. Dendy, 1995, Nucl. Fusion **35**, 1597.
Challis, C. D., *et al.*, 1989, Nucl. Fusion **29**, 563.
Chang, Z., J. D. Callen, E. D. Fredrickson, R. V. Budny, C. C. Hegna, K. M. McGuire, and M. Zarnstorff, 1995a, Phys. Rev. Lett. **74**, 4663.
Chang, Z., *et al.*, 1994, Nucl. Fusion **34**, 1309.
Chang, Z., *et al.*, 1995b, Nucl. Fusion **35**, 1469.
Chang, Z., *et al.*, 1996a, Phys. Rev. Lett. **77**, 3553.
Chang, Z., *et al.*, 1996b, Phys. Rev. Lett. **76**, 1071.
Chang, Z., *et al.*, 1997, Phys. Plasmas **4**, 1610.
Cheng, C. Z., 1991, Phys. Fluids B **3**, 2463.
Cheng, C. Z., and M. S. Chance, 1986, Phys. Fluids **29**, 3695.
Cheng, C. Z., L. Chen, and M. S. Chance, 1985, Ann. Phys. **161**, 21.
Cheng, C. Z., G. Y. Fu, and J. W. Van Dam, 1989, in *Theory of Fusion Plasmas, Proceedings of Joint Varenna-Lausanne International Workshop*, Chexbres, Switzerland, 1988 (Editrice Compositori, Bologna), p. 259.
Cheng, C. Z., *et al.*, 1995, in *Plasma Physics and Controlled Nuclear Fusion Research: Proceedings of the 15th International Conference*, Seville, Spain, 1994 (IAEA, Vienna), Vol. 3, p. 373.
Chong, G. P., 1995, "Measurement of Helium in Nickel Foils from the TFTR Alpha Collector Probe," MS Thesis (University of Toronto).
Coad, J. P., 1995, J. Nucl. Mater. **220**, 156.
Coppi, B., 1993, Phys. Lett. A **172**, 439.
Cordey, J. G., D. G. Muir, S. V. Neudachin, V. V. Parail, E. Springmann, and A. Taroni, 1995, Nucl. Fusion **35**, 101.
Cottrell, G. A., V. P. Bhatnagar, O. DaCosta, R. O. Dendy, J. Jacquinot, K. G. McClements, D. C. McCune, M. F. F. Nave, P. Smeulders, and D. F. H. Start, 1993, Nucl. Fusion **33**, 1365.
Craddock, G. G., and P. H. Diamond, 1991, Phys. Rev. Lett. **67**, 1535.
Craddock, G. G., P. H. Diamond, M. Ono, and H. Biglari, 1994, Phys. Plasmas **I**, 1944.
DIII-D Team, 1995, in *Plasma Physics and Controlled Nuclear Fusion Research: Proceedings of the 15th International Conference*, Seville, Spain, 1994 (IAEA, Vienna), Vol. 1, p. 83.
Darrow, D. S., 1997, Nucl. Fusion **37**, 939.
Darrow, D. S., H. W. Herrmann, D. W. Johnson, R. J. Marsala, R. W. Palladino, and S. J. Zweben, 1995, Rev. Sci. Instrum. **66**, 476.
Darrow, D. S., *et al.*, 1996a, Phys. Plasmas **3**, 1875.
Darrow, D. S., *et al.*, 1996b, Nucl. Fusion **36**, 509.
Darrow, D. S., *et al.*, 1996c, Nucl. Fusion **36**, 1.
DeLooper, J., 1994, Fusion Technol. **31**, 1051.
Dendy, R. O., *et al.*, 1994, Phys. Plasmas **1**, 1918.
Dendy, R. O., C. N. Lashmore-Davies, K. G. McClements, G. A. Cottrell, R. Majeski, and S. Cauffman, 1995, Nucl. Fusion **35**, 1733.
Diamond, P. H., *et al.*, 1997, Phys. Rev. Lett. **78**, 1472.
Drake, J. F., Y. T. Lau, P. N. Guzdar, A. B. Hassam, S. V. Novakovski, B. Rogers, and A. Zeiler, 1996, Phys. Rev. Lett. **77**, 494.
Duong, H. H., R. K. Fisher, J. M. McChesney, P. B. Parks, S. S. Medley, D. K. Mansfield, A. L. Roquemore, and M. P. Petrov, 1997a, Rev. Sci. Instrum. **68**, 340.
Duong, H. H., *et al.*, 1997b, Nucl. Fusion **37**, 271.
Durst, R. D., *et al.*, 1992, Phys. Fluids B **4**, 3707.
Efthimion, P. C., *et al.*, 1995a, Phys. Rev. Lett. **75**, 85.
Efthimion, P. C., *et al.*, 1995b, in *Plasma Physics and Controlled Nuclear Fusion Research: Proceedings of the 15 International Conference*, Seville, Spain, 1994 (IAEA, Vienna), Vol. 1, p. 289.
Ehst, D. A., and C. F. F. Karney, 1991, Nucl. Fusion **31**, 1933.
Ernst, D. R., *et al.*, 1995, Annual Meeting of the APS/DAP, Louisville, KY, 1995, Poster 9P31.
Ernst, D. R., S. D. Scott, and the TFTR Group, 1996, 1996 International Sherwood Fusion Theory Conference, Philadelphia, PA, Poster 1C38.
Equipe Tore Supra, 1997, in *Fusion Energy: Proceedings of the Sixteenth IAEA Fusion Energy Conference*, Montreal, 1996 (IAEA, Vienna), Vol. 2, p. 141.
Fasoli, A., *et al.*, 1995a, Nucl. Fusion **35**, 1485.
Fasoli, A., *et al.*, 1995b, in *Plasma Physics and Controlled Nuclear Fusion Research: Proceedings of the 15 International Conference*, Seville, Spain, 1994 (IAEA, Vienna), Vol. 1, p. 405.

Fasoli, A., *et al.*, 1995c, Phys. Rev. Lett. **75**, 645.
Fasoli, A., *et al.*, 1996, Phys. Rev. Lett. **76**, 1067.
Fisch, N. J., 1995, Phys. Plasmas **2**, (6), 2375.
Fisch, N. J., and M. C. Herrmann, 1995, Nucl. Fusion **35**, 1753.
Fisch, N. J., and J.-M. Rax, 1992, Phys. Rev. Lett. **69**, 612.
Fisch, N. J., E. J. Valeo, C. F. F. Karney, and R. Majeski, 1994, in *21st EPS Conference on Controlled Fusion and Plasma Physics*, Montpellier, VT, edited by E. Joffrin, P. Platz, and P. E. Stott (European Physical Society, Petit Lancy), Vol. 2, p. 640.
Fisch, N. J., *et al.*, 1997, in *Fusion Energy: Proceedings of the Sixteenth IAEA Fusion Energy Conference*, Montreal, 1996 (IAEA, Vienna), Vol. 1, p. 271.
Fisher, R. K., J. M. McChesney, P. B. Parks, H. H. Duong, S. S. Medley, A. L. Roquemore, D. K. Mansfield, R. V. Budny, M. P. Petrov, and R. E. Olson, 1995, Phys. Rev. Lett. **75**, 846.
Forest, C. B., *et al.*, 1996, Phys. Rev. Lett. **77**, 3141.
Fredrickson, E. D., *et al.*, 1995a, Phys. Plasmas **2**, 4216.
Fredrickson, E. D., *et al.*, 1995b, Nucl. Fusion **35**, 1457.
Fredrickson, E. D., K. M. McGuire, Z. Y. Chang, A. Janos, J. Manickam, and G. Taylor, 1996, Phys. Plasmas **3**, 2620.
Fredrickson, E. D., *et al.*, 1997, Phys. Plasmas **4**, 1589.
Freidberg, J. P., 1982, Rev. Mod. Phys. **54**, 801.
Fu, G. Y., C. Z. Cheng, R. Budny, Z. Chang, D. S. Darrow, E. Fredrickson, E. Mazzucato, R. Nazikian, and S. Zweben, 1995, Phys. Rev. Lett. **75**, 2336.
Fu, G. Y., and J. W. Van Dam, 1989, Phys. Fluids B **1**, 1949.
Fu, G. Y., *et al.*, 1996, Phys. Plasmas **3**, 4036.
Fu, G. Y., *et al.*, 1997, in *Nuclear Fusion: Proceedings of the Sixteenth IAEA Fusion Energy Conference*, Montreal, 1996 (IAEA, Vienna), Vol. 2, p. 453.
Fujita, T., *et al.*, 1997, Phys. Rev. Lett. **78**, 2377.
Furth, H. P., 1975, Nucl. Fusion **15**, 487.
Furth, H. P., R. J. Goldston, S. J. Zweben, and D. J. Sigmar, 1990, Nucl. Fusion **30**, 1799.
Galeev, A. A., 1970, Zh. Eksp. Teor. Fiz. **59**, 1378 [Sov. Phys. JETP **32**, 752 (1970)].
Gentle, K. W., 1995, Rev. Mod. Phys. **67**, 809.
Gibson, A., 1987, in *Plasma Physics and Controlled Nuclear Fusion Research: Proceedings of the Eleventh International Conference*, Kyoto, 1986, Vol. 3, p. 479.
Goldston, R., *et al.*, 1981, J. Comput. Phys. **43**, 61.
Goldston, R. J., R. B. White, and A. H. Boozer, 1981, Phys. Rev. Lett. **47**, 647.
Goldston, R., *et al.*, 1994, Plasma Phys. Controlled Fusion B 213.
Goloborod'ko, V., Ya. I. Kolesnichenko, and V. A. Yavorskij, 1987, Phys. Scr. **T16**, 46.
Gorelenkov, N. N., and C. Z. Cheng, 1995a, Phys. Plasmas **2**, 1961.
Gorelenkov, N. N., and C. Z. Cheng, 1995b, Nucl. Fusion **35**, 1743.
Gorelenkov, N. N., *et al.*, 1996, Nucl. Fusion **37**, (8), 1053.
Grisham, L., *et al.*, 1995, Nucl. Instrum. Methods Phys. Res. B **99**, 353.
Hahm, T. S., 1994, Phys. Plasmas **1**, 2940.
Hahm, T. S., and K. Burrell, 1995, Phys. Plasmas **2**, 1648.
Hahm, T. S., *et al.*, 1997, in *Fusion Energy: Proceedings of the Sixteenth IAEA Fusion Energy Conference*, Montreal, 1996 (IAEA, Vienna), Vol. 2. p. 335.
Hawryluk, R. J., 1980, in *Physics of Plasmas Close to Thermonuclear Condition,* edited by B. Coppi, G. G. Leotta, D. Pfirsch, R. Pozzoli, and E. Sindoni (Pergoma, New York/CEC, Brussels), Vol. 1, p. 19.
Hawryluk, R. J., *et al.*, 1991, Plasma Phys. Controlled Fusion **33**, 1509.
Hawryluk, R. J., *et al.*, 1994a, Phys. Rev. Lett. **72**, 3530.
Hawryluk, R. J., *et al.*, 1994b, Phys. Plasmas **1**, 1560.
Hawryluk, R. J., *et al.*, 1995, in *Plasma Physics and Controlled Nuclear Fusion Research: Proceedings of the 15th International Conference*, Seville, Spain, 1994 (IAEA, Vienna), Vol. 1, p. 11.
Heidbrink, W. W., *et al.*, 1991, Nucl. Fusion **31**, 1635.
Heidbrink, W. W., and G. J. Sadler, 1994, Nucl. Fusion **34**, 535.
Hemmerich, J. L., R. Lasser, and T. Winkel, 1992, Fusion Eng. Des. **19**, 161.
Hendel, H. W., *et al.*, 1990, Rev. Sci. Instrum. **61**, 1900.
Hender, T. C., *et al.*, 1996, in *Proceedings of the 23rd European Physical Society Meeting*, Kiev, Ukraine (European Physical Society, Petit Lancy), Vol. 38, p. 12A.
Herrmann, H., G. P. Chong, D. S. Darrow, R. G. Macauley-Newcombe, C. S. Pitcher, J. R. Timberlake, and S. J. Zweben, 1995, Rev. Sci. Instrum. **66**, 351.
Herrmann, M. C., and N. J. Fisch, 1997, Phys. Rev. Lett. **79**, 1495.
Herrmann, H., S. Zweben, D. Darrow, J. Timberlake, G. Chong, A. Haasz, R. Macaulay-Newcombe, and C. V. Pitcher, 1997, Nucl. Fusion **37**, 293.
Hill, K. W., H. Adler, M. Bitter, E. Fredrickson, S. von Goeler, H. Hsuan, A. Janos, D. Johnson, A. T. Ramsey, and G. Renda, 1995, Rev. Sci. Instrum. **66**, 913.
Hill, K. W., K. M. Young, and L. C. Johnson, 1990, PPPL Report 2690.
Hoang, G. T., *et al.*, 1994, Nucl. Fusion **34**, 75.
Horton, W., D. Lindberg, J. Y. Kim, J. Q. Dong, G. W. Hammett, S. D. Scott, M. C. Zarnstorff, and S. Hamaguchi, 1992, Phys. Fluids B **4**, 953.
Hosea, J., *et al.*, 1994, Fusion Technol. **26**, 389.
Hsu, C. T., C. Z. Cheng, P. Helander, D. J. Sigmar, and R. White, 1994, Phys. Rev. Lett. **72**, 2503.
Hugon, M., *et al.*, 1992, Nucl. Fusion **32**, 33.
Huguet, M., *et al.*, 1992, Fusion Eng. Des. **19**, 121.
Ide, S., T. Fujita, O. Naito, and M. Seki, 1996, Plasma Phys. Controlled Fusion **38**, 1645.
Ikeda, Y., K. Tobita, K. Hamamatsu, K. Ushigusa, O. Naito, and H. Kimura, 1996, Nucl. Fusion **36**, 759.
Itoh, K., 1994, Plasma Phys. Controlled Fusion **36**, A307.
Jaeger, E. F., D. B. Batchelor, and D. C. Stallings, 1993, Nucl. Fusion **33**, 179.
Janos, A. C., *et al.*, 1996, Nucl. Fusion **36**, 475.
Jassby, D. L., C. W. Barnes, L. C. Johnson, A. L. Roquemore, J. D. Strachan, D. W. Johnson, S. S. Medley, and K. M. Young, 1995, Rev. Sci. Instrum. **66**, 891.
Jassby, D. L., *et al.*, 1996, "TFTR Experiments with 2% Tritium Beam Fueling," PPPL-3205, submitted to Nucl. Fusion.
JET Team, 1992, Nucl. Fusion **32**, 187.
JET Team (presented by A. Gibson), 1993, in *Plasma Physics and Controlled Nuclear Fusion Research, Fourteenth Conference Proceedings*, Würzburg, Germany, 1992 (IAEA, Vienna), Vol. 1, p. 99.
JET Team (presented by D. Stork) 1995, in *Plasma Physics and Controlled Nuclear Fusion Research: Proceedings of the 15th International Conference*, Seville, Spain, 1994 (IAEA, Vienna), Vol. I, p. 51.
JET Team (presented by P. R. Thomas) 1997, in *Fusion Energy: Proceedings of the Sixteenth IAEA Fusion Energy Conference*, Montreal, 1996 (IAEA, Vienna), Vol. 1, p. 331.

JET Team (presented by J. Jacquinot) 1997, in *Fusion Energy: Proceedings of the Sixteenth IAEA Fusion Energy Conference*, Montreal, 1996 (IAEA, Vienna), Vol. 1, p. 57.
JET Team (presented by D. F. Start) 1997, in *Fusion Energy: Proceedings of the Sixteenth IAEA Fusion Energy Conference*, Montreal, 1996 (IAEA, Vienna), Vol. 1, p. 303.
JET Team (presented by C. Gormezano) 1997, in *Fusion Energy: Proceedings of the Sixteenth IAEA Fusion Energy Conference*, Montreal, 1996 (IAEA, Vienna), Vol. 1, p. 487.
JET Team (presented by A. Gibson) 1998, ''Deuterium-Tritium Plasmas in the Joint European Torus (JET): Behaviour and Implications,'' Phys. Plasmas (to be published).
Johnson, D., *et al.*, 1995, Plasma Phys. Controlled Fusion **37**, A69.
Johnson, L. C., C. W. Barnes, H. Duong, W. W. Heidbrink, D. L. Jassby, M. J. Loughlin, A. L. Roquemore, E. Ruskov, and J. D. Strachan, 1995, Rev. Sci. Instrum. **66**, 894.
Johnson, L. C., P. C. Efthimion, J. D. Strachan, E. Synakowski, M. Zarnstorff, D. McCune, A. L. Roquemore, M. Loughlin, and C. W. Barnes, 1994, in *21st EPS Conference on Controlled Fusion and Plasma Physics*, Montpellier, VT, edited by E. Joffrin, P. Platz, and P. E. Stott (Eureopean Physical Society, Petit Lancy), Vol. 1, p. 182.
Johnson, L. C., *et al.*, 1996, in *Diagnostics for Experimental Thermonuclear Fusion Reactors* (Plenum, New York), p. 369.
Kamada, Y., *et al.*, 1994, Nucl. Fusion **34**, 1605.
Kessel, C., *et al.*, 1994, Phys. Rev. Lett. **72**, 1212.
Kikuchi, M., and M. Azumi, 1995, Plasma Phys. Controlled Fusion **37**, 1215.
Kikuchi, M., *et al.*, 1990, Nucl. Fusion **30**, 343.
Kikuchi, M., *et al.*, 1995, in *Plasma Physics and Controlled Nuclear Fusion Research: Proceedings of the 15th International Conference*, Seville, Spain, 1994 (IAEA, Vienna), Vol. 1, p. 31.
Kinsey, Jon E., and G. Bateman, 1996, Phys. Plasmas **3**, 3344.
Kinsey, Jon E., G. Bateman, A. Kritz, and A. Redd, 1996, Phys. Plasmas **3**, 561.
Kinsey, Jon, C. Singer, T. Djemil, D. Cox, and G. Bateman, 1995, Phys. Plasmas **2**, 811.
Kissick, M. W., *et al.*, 1993, Phys. Fluids B **5**, 3618.
Kolesnichenko, Ya. I., 1980, Nucl. Fusion **20**, 727.
Kolesnichenko, Ya. I., D. Anderson, T. Fülöp, and M. Lisak, 1996, in *Fusion Energy: Proceedings of the Sixteenth IAEA Fusion Energy Conference,* Montreal, 1996 (IAEA, Vienna), Vol. 2, p. 487.
Kolesnichenko, Ya. I., V. V. Lutsenko, and Yu. V. Yakovenko, 1996, in *23rd EPS Conference on Controlled Fusion and Plasma Physics*, Kiev, Ukraine (European Physical Society, Petit Lancy), Pt. I, p. 331.
Kolesnichenko, Ya. I., and Yu. V. Yakovenko, 1996, Nucl. Fusion **36**, 159.
Kolesnichenko, Ya. I., *et al.*, 1992, Phys. Rev. Lett. **68**, 3881.
Kotschenreuther, M., W. Dorland, M. Beer, and G. Hammett, 1995, Phys. Plasmas **2**, 2381.
Ku, L. P., D. W. Johnson, and S. L. Liew, 1994, Fusion Technol. **26**, 933.
Ku, L. P., and S. L. Liew, 1994, in *Proceedings of the 8th International Conference on Radiation Shielding* (ANS, LaGrange Park, IL), p. 1062.
Kugel, H. W., G. Ascione, S. Elwood, and K. Rule, 1996, Fusion Technol. **30**, 1065.
Kugel, H. W., *et al.*, 1994, Fusion Technol. **26**, 963.
Kugel, H. W., *et al.*, 1995, Third International Symposium on Fusion Nuclear Technology, Los Angeles, CA, Fusion Eng. Des. **28**, 534.
Kumar, A., H. W. Kugel, and G. Ascione, 1996, Fusion Technol. **30**, 1113.
Kumar, A., H. W. Kugel, and G. Ascione, 1997, in *Fusion Energy: Proceedings of the Sixteenth IAEA Fusion Energy Conference*, Montreal, 1996 (IAEA, Vienna), Vol. 3, p. 517.
LaMarche, P. H., *et al.*, 1994, Fusion Technol. **26**, 427.
Lao, L. L., *et al.*, 1993, Phys. Rev. Lett. **70**, 3435.
Lazarus, E. A., *et al.*, 1991, Phys. Fluids B **3**, 2220.
Lazarus, E. A., *et al.*, 1992, Phys. Fluids B **4**, 3644.
Lazarus, E. A., *et al.*, 1996, Phys. Rev. Lett. **77**, 2714.
Lazarus, E. A., *et al.*, 1997, in *Fusion Energy: Proceedings of the Sixteenth IAEA Fusion Energy Conference*, Montreal, 1996 (IAEA, Vienna), Vol. 1, p. 199.
Levinton, F. M., L. Zakharov, S. H. Batha, J. Manickam, and M. C. Zarnstorff, 1994, Phys. Rev. Lett. **72**, 2895.
Levinton, F. M., *et al.*, 1995, Phys. Rev. Lett. **75**, 4417.
Levinton, F. M., *et al.*, 1997, in *Fusion Energy: Proceedings of the Sixteenth IAEA Fusion Energy Conference*, Montreal, 1996 (IAEA, Vienna), Vol. 1, p. 211.
Lin, Z., W. Tang, and W. W. Lee, 1997, Phys. Rev. Lett. **78**, 456.
Majeski, R., *et al.*, 1994, Phys. Rev. Lett. **73**, 2204.
Majeski, R., *et al.*, 1995, in *Plasma Physics and Controlled Nuclear Fusion Research: Proceedings of the 15th International Conference*, Seville, Spain, 1994 (IAEA, Vienna), Vol. 1, p. 443.
Majeski, R., *et al.*, 1996, Phys. Rev. Lett. **76**, 764.
Manfredi, G., and R. O. Dendy, 1996, Phys. Rev. Lett. **76**, 4360.
Manickam, J., *et al.*, 1997, in *Fusion Energy: Proceedings of the Sixteenth IAEA Fusion Energy Conference*, Montreal, 1996 (IAEA, Vienna), Vol. 1, p. 453.
Mansfield, D. K., *et al.*, 1995, Phys. Plasmas **2**, 4252.
Mansfield, D. K., *et al.*, 1996, Phys. Plasmas **3**, 1892.
Marcus, F. B., *et al.*, 1993, Nucl. Fusion **33**, 1325.
Mazzucato, E., *et al.*, 1996, Phys. Rev. Lett. **77**, 3145.
Mazzucato, E., *et al.*, 1997, in *Fusion Energy: Proceedings of the Sixteenth IAEA Fusion Energy Conference*, Montreal, 1996 (IAEA, Vienna) Vol. 1, p. 913.
McClements, K. G., R. O. Dendy, C. N. Lashmore-Davies, G. Cottrell, S. Cauffman, and R. Majeski, 1996, Phys. Plasmas **3**, 543.
McGuire, K. M., *et al.*, 1995, Phys. Plasmas **2**, 2176.
McGuire, K. M., *et al.*, 1997, in *Fusion Energy: Proceedings of the Sixteenth IAEA Fusion Energy Conference*, Montreal, 1996 (IAEA, Vienna), Vol. 1, p. 19.
McKee, G. R., R. J. Fonck, T. A. Thorson, and B. C. Stratton, 1995a, Rev. Sci. Instrum. **66**, 643.
McKee, G. R., *et al.*, 1995b, Phys. Rev. Lett. **75**, 649.
McKee, G. R., *et al.*, 1997, Nucl. Fusion **37**, 501.
Meade, D. M., 1995, Fusion Eng. Des. **27**, 17.
Meade, D. M., *et al.*, 1991, in *Proceedings of the 13th International Conference on Plasma Physics and Controlled Nuclear Fusion Research*, Washington, DC, 1990 (IAEA, Vienna), Vol. 1, p. 9.
Medley, S. S., H. Duong, R. Fisher, N. Gorelenkov, A. Khudoleev, D. Mansfield, J. McChesney, P. Parks, M. Petrov, and A. Roquemore, 1996b, Rev. Sci. Instrum. **67**, 3122.
Medley, S. S., R. K. Fisher, A. V. Khudoleev, D. K. Mansfield, J. M. McChesney, P. B. Parks, M. P. Petrov, C. K. Phillips, A.

L. Roquemore, and K. M. Young, 1995, in *22nd European Physical Society Conference on Controlled Fusion and Plasma Heating*, Bournemouth, UK (EPS, Geneva), Vol. 1, p. 409.
Medley, S. S., *et al.*, 1996a, Plasma Phys. Controlled Fusion **38**, 1779.
Morgan, P. D., 1992, in *Proceedings of the 17th Symposium on Fusion Technology*, Rome Italy, edited by C. Ferro, M. Gasparotto, and H. Knoepfel (Elsevier, Amsterdam), p. 722.
Mueller, D., *et al.*, 1996a, Fusion Technol. **30**, 840.
Mueller, D., *et al.*, 1996b, Fusion Technol. **30**, 251.
Mynick, H. E., and R. E. Duvall, 1989, Phys. Fluids B **1**, 750.
Mynick, H. E., and N. Pomphrey, 1994, Nucl. Fusion **34**, 1277.
Myra, J. R., *et al.*, 1993, Phys. Fluids B **5**, 1160.
Nagayama, Y., *et al.*, 1993, Phys. Fluids B **5**, 2571.
Nagy, A., *et al.*, 1995, in *Proceedings of the 16th IEEE/NPSS Symposium on Fusion Engineering,* Champaign, IL, edited by G. Miley, and C. Elliott (IEEE, Piscataway, NJ), Vol. 2, p. 573.
Navratil, G., *et al.*, 1991, in *Plasma Physics and Controlled Nuclear Fusion Research: Proceedings of the 13th International Conference*, Washington, DC, 1990 (IAEA, Vienna), Vol. 1, p. 209.
Nazikian, R., *et al.*, 1996, Phys. Plasmas **3**, 593.
Nazikian, R., *et al.*, 1997a, in *Fusion Energy: Proceedings of the Sixteenth IAEA Fusion Energy Conference,* Montreal, 1996 (IAEA, Vienna), Vol. 1, p. 281.
Nazikian, R., *et al.*, 1997b, Phys. Rev. Lett. **78**, 2976.
Ono, M., *et al.*, 1993, Phys. Fluids B **5**, 241.
Ozeki, T., *et al.*, 1993, in *Plasma Physics and Controlled Fusion Research: Proceedings of the Fourteenth International Conference*, Würzburg, Germany (IAEA Vienna), Vol. 2, p. 187.
Park, H. K., 1997, Phys. Plasmas **4**, 1699.
Park, W., Z. Chang, E. Fredrickson, G. Y. Fu, and N. Pomphrey, 1997, in *Fusion Energy: Proceedings of the Sixteenth IAEA Fusion Energy Conference*, Montreal, 1996 (IAEA, Vienna), Vol. 2, p. 411.
Park, W., E. D. Fredrickson, A. Janos, J. Manickam, and W. T. Tang, 1995, Phys. Rev. Lett. **75**, 1763.
Paul, S. F., J. L. Goldstein, R. D. Durst, and R. J. Fonck, 1995, Rev. Sci. Instrum. **66**, 1252.
Perkins, F. W., *et al.*, 1992, Phys. Fluids B **5**, 477.
Petrov, M. P., *et al.*, 1995, Nucl. Fusion **35**, 1437.
Petrov, M. P., *et al.*, 1997, in *Fusion Energy: Proceedings of the Sixteenth IAEA Fusion Energy Conference*, Montreal, 1996 (IAEA, Vienna), Vol. 1, p. 261.
Phillips, C. K., *et al.*, 1995, Phys. Plasmas **2**, 2427.
Pick, M., *et al.*, 1996, Fusion Technol. **30**, 634.
Raftopoulos, S., R. Scillia, P. Sichta, L. Dudek, G. Labik, J. Satkofsky, J. Langford, and D. Voorhees, 1995, in *Proceedings of the 16th IEEE/NPSS Symposium on Fusion Engineering*, Champaign, IL, edited by G. Miley and C. Elliott (IEEE, Piscataway, NJ), Vol. 1, p. 581.
Ramsey, A. T., 1995, Rev. Sci. Instrum. **66**, 871.
Redi, M. H., M. C. Zarnstorff, R. B. White, R. V. Budny, A. C. Janos, D. K. Owens, J. F. Schivell, S. D. Scott, and S. J. Zweben, 1995a, Nucl. Fusion **35**, 1191.
Redi, M. H., *et al.*, 1995b, Nucl. Fusion **35**, 1509.
Rogers, B., and L. Zakharov, 1995, Phys. Plasmas **2**, 3420.
Rogers, J. H., *et al.*, 1994, in *21st EPS Conference on Controlled Fusion and Plasma Physics*, Montpellier, VT, edited by E. Joffrin, P. Platz, and P. E. Stott (European Physical Society, Petit Lancy), Pt. 2, p. 988.
Rogers, J. H., *et al.*, 1997, in *Fusion Energy: Proceedings of the Sixteenth IAEA Fusion Energy Conference*, Montreal, 1996 (IAEA, Vienna), Vol. 3, p. 317.
Rose, D. J., and M. Clark, Jr., 1961, *Plasmas and Controlled Fusion* (MIT, Cambridge, MA, and Wiley, New York).
Ruskov, E., W. W. Heidbrink, and R. V. Budny, 1995, Nucl. Fusion **35**, 1099.
Sabbagh, S. A., *et al.*, 1991, Phys. Fluids B **3**, 2277.
Sabbagh, S. A., *et al.*, 1995a, in *Plasma Physics and Controlled Nuclear Fusion Research: Proceedings of the 15th International Conference*, Seville, Spain, 1994 (IAEA, Vienna), Vol. 1, p. 663.
Sabbagh, S. A., *et al.*, 1995b, in *Tokamak Concept Improvement: Proceedings of the Workshop held at the 1994 International School of Plasma Physics*, Varenna, Italy, edited by S. Bernabei, N. Sauthoff, and E. Sindoni (Editrice Compositori, Bologna, Italy), p. 219.
Sabbagh, S. A., *et al.*, 1997, in *Fusion Energy: Proceedings of the Sixteenth IAEA Fusion Energy Conference*, Montreal, 1996 (IAEA, Vienna), Vol. 1, p. 921.
Saibene, G., R. Sartori, P. Andrew, J. How, Q. King, and A. T. Peacock, 1992, Fusion Eng. Des. **19**, 133.
Saigusa, M., *et al.*, 1995, Plasma Phys. Controlled Fusion **37**, 295.
Saville, C., G. Ascione, S. Elwood, A. Nagy, S. Raftopoulos, R. Rossmassler, J. Stencel, D. Voorhees, and C. Tilson, 1995, Fusion Technol. **28**, 1078.
Scott, S., *et al.*, 1990a, Phys. Rev. Lett. **64**, 531.
Scott, S., *et al.*, 1990b, Phys. Fluids B **2**, 1300.
Scott, S. D., *et al.*, 1995a, Phys. Plasmas **2**, 2299.
Scott, S. D., *et al.*, 1996b, Phys. Scr. **51**, 394.
Scott, S. D., *et al.*, 1997, in *Fusion Energy: Proceedings of the Sixteenth IAEA Fusion Energy Conference*, Montreal, 1996 (IAEA, Vienna), Vol. 1, p. 573.
Shaing, K. C., E. C. Crume Jr., and W. A. Houlberg, 1990, Phys. Fluids B **2**, 1492.
Sigmar, D. J., 1987, Phys. Scr. **T16**, 6.
Skinner, C., H. Adler, R. V. Budny, J. Kamperschroer, L. C. Johnson, A. T. Ramsey, and D. P. Stotler, 1995a, Nucl. Fusion **35**, 143.
Skinner, C. H., J. Kamperschroer, D. Mueller, A. Nagy, and J. Stotler, 1997a, J. Nucl. Mater. **241-243**, 887–891.
Skinner, C. H., D. P. Stotler, H. Adler, and A. T. Ramsey, 1995b, Rev. Sci. Instrum. **66**, 646.
Skinner, C. H., *et al.*, 1996, J. Vac. Sci. Technol. A **14**, 3267.
Skinner, C. H., *et al.*, 1997b, J. Nucl. Mater. **241-243**, 214–226.
Spong, D. A., C. L. Hedrick, and B. A. Carreras, 1995, Nucl. Fusion **35**, 1687.
Stencel, J. R., J. D. Gilbert, J. D. Levine, and G. Ascione, 1994, J. Appl. Health Phys. **11**, 27.
Stevenson, T., *et al.*, 1995, 16th IEEE/NPSS Symposium on Fusion Engineering, Champaign, IL, edited by G. Miley and C. Elliott (IEEE, Piscataway, NJ), Vol. 1, p. 537.
Stix, T. H., 1992, *Waves in Plasmas* (AIP, New York).
Stotler, D. P., C. H. Skinner, R. V. Budny, and A. T. Ramsey, 1996, Phys. Plasmas **3**, 4084.
Strachan, J. D., 1994, Nucl. Fusion **34**, 1017.
Strachan, J. D., C. W. Barnes, M. Diesso, D. Jassby, L. Johnson, M. Loughlin, S. McCauley, T. Munsat, and A. L. Roquemore, 1995, Rev. Sci. Instrum. **66**, 1247.
Strachan, J. D., R. E. Chrien, and W. W. Heidbrink, 1983, J. Vac. Sci. Technol. A **1**, 811.
Strachan, J. D., *et al.*, 1987, Phys. Rev. Lett. **58**, 1004.

Strachan, J. D., *et al.*, 1989, in *Proceedings of the 10th International Conference on Plasma Physics and Controlled Nuclear Fusion Research*, Nice (IAEA, Vienna), Vol. 1, p. 257.
Strachan, J. D., *et al.*, 1990, Rev. Sci. Instrum. **61**, 3501.
Strachan, J. D., *et al.*, 1992, J. Nucl. Mater. **96**, 28.
Strachan, J. D., *et al.*, 1994a, Phys. Rev. Lett. **72**, 3526.
Strachan, J. D., *et al.*, 1994b, Plasma Phys. Controlled Fusion **36**, B3.
Strachan, J. D., *et al.*, 1994c, J. Nucl. Mater. **217**, 145.
Strait, E. J., *et al.*, 1993, Nucl. Fusion **33**, 1849.
Strait, E. J., *et al.*, 1995, Phys. Rev. Lett. **75**, 4421.
Stratton, B., R. Fonck, G. McKee, R. Budny, Z. Chang, F. Wising, and A. Ödblom, 1996, Nucl. Fusion **36**, 1586.
Synakowski, E. J., *et al.*, 1993, Phys. Fluids B **5**, 2215.
Synakowski, E. J., *et al.*, 1995a, Phys. Rev. Lett. **75**, 3689.
Synakowski, E. J., *et al.*, 1995, in *Proceedings of the 22nd European Conference on Controlled Fusion and Plasma Physics*, Bournemouth, U.K., 1995, Vol. 19C of Europhysics Conference Abstracts, pp. 13–16 (EPS, Petit-Lancy, Switzerland), Part III.
Synakowski, E. J., *et al.*, 1997a, Phys. Plasmas **4**, 1736.
Synakowski, E. J., *et al.*, 1997b, Phys. Rev. Lett. **78**, 2972.
Tang, W. M., J. W. Connor, and R. J. Hastie, 1980, Nucl. Fusion **20**, 1439.
Taylor, G., *et al.*, 1995, in *Plasma Physics and Controlled Nuclear Fusion Research: Proceedings of the 15th International Conference*, Seville, Spain, 1994 (IAEA, Vienna), Vol. 1, p. 431.
Taylor, G., *et al.*, 1996a, Plasma Phys. Controlled Fusion **38**, 723.
Taylor, G., *et al.*, 1996b, Phys. Rev. Lett. **76**, 2722.
Terry, J. L., *et al.*, 1991, in *Proceedings of the 13th International Conference on Plasma Physics and Controlled Nuclear Fusion Research*, Washington, DC, 1990 (IAEA, Vienna), Vol. 1, p. 393.
Thomas, P. R., 1996, "Divertor Diagnostics for JET" in *Diagnostics for Experimental Thermonuclear Fusion Reactors* (Plenum, New York), p. 531.
Tibone, F., 1993, Nucl. Fusion **33**, 1319.
Tobita, K., *et al.*, 1997, in *Fusion Energy: Proceedings of the Sixteenth IAEA Fusion Energy Conference*, Montreal, 1996 (IAEA, Vienna), Vol. 1, p. 497.
Troyon, F., R. Gruber, H. Saurenmann, S. Semenzato, and S. Succi, 1984, Plasma Phys. Controlled Fusion **26**, 209.
Turnbull, A. D., *et al.*, 1995, Phys. Rev. Lett. **74**, 718.
Ulrickson, M., *et al.*, 1990, J. Nucl. Mater. **176/177**, 44.
Ushigusa, K., and the JT-60 Team, 1997, in *Fusion Energy: Proceedings of the Sixteenth IAEA Fusion Energy Conference*, Montreal, 1996 (IAEA, Vienna), Vol. 1, p. 37.
Valeo, E. J., and N. J. Fisch, 1994, Phys. Rev. Lett. **73**, 3536.
Wagner, F., *et al.*, 1982, Phys. Rev. Lett. **49**, 1408.
Wang, S., and S. J. Zweben, 1996, "Model of Alpha Particle Diffusion in the Outer Limiter Shadow of TFTR," PPPL-3186.
Ward, D. J., 1996, Plasma Phys. Controlled Fusion **38**, 1201.
Wesson, John, 1987, *Tokamaks* (Oxford University Press, Oxford).
Wesson, J. A., and B. Balet, 1996, Phys. Rev. Lett. **77**, 5214.
White, R. B., E. Fredrickson, D. Darrow, M. Zarnstorff, R. Wilson, S. Zweben, K. Hill, Y. Chen, and G. Fu, 1995a, Phys. Plasmas **2**, 2871.
White, R. B., R. J. Goldston, M. H. Redi, and R. V. Budny, 1996, Phys. Plasmas **3**, 3043.
White, R. B., Y. Wu, Y. Chen, E. D. Fredrickson, D. S. Darrow, M. C. Zarnstorff, J. R. Wilson, S. J. Zweben, K. W. Hill, and G. Y. Fu, 1995b, Nucl. Fusion **35**, 1707.
Williams, M. D., and the TFTR Group, 1997, Symposium on Fusion Technology, September 16–20, 1996, Lisbon, Portugal, Fusion Eng. Des. **36**, 135.
Wilson, J. R., *et al.*, 1993, in *Plasma Physics and Controlled Nuclear Fusion Research, Fourteenth Conference Proceedings*, Würzburg, Germany 1992 (IAEA, Vienna), Vol. 1, p. 661.
Wilson, J. R., *et al.*, 1995, Phys. Rev. Lett. **75**, 842.
Wong, K. L., *et al.*, 1991, Phys. Rev. Lett. **66**, 1874.
Wong, K. L., *et al.*, 1992, Phys. Fluids B **4**, 2122.
Wong, K. L., *et al.*, 1996, Phys. Rev. Lett. **76**, 2286.
Wong, K. L., *et al.*, 1997, Phys. Plasmas **4**, 393.
Young, K. M., 1997, J. Fusion Eng. Design **34-35**, 3.
Young, K. M., and D. W. Johnson, 1992, Plasma Phys. Controlled Fusion **34**, 2001.
Yushmanov, P. N., T. Takizuka, K. S. Riedel, O. J. W. F. Kardaun, J. G. Cordey, S. M. Kaye and D. E. Post, 1990, Nucl. Fusion **30**, 1999.
Zakharov, L. and B. Rogers, 1992, Phys. Fluids B **4**, 3285.
Zakharov, L., B. Rogers, and S. Migliuolo, 1993, Phys. Fluids B **5**, 2498.
Zarnstorff, M. C., *et al.*, 1988a, in *15th European Conference on Controlled Fusion and Plasma Heating*, Dubrovnik, Contributed Papers edited by S. Pesic and J. Jacquinot (EPS, Geneva), Vol. 12B, Part 1, p. 95.
Zarnstorff, M. C., *et al.*, 1988b, Phys. Rev. Lett. **60**, 1306.
Zarnstorff, M. C., *et al.*, 1989a, in *Plasma Physics and Controlled Nuclear Fusion Research: Proceedings of the Twelfth International Conference*, Nice, 1988 (IAEA, Vienna), Vol. 1, p. 183.
Zarnstorff, M. C., *et al.*, 1989b, *Controlled Fusion and Plasma Physics, Proceedings of the Sixteenth European Conference*, Venice, 1989 (European Physical Society, Petit Lancy), Vol. 13B, Part 1, p. 35.
Zarnstorff, M. C., *et al.*, 1990, in *Controlled Fusion and Plasma Heating, Proceedings of the Seventeenth European Conference*, Amsterdam, 1990 (European Physical Society, Petit Lancy), Vol. 14B, Part 1, p. 42.
Zarnstorff, M. C., *et al.*, 1991, in *Proceedings of the Thirteenth International Conference on Plasma Physics and Controlled Nuclear Fusion Research*, Washington, DC, 1990 (IAEA, Vienna), Vol. 1, p. 109.
Zarnstorff, M. C., *et al.*, 1995, in *Plasma Physics and Controlled Nuclear Fusion Research: Proceedings of the 15th International Conference*, Seville, Spain, 1994 (IAEA, Vienna), Vol. 1, p. 183.
Zhao, Y. and R. White, 1997, Phys. Plasmas **4**, 1103.
Zweben, S. J., D. S. Darrow, H. W. Herrmann, M. H. Redi, J. F. Schivell, and R. B. White, 1995, Nucl. Fusion **35**, 1445.
Zweben, S. J., *et al.*, 1990, Nucl. Fusion **30**, 1551.
Zweben, S. J., *et al.*, 1991, Nucl. Fusion **31**, 2219.
Zweben, S. J., *et al.*, 1993a, Nucl. Fusion **33**, 705.
Zweben, S. J., *et al.*, 1993b, in *Plasma Physics and Controlled Nuclear Fusion Research: Proceedings of the 14th International Conference*, Würzburg, Germany, 1992 (IAEA, Vienna), Vol. 1, p. 363.
Zweben, S. J., *et al.*, 1994, Phys. Plasmas **1**, 1469.
Zweben, S. J., *et al.*, 1995b, Nucl. Fusion **35**, 893.
Zweben, S. J., *et al.*, 1996, Nucl. Fusion **36**, 987.
Zweben, S. J., *et al.*, 1997, Plasma Phys. Controlled Fusion **39**, A275.